1-1-2014

Post-Transcriptional Shaping of Neurons: The Role of miRNAs and FMRP-Interacting P-Body Components in Regulating Neuronal Structure

Breanna Symmes
University of Denver

Post-Transcriptional Shaping of Neurons:
The Role of miRNAs and FMRP-Interacting P-Body Components in Regulating Neuronal Structure

_____

A Dissertation

Presented to

the Faculty of Natural Sciences and Mathematics

University of Denver

_____

In Partial Fulfillment

of the Requirements for the Degree

Doctor of Philosophy

_____

by

Breanna A. Symmes

June 2014

Advisor: Dr. Scott A. Barbee, Ph.D.

Author: Breanna A. Symmes
Title: Post-Transcriptional Shaping of Neurons: The Role of miRNAs and FMRP-Interacting P-Body Components in Regulating Neuronal Structure
Advisor: Scott A. Barbee, Ph.D.
Degree Date: June 2014

Abstract

Changes in synaptic structure in response to neuronal stimulation are believed to underlie the processes of learning and long-term memory. However, the mechanisms for these structural modifications are poorly understood. It is well-known that activity-dependent synaptic modifications rely upon new protein synthesis, and rapid new protein synthesis, at that. Therefore, it is widely believed that pools of messenger RNAs held in a state of translational repression are transcribed in a neuronal cell body prior to stimulation, and transported to the synapse, where they reside until stimulation occurs.

This study investigates the roles and interactions of translational repression mechanisms to better understand how new synaptic growth is repressed or enhanced for the purposes of long-term memory and learning. We found that miRNAs -315, -275, -11 and the miR-9 family are of particular interest for neuronal growth in *Drosophila* larvae because they are extremely enriched in the larval CNS compared to the adult brain, and are predicted to regulate mRNA targets that significantly contribute to neuronal development. Furthermore, miR-315 and the miR-9 family bind and regulate a *Futsch* (*Drosophila* homolog of mammalian MAP1B known to affect synaptic growth) reporter *in vitro*, and the miR-9 family exhibits an increase in bouton numbers at muscles 6/7 of the NMJ characteristic of an increase in Futsch levels when under-expressed. Curiously, this same effect with seen with miR-9 family overexpression.

While miRNAs are translational repressors and can clearly affect synaptic structure on their own, components of the miRNA pathway further interact with other translational repressors, including the Fragile-X Mental Retardation Protein (FMRP). Although FMRP has been shown to interact with the miRNA pathway, and to regulate *Futsch*, we could not discern down-regulation of a *Futsch* reporter from FMRP overexpression in S2 cells, nor an interaction between FMRP and these miRNAs that regulated a *Futsch* reporter *in vitro*. However, FMRP did interact with several P-body components, including co-localization with HPat, Twin, and Me31B, as well as co-immunoprecipitation with HPat, Me31B and Dcp1. Genetic interactions between FMRP and HPat and FMRP and Twin produced discernible phenotypes at the *Drosophila* NMJ, suggesting this interaction is important for synaptic growth.

Acknowledgements

First and foremost, I would like to thank my incredibly supportive family, for encouraging me throughout my life to work as hard as possible to achieve and to succeed. I would also like to thank the love of my life for the same reason, and for helping me throughout the endeavors of the last five years.

I would like to thank previous lab members for helping me to learn new techniques to apply to my research, including Bob Sand and Sarala Pradhan. I am grateful to Leslie Rozeboom and Nathan Boin for their contributions to this research. I would also like to thank Marissa Kuhl and Jodie for making fly food for us every week to maintain our stocks, and Zack Drum for his reliable efforts as a work-study assisting in making up solutions, scrambling data, etc.

I would especially like to thank members of the University of Denver Biology Department for their support and guidance, particularly Randi Flageolle, Kristin Andrud, and Angie Hebel. Also: my fellow graduate student, Katherine Nesler, for her immeasurable help with procedures, suggestions, and moral support.

Finally, I would like to thank the members of my committee: Dr. Joe Angleson, Dr. Todd Blankenship, and Dr. Michelle Knowles for their guidance in shaping this project, and Dr. Scott Barbee for inviting me into his lab to design and work on this project, and offering me the opportunity to pursue this research.

Table of Contents

List of Tables

List of Figures

Chapter One: Introduction

Chapter 1.1.: Translational Regulation: The Key to Long-Term Memory and Learning

There is a philosophy in science that form fits function. Every structure exists for a purpose, and is structured the way it is in order to fit that function for the overall benefit of the organism. Though modern understanding of learning and long-term memory mechanisms is still somewhat limited, evidence dating back decades suggests that the structure of the synapse underlies learning and long-term memory processes (Davis, 1993; Heisenberg et al., 1985; Bailey and Chen, 1983). Synaptic stimulation triggers protein synthesis-dependent synaptic growth and structural modifications (Schwartz et al., 1971; Bliss and Lomo, 1973; Matsuzaki et al. 2004), and dysregulation of this synaptic remodeling is correlated with neurological diseases (Steele et al., 2014; Kim et al., 2013; Rage et al., 2013; Morris et al., 1990). Given the requirement for new protein synthesis in this model, and the rapidity with which modifications begin to occur, researchers turn to translational regulation as the key to learning and long-term memory processes (Mikl et al., 2010).

Chapter 1.2: The Role of Ribonucleoproteins in Long-Term Memory and Learning

Ribonucleoprotein complexes (RNPs) are conglomerates of RNAs and proteins, which can include components of the microRNA (miRNA) pathway, Processing Bodies

(P-bodies), ribosomes and spliceosomes, and much more (Weil et al., 2012; Staley and Woolford, 2009; Dostie et al., 2003). Given their diverse structures, RNPs can act as chaperones to mediate mRNA folding, translational repression, or degradation (Lorsch, 2002; Fritzsche et al., 2013; Sheth and Parker, 2003). Special subsets of RNPs exist in neurons and perform similar functions. Ergo, these complexes are the subject of great speculation as potential mediators of learning and long-term memory disorders (Sleeman, 2013). For the purposes of this study, the focus on RNPs is restricted to their role as potential mediators of mRNA translational repression and decay.

Chapter 1.3: The Role of microRNAs in Synaptic Growth

One of the more recent discoveries in RNPs is the involvement of small RNAs known as microRNAs (miRNAs), and their pathway for translational repression: the RNA-induced Silencing Complex (RISC; Keene, 2010). When combined, these form a complex referred to as the miRISC (Nottrott et al., 2006). miRNAS are small endogenous 21-22 nucleotide sequences that are initially transcribed as a primary miRNA molecule in the nucleus, which includes a hairpin loop and excess sequence on each end (Moss, 2002; see Figure 1). From there, the primary transcript is processed into a pre-miRNA sequence by the enzyme Drosha, which cleaves off any sequence surrounding the hairpin loop, and then the hairpin loop is exported from the nucleus by Exportin-5 to the cytoplasm (Han et al., 2004; Yi et al., 2003). Dicer then cleaves off the hairpin loop and processes the sequence to form a 21-22 nucleotide duplex (Bernstein et al., 2001). One strand of the duplex associates with the RISC and base-pair matches to its target mRNA sequence to induce translational silencing when the base-pair match is imperfect, or

degradation in the presence of perfect base-pair complementarity (Hammond et al., 2000; Hammond, 2005; Filipowicz et al., 2005). The RISC is composed of Dicer, Argonaute proteins, RNA-binding proteins, and other components that mediate translational repression (Chu and Rana, 2006).

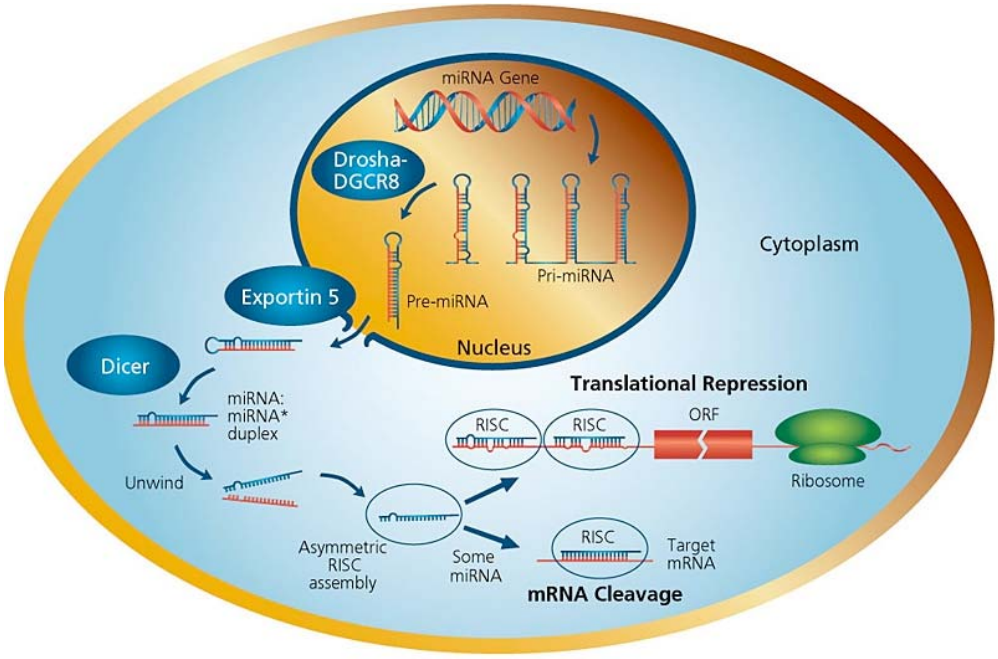

Figure 1: The miRNA Process: From Transcription to Translational Regulation

The image above is from the Sigma-Aldrich miRNA Introduction webpage: http://www.sigmaaldrich.com/life-science/functional-genomics-and-rnai/mirna/learning-center/mirna-introduction.html. It illustrates the transcription and processing of miRNAs from primary transcripts to mature sequences associated with the RISC to induce translational repression or degradation of mRNA targets. Copyright 2014, permission requested.

miRNA mis-expression can lead to dysregulation of target mRNAs. Ergo, miRNAs are implicated in neuronal diseases such as Alzheimer's Disease (Garza-Manero

et al., 2013) and epilepsy (Gorter et al. 2014). miRNAs affect synaptic growth and maturation by selectively targeting the mRNAs of proteins involved in synaptogenesis (Siegel et al., 2011; Olde Loohuis et al., 2012; Nesler et al., 2013; Sun et al., 2013). To understand their role in development, a key first step is to analyze the abundance of these molecules at different stages of development in order to better understand how miRNA expression contributes to development. Part of this study will investigate the differential expression of miRNAs in the *Drosophila* larval CNS and adult CNS for the purposes of guiding us to finding the most important miRNAs involved in synaptic development between the larval and adult stages.

Chapter 1.4: The Role of the Fragile-X Mental Retardation Protein in Synaptic Growth

RNPs are known to be comprised of components of the miRNA pathway, as well as numerous RNA-binding proteins, including the Fragile-X Mental Retardation Protein (FMRP), (Kanai et al., 2004; Höck et al., 2007). FMRP is so named because of its relationship to the human disease known as Fragile-X Syndrome (FXS). FXS is phenotypically characterized by facial dysmorphism, and macroorchidism, and is strongly correlated with autism-spectral social and behavioral disorders (Bardoni et al., 2000; Maurin et al., 2014; Reddy, 2005; Hatton et al., 2006; Hagerman et al., 2010). It is the leading cause of genetically inherited mental retardation in males (McLennan et al., 2011), caused by a genetically inherited expansion of the CGG trinucleotide repeat domain preceding the gene *Fmr1* (Verkerk et al., 1991). Expansion of this trinucleotide to repeats above 200 leads to hypermethylation in the non-coding region upstream of *Fmr1*, leading to transcriptional silencing of FMRP (Pieretti et al., 1991; Lightbody and

Reiss, 2009). Absence of FMRP leads to increased numbers of dendritic spines in the brain that are characteristically elongated and thin, reminiscent of immature dendritic spines in both *Fmr1* knock-out mice, as well as humans with FXS (Bakker et al., 1994; Irwin et al., 1999; Irwin et al., 2000); this structural abnormality is thought to underlie the cognitive impairments associated with the disease (Loesch et al., 2004). Therefore, understanding the mechanisms by which FMRP normally inhibits this synaptic overgrowth is key to revealing the pathology and potential therapeutic targets of FXS.

Chapter 1.5: The Fragile-X Mental Retardation Protein is a Translational Repressor: The Molecular Theory of Fragile-X Syndrome

FMRP contains RNA-binding domains, including the RGG motif as well as two KH-homology domains (Kiledjian and Dreyfuss, 1992; Siomi et al., 1993a). It is an RNA-binding protein, and point-mutation of one of the KH-homology domains alone is sufficient to induce Fragile-X Syndrome in humans, suggesting the RNA-binding property of FMRP underlies its effects on cognition (Ashely et al., 1992; Siomi et al., 1993b; de Boulle et al., 1993; Siomi et al., 1994). FMRP acts as a translational repressor and its absence results in increased abundance of proteins related to synaptic growth (Laggerbauer et al., 2001; Li et al., 2001). These proteins are most often synthesized under the metabotropic Glutamate Receptor (mGluR) pathway, where activation of mGluR1 and mGluR5 by synaptic stimulation induces local mRNA translation and thus, synaptic growth associated with plasticity (Weiler and Greenough, 1993). This association of FMRP with proteins linked to the mGluR pathway has led to the mGluR Theory of FXS (See Figure 2; Dölen et al., 2007). Briefly, Figure 2 illustrates the mGluR Theory of FXS derived from a previously-published figure (Penagarikano et al., 2007).

Under normal conditions, local pools of mRNAs are present at the synapse. Stimulation of mGluRs 1 or 5 in mammals leads to local translation of some of these mRNAs, while FMRP represses the translation of others. In the absence of FMRP (as in the case of FXS), stimulation leads to universal translation of the local pool of mRNAs, including those that would normally be translationally repressed by FMRP, leading to overproduction of proteins responsible for synaptic growth, thus inducing the synaptic overgrowth phenotype of FXS. In *Drosophila*, only two mGluRs exist: DmGluRA and DmGluRB, but inhibition of these receptors in flies lacking FMRP imitates the phenotypic effects seen when mGluRs 1 and 5 in mammalian models lacking FMRP are blocked (McBride et al., 2005).

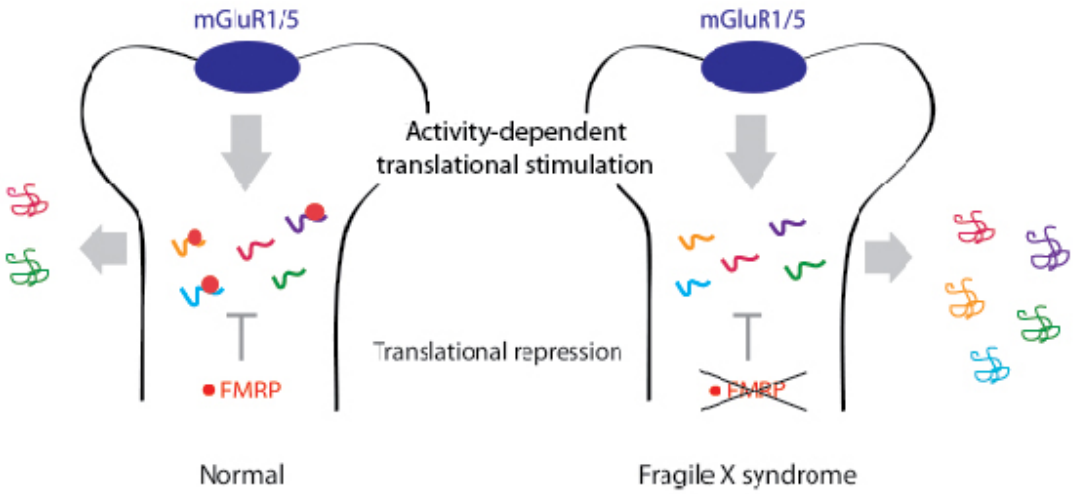

Figure 2: The mGluR Theory of Fragile-X Syndrome

This image is derived from Penagarikano et al. (2007), and depicts the metabotrophic Gluatamate Receptor Theory of Fragile-X Syndrome, whereby synaptic stimulation of mGluRs 1 or 5 induces translation of local pools of messenger RNAs at the synapse, and in the absence of FMRP, this leads to translation of targets that would normally be repressed. Copyright 2007 by Copyright Clearance Center, used with permission.

Part of the intention of this research is to use *Drosophila* as a model to reveal the pathology mechanisms of FXS. The *Drosophila* neuromuscular junction (NMJ) is an excellent model for studying neuronal function because it is accessible, easily manipulable due to simple genetics, and the synapses are glutamatergic, and thus present similar mechanisms to synapses in the mammalian central nervous systems (Collins and DiAntonio, 2007). The *Drosophila* model of FXS, induced by deletion or mutation of the gene *Dfmr1*, recapitulates the synaptic overgrowth reminiscent of the human disease. Additionally, flies with FMRP mis-expression exhibit altered circadian behaviors that mimic sleep problems in humans with FXS (Bakker and Oostra, 2003). Thus, *Drosophila* is a widely-accepted model for investigating FXS.

Chapter 1.6: The Fragile-X Mental Retardation Protein Interacts with Microtubule-Associated Protein 1B and Its *Drosophila* Homolog Futsch

Among the interactions of FMRP, one of the best-known and well-studied is its interaction with the microtubule-associated protein 1B (MAP1B). *MAP1B* and its *Drosophila* homolog *Futsch* mRNAs immunoprecipitate with FMRP, and FMRP overexpression is directly correlated to decreased expression of these respective proteins, as well as a decrease in synaptic growth. Similarly, under-expression of FMRP up-regulates MAP1B and Futsch expression, and correspondingly, synaptic growth (Lu et al., 2004; Zhang et al., 2001). Thus, FMRP is presumed to bind to the *MAP1B/Futsch* mRNA in order to prevent translation under normal conditions, and in the absence of FMRP, MAP1B dysregulation causes the synaptic overgrowth characteristic of FXS.

Given the clear association of FMRP with MAP1B, and the role of MAP1B in axonal growth (Mack et al., 2000; Lucas et al., 1998) one of the most important goals in

revealing FXS pathology using *Drosophila* as a model is to identify where and how FMRP binds to the *Futsch* mRNA. FMRP is known to bind to secondary and tertiary RNA structures such as the loop-loop pseudoknot, also known as the "kissing complex" (Darnell et al., 2005), and the G-quartet (Darnell et al., 2001). Although specific G-quartets are difficult to identify, there are several sites for potential G-quartets within the *Futsch* mRNA that are candidate sites for FMRP binding and repression. This study will investigate FMRP binding to a *Futsch* reporter.

Chapter 1.7: The Fragile-X Mental Retardation Protein Associates with the microRNA Pathway

In addition to FMRP's role as an RNA-binding protein, part of its association with RNPs involves association with components of the RNA Induced Silencing Complex (RISC), and the miRNA pathway. FMRP co-immunoprecipitates with RISC component Argonaute-2 (Ago2; Caudy et al., 2002), miRNA components Dicer (Ishizuka et al., 2002) and Argonaute-1 (Ago1) in *Drosophila*, and the mammalian homologue of Ago1, EIF2C2. Further, knockdown of Ago1 in *Drosophila* inhibits FMRP's ability to induce a rough-eye phenotype in flies when overexpressed in that tissue, implicating the miRNA pathway as a necessary component for FMRP function (Jin et al., 2004). FMRP has been shown to specifically immunoprecipitate with miRNAs (Edbauer et al., 2010). Thus, this research will investigate the potential interaction between FMRP and miRNAs to induce translational repression of mRNAs involved in synaptic growth.

We propose a model whereby FMRP binds to its target mRNAs using its RNA-binding domains, and then recruits the miRISC to that mRNA to induce translational repression (see Figure 3).

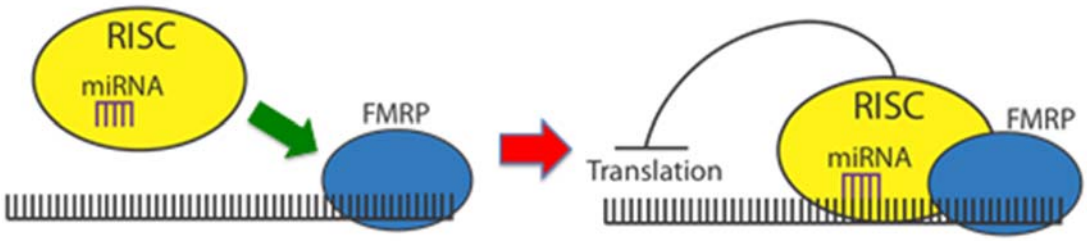

Figure 3: Proposed Model for FMRP Interaction with the miRNA Pathway

Above demonstrates the hypothetical model we propose for FMRP interaction with the miRNA pathway for the purposes of FMRP-mediated translational repression of mRNAs associated with synaptic growth. FMRP binds directly to the mRNA, and recruits the miRISC, which then binds to the mRNA by miRNA base-pair matching to the target, leading to translational repression.

Chapter 1.8: The Role of Processing Bodies in Synaptic Growth

Neuronal RNPs are composed not only of RNA-binding proteins and components of the miRISC, but also components of other conglomerates such as P-bodies. P-bodies include protein components such as Dcp1, Dcp2, Xrn1 (Coller and Parker, 2004), Staufen, CCR4, Me31B, Trailerhitch, and HPat (Eulalio et al., 2007). Homologues for many of these components can be found together in yeast, *Drosophila*, and mammalian cells (Hillebrand et al., 2007). P-bodies contain mRNAs and can serve several purposes for these mRNAs: transport (Krichevsky et al., 2001), degradation (Sheth and Parker, 2003), or translational repression. P-bodies interact physically with FMRP (Barbee et al., 2006; Oh et al., 2013), as well as the miRISC (Chan and Slack, 2006). Given the role of both FMRP and miRNAs as translational repressors, their interaction with P-bodies suggests that these components may act in concert to regulate translation of target mRNAs. This research will investigate the potential interactions between FMRP and P-

body components, specifically Me31B, Twin (*Drosophila* homolog of CCR4), HPat, and Dcp1.

Each component of P-bodies plays a different role in regards to mRNA targets. Me31B is the *Drosophila* homolog of mammalian Rck, a DEAD Box helicase that acts as an enhancer of mRNA decapping (de Valoir, 1991). Me31B co-localizes with FMRP in embryos (Monzo et al., 2006) and co-immunoprecipitates with FMRP and other P-body components in *Drosophila* head extract. When Me31B expression is diminished, it ameliorates the rough-eye phenotype induced by FMRP overexpression in that tissue, suggesting Me31B may mediate the function of FMRP (Barbee et al., 2006). In contrast, CCR4 (Twin in *Drosophila*) is a primary and essential component of the deadenylation complex in *Saccharomyces cerevisiae* (Behm-Ansmant, 2006; Daugeron et al., 2001; Tucker et al., 2001), *Drosophila*, (Temme et al., 2004), and humans (Yamashita et al., 2005). It associates in a complex with NOT1 and CAF1 for the purposes of deadenylating mRNAs prior to degradation (Temme et al., 2010). Genetic knockdown of Twin by itself produces a synaptic overgrowth phenotype at the *Drosophila* NMJ, which is exacerbated by simultaneous knockdown of HPat (Pradhan et al., 2012). HPat is involved in the 5' to 3' mRNA decay pathway and is an activator of decapping. Its role and its association to P-bodies are highly conserved in yeast, flies, and humans (Marnef and Standart, 2010). HPat acts as a negative regulator of synaptic terminal growth at the *Drosophila* NMJ (Pradhan et al., 2012). Finally, Dcp1 is the enzyme responsible for mRNA decapping and acts in concert with its co-enzyme Dcp2. Dcp1 is essential for miRNA-mediated gene

silencing (Rehwinkel et al., 2005). Ultimately, all of these P-body components work in concert to transport, degrade or repress mRNA targets.

Chapter 1.9: Goals For This Study: Identifying Roles for RNP Components in Synaptic Growth

Altogether, the goal of this study is to investigate the interactions and overall roles of components of neuronal RNPs for the purposes of affecting synaptic growth at the *Drosophila* NMJ. The abundance of miRNAs at the *Drosophila* CNS at different developmental stages suggests it will be important in the future to analyze roles of miRs -315, -275, and -11, as well as the miR-9 family in synaptic development. Testing and identification of real targets of these miRNAs from lists of predicted targets with known roles in synaptic growth is key to furthering our understanding of how these small molecules contribute to synaptic development.

FMRP is known to interact with components of the miRNA pathway and P-bodies, as well as the *Futsch* mRNA. This investigation elucidates the nature of some of those interactions involved in mediating FMRP's function as a repressor of synaptic overgrowth by demonstrating that some of the most larvally-enriched miRNAs (miR-315 and the miR-9 family) repress the reporter of a published and presumed FMRP target, *Futsch*. Although FMRP has been shown to regulate Futsch expression *in vivo*, our results indicate that FMRP does not bind to a *Futsch* reporter to repress translation *in vitro*, nor does FMRP interact in a physical complex with the miRNAs that do repress a *Futsch* reporter *in vitro*.

The roles and interactions of P-body components is also elucidated. FMRP interacts physically and genetically with components of P-bodies that, in some cases,

leads to a change in the number of boutons at the NMJ. P-body components Me31B, Twin, and HPat co-localize with FMRP in cultured neurons, and P-body components Me31B, HPat, and Dcp1 co-immunoprecipitate with FMRP in cultured cells. Some of these P-body components clearly play their own role in regulating synaptic growth, but also enhance the effects of loss of FMRP at the NMJ. Loss of FMRP and either Twin or HPat leads to a significant increase in the number of boutons at the NMJ, suggesting an interaction between FMRP and these P-body components that affects synaptic growth.

Chapter Two: Materials and Methods

Chapter 2.1: Differential Expression of miRNAs

RNA Isolation

For the RNA isolation from each of adult and larval brains, more than 100 total brains were dissected out by 3 separate individuals, cleared of any structures other than the optic lobes and ventral ganglia, and inserted into 333 µl of Trizol Reagent (Ambion). Each of the 3 tubes generated by these individuals were then homogenized using a Kontes Pellet Pestle Motor, then allowed to sit in Trizol for 5 minutes incubating to complete lysis, and pooled. 200 µl of chloroform was added to the tube and mixed by hand-shaking for 15 seconds. The tube was then incubated for 2.5 minutes at room temperature and centrifuged for 15 minutes at 12,000 x g and 4˚C. The aqueous (top) layer was removed and placed into a new RNase-free 1.5 mL conical tube, and 0.5 µl of 20 µg/µl glycogen was added and mixed. 500 µl 100% isopropanol was then added and mixed, and the samples were incubated at room temperature for 10 minutes, then centrifuged at 12,000xg at 4˚C for 10 minutes. The isopropanol was gently removed using a micropipettor and discarded. 1 mL of RNase-free 75% ethanol was added to the RNA pellet; this was mixed by briefly vortexing, then placed at -20˚C.

RNA Sample Quantity and Quality Analysis

RNA samples were centrifuged and ethanol was removed from the pellets. The pellets were then dried and resuspended in 50 µl RNase-free water. Small aliquots were saved for analysis and the remainder was flash-frozen on liquid nitrogen and stored at -80˚C. RNA samples were then analyzed using a NanoDrop-1000 version 3.5.2 spectrophotometer and then using the Experion Standard Sensitivity RNA Analysis Kit (BioRad). The primary samples were then submitted to the Genomics and Microarray Core at the University of Colorado Denver for Next-Generation Sequencing.

RNA-Sequencing Analysis

Raw RNA-Sequencing reads were manipulated and analyzed using the Galaxy program at UseGalaxy.org (Giardine et al., 2005; Blankenberg et al., 2010; Goecks et al., 2010). Files were converted to FastQSanger format using the NGS: QC and Manipulation FastQ Groomer tool. Reads were then trimmed of the adapter sequence TGGAATTCTCGGGTGCCAAGG using the NGS: QC and Manipulation Clip tool, and filtered for quality with a minimum quality score of 20, a maximum quality score of zero, a minimum size of 18 base-pairs, and a maximum size of 27 base-pairs for non-paired-end reads allowing for zero base-pairs outside of the quality range.

Trimmed sequences filtered for quality were next uploaded to the MPI-HLR: miRNA Identification miRNA pipeline (MIRPIPE; Kuene et al., 2014) using the FTP server FileZilla. MIRPIPE combined clustered reads (isomiRs), mapped them to the miRBase database (Kozomara and Griffiths-Jones, 2014; Kozmara and Griffiths-Jones,

2011; Griffiths-Jones et al., 2008; Griffiths-Jones et al., 2006; Griffiths-Jones, 2004), and quantified the number of reads.

To ensure that miRNAs were not overrepresented merely from obtaining more reads in a particular tissue, each quantity was normalized by dividing the number of reads of each miRNA by the total number of reads per tissue, then multiplying by 10^6 to translate each quantity to reads per million. The reads per million in adult tissue were then subtracted from the reads per million in larval tissue to find absolute enrichment for each miRNA in larval CNS compared to adult brain. The top 15 most abundantly enriched miRNAs in the larval CNS were then further processed by dividing the reads per million in larval CNS by the reads per million in adult brain to show fold-enrichment.

For the purposes of target analysis, miRNA families were grouped together with their number of reads, because these miRNAs have the same seed region binding sequence and are therefore predicted to target the same mRNAs (Lucas and Raikhel, 2013). Lists of potential targets for the top 10 most enriched miRNAs/ miRNA families were then compiled using the program TargetScanFly version 6.2 (Lewis et al., 2005; Ruby et al., 2007; Bartel et al., 2007; Kheradpour et al., 2007). Target lists were then processed using the cluster annotation function from the Database for Annotation, Visualization, and Integrated Discovery (DAVID; Huang et al., 2009a; Huang et al., 2009b) to analyze potential functional roles for these highly-enriched miRNAs. Those miRNAs whose targets showed the greatest enrichment in functional annotation clusters attributed to neuronal growth were analyzed further. The lists of compiled predicted

targets for these miRNAs were compared for overlap in Microsoft Excel, then these lists of overlapping targets were processed with the DAVID Bioinformatics program.

Chapter 2.2: Interaction Between FMRP and miRNAs to Target *Futsch*

In Silico Analysis

Leslie Rozeboom initially performed analysis using miRNA target prediction algorithm, TargetScanFly at http://www.targetscan.org/fly_12/ (Release 5.1 Friedman, et al. 2009). She input "Futsch" as the FlyBase symbol or ID and found that the miR-9 family and miRs -315, -963, and -976 were predicted to bind to the *Futsch* 3'UTR. Of these, only miRs -9A, -9B, -9C, and -315 were found by microarray analysis and qRT-PCR to be expressed in the larval CNS (Rozeboom, 2011).

S2 Cell Maintenance and Care

SL2 cells obtained from the *Drosophila* RNAi Screening Center were thawed from a new vial and passaged every 3-7 days as per the instructions found at http://www.flyrnai.org/DRSC-PRC.html. Briefly, a 1 mL vial of frozen cells was thawed rapidly using room-temperature media and transferred to 4 mL fresh Complete Schneider's Media in a 25 cm^2 culture flask (CellTreat). Cells were allowed to adhere for 2 hours prior to gently removing the media and adding back 5 mL fresh media. Cells were then allowed to grow for 1-2 weeks to reach 100% confluence. After that point, cells were allowed to grow to 70%-100% confluence before passaging 3 mL mature cells into 12 mL fresh Complete Schneider's Media treated with 0.2% Fungizone (Gibco) in a 75 cm^2 culture flask (CellTreat) every 3-7 days as needed. Cells were loosened from the adherent surface by banging the flask against the lab bench prior to each passage.

4 days prior to an experiment, cells were passaged. The SL2 cell population was split in a 250 mL suspension flask (CellTreat) 24 hours prior to seeding using Complete Schneider's Media. The day of transfection, cell density was calculated using a Phase Counting Chamber (Hausser Scientific). The appropriate volume of cells was then removed from the flask and centrifuged in a 50 mL conical tube at 2,500 rpm for 3 minutes. The media was decanted and the pellet was resuspended in 15 mL Phosphate Buffered Saline (PBS). The cells were centrifuged again at 2,500 rpm for 3 minutes, and the supernatant was decanted. The cells were resuspended in an appropriate volume of Complete Schneider's Media to obtain 2 x 10^6 cells in 1.6 mL media for a 6-well plate, or 1 x 10^6 cells in 0.8 mL media for a 12-well plate. 1.6 mL of resuspended cells were seeded into each well of a 6-well plate, or 0.8 mL of resuspended cells in each well of a 12-well plate.

Plasmid Design for S2 Cell Dual-Luciferase Experiments

Leslie Rozeboom designed each of the constructs for inserting miRs -9A, -9B, -9C, -315 into S2 cells, as well as the reporter Firefly Luciferase-*Futsch* 3'UTR. Briefly, the *Futsch* 3'UTR was PCR-amplified from a BAC vector from the *Drosophila* Genomics Resource Center (DGRC), then cloned into pENTR using to TOPO Reaction for Gateway system (Invitrogen), and then inserted into pAc5.1-FireflyLuciferase-Invitrogen Gateway Reading Frame Cassette A using the LR Recombination from the Invitrogen Gateway system. The Renilla Luciferase vector was generated similarly, with an SV40 3'UTR in place of the Gateway Reading Frame Cassette. Each miRNA expression vector was generated by PCR-amplifying 100-200 base-pairs upstream and downstream of the pre-

miRNA sequence found on miRBase.org from *w1118* larval genomic DNA and inserting into pENTR using the TOPO Reaction for Gateway system (Invitrogen), and then inserted into pAc5.1: Gateway Reading Frame Cassette A using LR Recombination from the Invitrogen Gateway system. To generate the Empty Vector used for a negative control, the Reading Frame Cassette was cut out of the pAc5.1-Reading Frame Cassette A vector and the vector was re-ligated together (Rozeboom, 2011).

Reporters for the miR-9 and miR-315 sponges were designed by PCR-amplifying the miR-9 sponge from pBSTM the miR-315 sponge from pBSTM using primer sequences: 5'-CACCCTCACTAAAGGGAACAAAAGC-3' and 5'- CGGGCC CGGGATCCGATA-3'. Each sponge construct was then cloned into pAc5.1-Reading Frame Cassette A for expression of the sponge constructs, and pAc5.1-Firefly Luciferase-Reading Frame Cassette A for a sponge reporter, using the Gateway Cloning System (Invitrogen).

An FMRP overexpression vector was generated by PCR-amplification of *DFmr1* from cDNA plasmid LD09557 (DGRC) using primer sequences 5'-CACCATGGAAGATCTC CTCGTGGA-3' and 5'-TTAGGACGTGCCATTGACCA-3' followed by insertion into pENTR and subsequently into pAc5.1-Reading Frame Cassette A using the Gateway System (Invitrogen).

The *Futsch* sequence was obtained from Flybase.org (St. Pierre et al., 2014). All of the *Futsch* coding sequence fragment reporters were generated using the primers listed in Table 1. Each fragment was PCR-amplified from *w1118* larval genomic DNA, then

inserted into pAc5.1-Firefly Luciferase-Reading Frame Cassette A using the Gateway System. Nathan Boin performed most of these cloning reactions.

Table 1: PCR-Amplification of Futsch Coding Sequence Fragments

Futsch CDS Fragment Name	Forward PCR Primer	Reverse PCR Primer
A	5'-CACCGATTCCTCTCCTGGGACGTTT-3'	5'-CCTTCCGGTTGTTGGCC-3'
B	5'-CACCTGCTCGAGTCCAAGCAGC-3'	5'-TTGGCTGATTTGGGTGGC-3'
C	5'-CACCATCCGATGATGAGCTTCCTG-3'	5'-AAGGAGATTTTTCGGCCACT-3'
D	5'-CACCAGTGGCCGAAAAATCTCCTT-3'	5'-CCTTCAAAACTTGCGGTGAT-3'
E	5'-CACCATCACCGCAAGTTTTGAAGG-3'	5'-TGGTCTGGAAACTTCCTTGG-3'
F1	5'-CACCATCACAGGCAGCCATAAAGC-3'	5'-TCGCCTTGATTCTTCTTTGG-3'
F2	5'- CACCTGCAGAAAGTGTTCAGGACG-3'	5'- AGGCTGTATGCCCAGTATCG-3'
G	5'-CACCAGGCGGAGAGTATCAAGGGT-3'	5'-TTCAGTGCTGAAGGCTTCCT-3'
H	5'-CACCAGCCACTAAGTCGGCCGA-3'	5'-CTGCATTTCCAGAGACTTAAGCTC-3'
I	5'-CACCACTCGCAGGAGCAG-3'	5'-CCAACTCCTTGTCCTCCCAT-3'
J	5'-CACCAGGTCACCATTATACCTACGTACGAC-3'	5'-CTAGAACTCTAGGCGGTAGGCC-3'

Fragments column of the *Futsch* coding sequence labeled according to the left column were PCR-amplified from *w1118* genomic DNA using the primers listed, then inserted into pENTR then pAc5.1-Firefly Luciferase using Gateway cloning.

The *Futsch* 5'UTR reporter was generated using primer sequences 5'-GCATTCGGTACCTCAGCTGTTCGGCTCCGCTT-3' and 5'-GCATTCGAATTCTTGGACGTGGATTAGCTGTGC-3' from *w1118* larval genomic DNA, cut with restriction enzymes KpnI and EcoRI then cloned into pAc5.1-Firefly Luciferase-*Futsch* 3'UTR upstream of Firefly Luciferase using standard cloning techniques.

All plasmid sequences were verified by sequencing from the University of Colorado DNA Sequencing and Analysis Core.

Dual Luciferase Assay

Transfection mixtures were prepared using the Qiagen Effectene Transfection Reagent Kit according to the instructions from Qiagen. Each construct for the DNA mixture was prepared using an endotoxin-free maxi-prep (Qiagen or Promega). DNA mixtures were prepared as follows: 0.1 μg Firefly Luciferase-Target constructs, 0.4 μg Renilla Luciferase, 0.5 μg miRNA overexpression or sponge construct, empty vector control, or FMRP expression construct, per transfection for a 6-well experiment. For a 12-well experiment, each of these quantities was cut in half. DNA mixtures were prepared in triplicate in a total volume of 300 μl EC Buffer. To each mixture, 24 μl Enhancer was added for a 6-well experiment, or 12 μl Enhancer for a 12-well experiment, and mixed by flicking. Each mixture was then incubated for 3 minutes at room temperature. Next, to each mixture, 30 μl Effectene reagent was added for a 6-well experiment, or 15 μl Effectene reagent for a 12-well experiment, and mixed by vortexing for 10 seconds. The mixtures were incubated at room temperature for 7 minutes, during which they were transferred to a sterile hood containing the seeded 6-well or 12-well plates. At the end of the incubation, 3 mL Complete Schneider's Media was added to each mixture for a 6-well experiment, or 1.5 mL Complete Schneider's Media for a 12-well experiment, and mixed by pipetting up and down. 1.1 mL of each mixture was added drop-wise to each of 3 wells (biological triplicate) containing the SL2 cells on the 6-well plate while swirling the plate; half the volume for a 12-well experiment.

Each 6-well or 12-well plate was placed in a lidded plastic box to prevent contamination of the cells, and each box was in turn placed in an incubator at room temperature for 72 hours. At the end of the 72-hour incubation, cells were scraped from the bottom of the plate using a p1000 micropipettor tip. The cells from each well were then pipetted up and down to thoroughly and homogeneously resuspend them. Next, 75 µl of resuspended cells from each well of the 6-well or 12-well plate were added to each of 3 separate wells (technical triplicate) of a 96-well plate (CoStar). To each of these wells was then added 75 µl Dual-Glo Luciferase Reagent from the Dual-Glo Luciferase Assay System (Promega). This was added as simultaneously as possible using a multi-channel micropipettor. The plate was allowed to incubate for 10 minutes in a foil-covered box, as the reagent is light-sensitive. The 96-well plate was then placed in a Synergy HT microplate reader and luminescence was quantified as Firefly Luciferase luminescence. Next, 75 µl Dual-Glo Stop and Glo Reagent from the Dual-Glo Luciferase Assay System (Promega) was added to each cell-containing well of the 96-well plate, and the plate was immediately placed into the microplate reader again, this time to quantify Renilla Luciferase luminescence.

Normalized FLuc/RLuc ratios were determined by an Excel spreadsheet I designed. Briefly, a Firefly Luciferase to Renilla Luciferase (FLuc/RLuc) ratio was generated for each well by dividing the raw FLuc value obtained from the microplate reader by the raw RLuc value obtained from the microplate reader. Next, an average was taken for each set of 3 technical replicates (each biological replicate) by using the "Average" function in Excel. The ratio for each experimental set was then normalized to

the empty vector control by dividing each averaged biological replicate FLuc/RLuc ratio by an average of all 3 biological replicates of the empty vector control. Statistics were calculated using ANOVA in Prism.

Protein Extraction

For the protein extraction from fly head extract followed by qRT-PCR, *w1118* flies were aged 3-5 days, then flies were anesthetized with carbon dioxide gas, poured into a tube on ice, then frozen on liquid nitrogen for preservation of tissue. The tube containing frozen flies was then vortexed 15-30 seconds, then poured onto the top of two stacked mesh filters previously frozen with liquid nitrogen. The filters were tapped for up to 30 seconds. Wing, leg, and other small particles fell through both filters, while heads remained between the first and second filter, and the large bodies remained on the top of the first filter. All heads from between the first and second filter were funneled into a frozen 2 mL round-bottom tube, then homogenized using a TissueRuptor (Qiagen) in Buffer TBT (Dokudovskaya et al., 2006) containing Superase RNase Inhibitor (Invitrogen), and antifoam B (Sigma), and Solution P as indicated in Oeffinger et al. (2007), which includes PMSF, which we substituted with EDTA-free protease inhibitor tablets (Roche), and Pepstatin A (Fisher Scientific). Homogenate was centrifuged at 3,000 x g for 3 minutes and the supernatant was flash-frozen on liquid nitrogen and stored at -80°C to be used for downstream applications.

Immunoprecipitation Followed by qRT-PCR

All materials for the following procedure were kept on ice when not at 4°C on a rotator. All materials and reagents were RNase-free and all work was performed in an RNA hood sprayed down with RNase-Away (Molecular BioProducts) and dried.

Immunoprecipitation

Protein G-coated magnetic beads (Invitrogen) were washed 3 times with 1X PBS plus 0.2% Tween, and then half of these beads were blocked with 100 µg/mL yeast tRNA diluted in 1X PBS + 0.02% Tween. Half of these pre-blocked beads were applied to three extracts, each containing 100 µg of *w1118* protein extract, to pre-clear the protein samples. The other half of the pre-blocked beads were used downstream for the "beads only" immunoprecipitation. Half of the unblocked Protein G-coated magnetic beads were incubated with antibody Mouse IgG (Invitrogen), and half with Mouse anti-DFmr1 (6A15; Abcam) for 10 minutes at 4°C, then blocked with 100 µg/mL yeast tRNA diluted in 1X PBS + 0.02% Tween for 30 minutes at 4°C. These beads were then washed 4 times with Buffer TBT containing 10 µg yeast tRNA, and each was then incubated with pre-cleared 100 µg of *w1118* protein extract for 2 hours at 4°C. The additional pre-cleared extract was incubated for 2 hours at 4°C with the pre-blocked beads that had not been incubated with antibody (described earlier). All beads were then washed 4 times with Buffer TBT and protein was eluted using 180 µl of 100 mM Glycine-HCl [pH 2.8]. 20 µl of 1M Tris [pH 7.5] was added to each tube of eluted protein to neutralize the pH before proceeding to RNA Isolation.

RNA Isolation from Eluted Extract

Samples were allowed to return room temperature. Next 60 µl chloroform was added to each sample; samples were mixed thoroughly, incubated for 2-3 minutes, then centrifuged at 12,000 x g for 15 minutes. The upper aqueous phase was transferred to a new tube, to which was added 1 volume of 100% ethanol. After mixing, each sample was transferred to an RNeasy spin column (Qiagen). RNA was then extracted using the RNeasy Mini Kit from Qiagen following manufacturer's instructions, and stored at -80°C for use in later qRT-PCR analysis.

qRT-PCR analysis

RNA was precipitated using an ethanol precipitation and the visualization agent GlycoBlue (Ambion). RNA was converted to cDNA using the Qiagen miScript Reverse Transcription for Quantitative Real-Time PCR Kit by following manufacturer's instructions. qRT-PCR was then performed on each extract using the miScript SYBR Green PCR Kit and miScript primer assays (Qiagen) for miRs -9A, -9B, -9C, -315, and small RNA U1 using two technical replicates per reaction in a 96-well plate. One replicate containing only water was included for each reaction as a negative control. PCR was performed on the iCycler Thermocycler (BioRad) and fluorescence was read by the iQ5 Multicolor RT-PCR Quantification System (BioRad) and quantified using the iQ5 Optical System Software version 1.2.

Chapter 2.3: Analyzing the Effects of miRNA Expression on NMJ Structure

Generation of Transgenic Fly Lines

Overexpression and Under-Expression Fly Lines for miRs -9A, -9B, -9C and -315

Using the Gateway Cloning System, Leslie Rozeboom inserted the same sequences used for overexpression of each of miRs -9A, -9B, -9C, and -315 into a pUASM-mCherry-RFB vector. These plasmids were sequenced, maxi-prepped using a Qiagen Maxi-Prep Kit, and sent to BestGene for insertion into fly lines and balancing.

Using the Gateway Cloning System, the same miR-9sponge(15x repeat) and miR-315 sponge(20x repeat) sequences used in S2 experiments were inserted into pUASM-mCherry-RFB, sequenced, maxi-prepped using the Promega Maxi-Prep Kit, and sent to BestGene for insertion into fly lines. The miR-315 sponge lines were balanced by BestGene. Due to a BestGene error, the miR-9 sponge lines were balanced by me. To do this, flies were first examined for a transgene on the sex chromosome, knowing that in the generation of flies we received, if a transgene was X-linked, females would express the transgene and not males. None of the lines contained an X-linked transgene. To balance the miR-9 sponge lines, I crossed males from each transgenic line, which expressed the *Mini-white* gene, to the BL 7199 (Bloomington) line, which expresses Kruppel/Curly-wing; Tubby-Stubble/Dichaete (Kr/CyO; TbSb/DI). Red-eyed, curly-wing, stubble adult offspring were isolated and back-crossed to the BL 7199 line again. Flies containing the transgene on the second chromosome would have red eyes, and could not be both kruppel and curly-winged, so if a line showed this, a male was isolated, and a virgin female with the mini-white and curly-wing phenotypes, and also TbSb/DI (when possible) for a single-pair mating to generate a stable double-balanced line. On the other

hand, flies containing the transgene on the third chromosome would have red eyes, and could not be both tubby-stubble and dichaete, so if a line showed this, a male was isolated, and a virgin female with the mini-white and tubby-stubble phenotypes, and also Kr/CyO (when possible) for a single-pair mating to generate a stable balanced (or double-balanced) line.

To perform analyses using more than one copy of a sponge transgene, double-miRNA sponge lines were generated. To do this, double-balanced miR-315 sponge lines were first generated by crossing males from the miR-315 sponge lines previously analyzed to BL 7199 virgin females. Male offspring expressing mini-white, curly wings, and stubble were isolated and back-crossed to BL 7199 virgin females. Offspring that were either transgene/CyO; TbSb/DI for transgenes on the second chromosome, or offspring that were Kr/CyO; transgene/TbSb for transgenes on the third chromosome were isolated. When transgenic lines were viable as homozygotes, the homozygotes were isolated. Single-pair mating for each double-balanced transgenic line were performed a to generate the following: Kr/CyO; UAS: mCherry-miR-315sp(20x)(Line 1)/TbSb, Kr/CyO; UAS: mCherry-miR-315sp(20x)(Line 2)/TbSb, and UAS: mCherry-miR-315sp(20x)(Line 6) on II; TbSb/DI.

To generate double-sponge lines, the following crosses were performed:

UAS: mCherry-miR-315sp(20x) (Line 6) on II; TbSb/DI x

Kr/CyO; UAS: mCherry-miR-315sp(20x) (Line 1) /TbSb,

UAS: mCherry-miR-315sp(20x) (Line 6) on II; TbSb/DI x

Kr/CyO; UAS: mCherry-miR-315sp(20x) (Line 2) /TbSb,

UAS: mCherry-miR-315sp(20x) (Line 6) on II; TbSb/DI x

Kr/CyO; UAS: mCherry-miR-9sp(15x) (Line 2) / TbSb

UAS: mCherry-miR-315sp(20x) (Line 6) on II; TbSb/DI x

Kr/CyO; UAS: mCherry-miR-9sp(15x) (Line 5) / DI

UAS: mCherry-miR-9sp(15x) (Line 1)/CyO ; TbSb/DI x

Kr/CyO; UAS: mCherry-miR-9sp(15x) (Line 2) / TbSb

UAS: mCherry-miR-9sp(15x) (Line 1)/CyO ; TbSb/DI x

Kr/CyO; UAS: mCherry-miR-9sp(15x) (Line 5) / DI

Non-kruppel, non-dichaete, curly-winged, stubble offspring were selected and mated. When possible, offspring with homozygous expression of a transgene were selected for single-pair matings. Otherwise, single-pair matings were performed with heterozygous-expression offspring.

Fly Crosses Performed for NMJ Analysis

For overexpression of miRs -9A, -9B, -9C, and -315, virgin female P{w[+mW.hs]=GawB}elav[C155] flies were crossed to males from each of the following lines: UAS: mCherry-miR-9A (Line 1)/Tm3Sb, UAS: mCherry-miR-9A (Line 2)/CyO, UAS: mCherry-miR-9B (Line 1)/ CyO, UAS: mCherry-miR-9B (Line 2)/Tm3Sb, mCherry-miR-9C (Line 1)/ CyO, UAS: mCherry-miR-9C (Line 3)/Tm3Sb, UAS: mCherry-miR-315 (Line 1)/CyO, UAS: mCherry-miR-315 (Line 2)/ CyO. Another overexpression experiment was performed by crossing males from the same miR-9 and miR-315 overexpression transgenic lines each to C380-Gal4 virgin females. In both

cases, larvae demonstrating overexpression of the transgene were isolated by examining them for mCherry expression using an Olympus SZX10 Research Stereo Microscope.

For under-expression of miRNAs, virgin female C380-Gal4 flies were crossed to males from the following transgenic fly lines: UAS: mCherry-miR-9sp(15x)(Line1)/CyO; TbSb/DI, Kr/CyO; UAS: mCherry-miR-9sp(15x)(Line 2)/TbSb, and Kr/CyO; UAS: mCherry-miR-9sp(15x)(Line 5)/DI. In both cases, larvae demonstrating expression of the transgene were isolated by examining them for mCherry expression using an Olympus SZX10 Research Stereo Microscope. Larvae displaying the Tubby phenotype were also selected against to avoid complications involving larval shape.

NMJ Analysis: Dissection, Staining and Imaging

NMJ analysis was performed on each cross first by vivisecting the larvae. This was done by pinning larvae at the posterior and anterior to a Sylgard plate in hemolymph-like 3 buffer (HL-3; Stewart et al., 1994), cutting the larvae open, removing the guts and CNS, then pinning each larva open at 2 points along either side of the mid-section. These preps were fixed for 20 minutes in 3.5% paraformaldehyde, washed 3 times for 10 minutes on a shaker with 1X PBS, then once with 1X PBS plus 0.1% Triton X-100. Preps were blocked for 1 hour at room temperature, then incubated with a 1:100 dilution (in block) of the primary antibody Mouse anti-Discs Large either at 4˚C overnight or for 2 hours at room temperature. Preps were then quick-washed twice with 1X PBS plus 0.1% Triton X-100, then 6 times for 10 minutes on a shaker. They were then incubated for 1 hour at room temperature with a 1:100 mixture (in block) of Goat anti-HRP_Dylight649

and 1:500 mixture of Goat anti-Mouse_AlexaFluor488. Preps were quick-washed twice with 1X PBS plus 0.1% Triton X-100, then twice for 10 minutes on a shaker. Finally, preps were rinsed for 10 minutes on a shaker with 1X PBS and retained in 1X PBS at 4˚C no more than a day until they could be mounted.

Preps were mounted onto slides by removing the pins and blotting the preps dry with a Kimwipe applied to the posterior end, then adding a drop of VectaShield (Vector Laboratories) containing DAPI to a glass slide and placing the preps gently on the slide. Each prep was covered with a glass coverslip and the coverslip was secured using clear nail polish. Preps were imaged on an Olympus FV1000 Scanning Confocal microscope at a 100X magnification. Fluoview software was used to distinguish fluorescence by coloring the 649 fluorescence with red, and the 488 fluorescence with green.

NMJ Analysis: Quantification of Boutons and Morphology Analysis

Images from each experiment were scrambled and blindly analyzed for the number of 1B and 1S boutons, terminal tips, etc. using the Cell Counter analysis function of the program ImageJ. Data were then compiled and analyzed in the program Prism for mean and standard error calculations.

For analysis of Bouton morphology, colored channels were separated in ImageJ and the red channel was used for morphology analysis. Boutons were circled using a hand-drawing tool, and the ROI manager was used to quantify various aspects of the circled areas, including Area, Roundness, and Feret's Diameter.

Chapter 2.4: Analyzing the Effects of P-Bodies and Their Interactions with DFmr1 on Synaptic Structure

For crosses investigating the interactions between FMRP and P-body components, or the role of P-body components themselves, see Table 2. Larvae were dissected, stained, and imaged as previously described (2.3 "NMJ Analysis: Dissection, Staining and Imaging").

Table 2: Genetic Fly Crosses Performed to Analyze the Role of P-Body Components In Affecting NMJ Structure		
Virgin Females	Males	Selection Markers
CantonS	*w1118 (Iso31)*	None
w1118 (Iso31)	*Pat1[Δ3]/Tm3SerGFP*	GFP
w1118 (Iso31)	*w1118; DFmr1[Δ113M]/TM6B, Tb[1]*	Tubby
w1118 (Iso31)	*w1118; DFmr1[Δ50M]/TM6B, Tb[1]*	Tubby
Pat1[Δ3]/Tm3SerGFP	*w1118; DFmr1[Δ113M]/TM6B, Tb[1]*	GFP, Tubby
Pat1[Δ3]/Tm3SerGFP	*w1118; DFmr1[Δ50M]/TM6B, Tb[1]*	GFP, Tubby
Pat1[Δ3]/Tm3SerGFP	*Pat1[Δ3]/Tm3SerGFP*	GFP
w1118; DFmr1[Δ113M]/TM6B, Tb[1]	*w1118; DFmr1[Δ50M]/TM6B, Tb[1]*	Tubby
w1118 (Iso31)	*Me31BΔ1, FRT40A/CyOGFP*	GFP
w1118 (Iso31)	*Me31BΔ2,FRT40A/CyOGFP*	GFP
w1118 (Iso31)	*y[1] w[67c23]; P{w[+mC]=GSV6}twin[GS12209] / Tm6C,Sb,Tb*	Tubby
w1118 (Iso31)	*y[1] w[67c23]; P{w[+mC]=GSV3}twin[GS8115] / Tm6C,Sb,Tb*	Tubby
w1118 (Iso31)	*dDcp1b53/CyOGFP; T3/Tm6**	GFP
w1118 (Iso31)	*W;FRTG13,Dcp1442P/CyOGFP*	GFP
w1118; DFmr1[Δ113M]/TM6B, Tb[1]	*Me31BΔ2,FRT40A/CyOGFP*	GFP, Tubby
w1118; DFmr1[Δ113M]/TM6B, Tb[1]	*y[1] w[67c23]; P{w[+mC]=GSV6}twin[GS12209] / Tm6C,Sb,Tb*	Tubby
w1118; DFmr1[Δ113M]/TM6B, Tb[1]	*W;FRTG13,Dcp1442P/CyOGFP*	GFP, Tubby
Me31BΔ2,FRT40A/CyOGFP	*Me31BΔ1, FRT40A/CyOGFP*	GFP
y[1] w[67c23]; P{w[+mC]=GSV6}twin[GS12209] / Tm6C,Sb,Tb	*y[1] w[67c23]; P{w[+mC]=GSV3}twin[GS8115] / Tm6C,Sb,Tb*	Tubby
W;FRTG13, Dcp1442P/ CyOGFP	*dDcp1b53/CyOGFP; T3/Tm6**	GFP

Fly crosses were performed as detailed above, and larval offspring were selected by selecting against the marker(s) indicated.

*To generate this fly line, I first had to generate a double-balancer line containing the larval marker GFP. To do this, I crossed males from the line Inversion/CyOGFP (Inv/CyOGFP) to virgin female BL 7199 Kr/CyO; TbSb/DI flies, isolated red-eyed males expressing curly-wings and stubble, and back-crossed these to BL 7199 virgin females. I performed a single-pair mating to get a stable line of Kr/CyOGFP; TbSb/DI flies. I then crossed virgin females of these flies to males from the existing dDcp1^{b53}/CyOGFP; T3/Tm6 line as described above.

Chapter 2.5: Expression of Tagged P-Body Components in S2 Cells

For expression of tagged P-body components in S2 cells, each component was cloned into the pAc5.1: V5-HisA using standard cloning techniques. See Table 3 for details.

Table 3: Cloning of P-Body Components into pAc5.1: V5-HisA

P-Body Protein	cDNA Used	Forward Primer	Reverse Primer	Restriction Enzymes
Me31B	LD21247	5'-GCATTCGCGGCC GCATGATGACTGAA AAGTTAAATTC-3'	5'-GCATTCTCTAG ATTTGCTAACGTTG CCCTCCT-3'	NotI, XbaI
Twin	LD18435	5'-GCATTCGGTACC ATGAAAGGCAATCA T-3'	5'-GCATTCGAATT CCCGGCGATTGAT CAGCCCG-3'	KpnI, EcoRI
HPat	RE36948	5'-GCATTCGCGGCC GCATGGATGACTCG TT TTTCGGC-3'	5'-GCATTCTCTAG AATCAATTTGATGC CTGGCTTC-3'	NotI, XbaI
Dcp1	GH04763	5'-GCATTCGGTACC ATGGCCGACGAGAG CATCA-3'	5'-GCATTCGAATT CTTGATATGTGGAG CTGGAGTCCAGC-3'	KpnI, EcoRI

Each P-body component was PCR-amplified from a cDNA from the *Drosophila* Genomics Resource Center (DGRC) listed using the primers listed, which did not include the stop codon for any of the sequences. Sequences were cloned into pAc5.1: V5-HisA from Invitrogen using the restriction enzymes listed to insert each sequence upstream and in-frame with the V5 and His tags. Constructs were verified by sequencing.

Chapter 2.6: Stable Expression of FLAG-HA-FMRP in S2 Cells

The vector pENTR: *DFmr1* had previously been generated (Chapter 2.2, "Plasmid Design for S2 Cell Dual-Luciferase Experiments"). Using the same Gateway Cloning

Technique, an LR Recombination reaction was used to insert the *DFmr1* sequence into the vector pAFHW from the *Drosophila* Genomics Resource Center (DGRC), in-frame with a 3x-FLAG, 3x-HA tag. Once the sequence was verified and overexpression of FMRP was tested by transfection into S2 cells using the Qiagen Effectene Transfection Reagent Kit, a stable-expression S2 cell line was generated.

To generate a stable-expression S2 line for permanent expression of pAFHW-*DFmr1*, 3.8 μg of pAFHW-*DFmr1* and 0.2 μg pCoBlast—a plasmid conferring cellular resistance to the eukaryotic cell antibiotic Blasticidin—(Invitrogen), were transfected into 1 x 10^6 S2 cells each of 2 wells in a 6-well plate (CoStar) using Effectene as described previously (Chapter 2.2 "Dual-Luciferase Assay"). Cells were allowed to grow for 72 hours, at which point, the media was gently siphoned from the cells, and cells were dislodged by roughly pipetting with fresh Complete Schneider's Media plus 12.5 μg/mL Blasticidin. Resuspended cells were transferred to a new 6-well plate and allowed to grow to optimal density over the course of 1-2 weeks. Cells were maintained by siphoning off media every 3-4 days and replacing with fresh media. Once cells had reach optimal density in a 6-well plate, they were transferred to a 25 cm^2 coated culture flask (CellTreat) and allowed to grow to optimal density again before transfer to a 75 cm^2 coated culture flask (CellTreat). At this point, some of the cells were frozen following protocols from the *Drosophila* RNAi Screening Center (DRSC), while others were tested for expression of the tagged FMRP.

Chapter 2.7: Overall Western Blot Procedures

Fly Head Extracts Preparation

Extracts from fly heads were prepared using Buffer TBT as described previously (Chapter 2.2 "Protein Extraction"). Samples were quantified using the BioRad RC DC Protein Assay Kit as per manufacturer's instructions. Measured quantities of protein extract were combined with Laemmli Sample Buffer (BioRad) in at least a 1:1 ratio, to which was added 10% 1M Dithiothreitol (DTT) by volume.

S2 Cells Protein Sample Preparation

S2 cell protein extracts were prepared by scraping cells from an adherent plate using a p1000 pipet tip. Cells were then transferred to a microcentrifuge tube and centrifuged at 3,000 x g for 3 minutes. Supernatant was pipetted off and additional cells from the same well were added. This process was repeated until all cells from all wells were spun down and the supernatant was pipetted off. Cells were washed in 1X PBS, then resuspended in NET Buffer (Huntzinger et al., 2010) plus Solution P (Oeffinger et al., 2007) where we substituted EDTA-free protease inhibitor tablets for PMSF, and Superase RNase Inhibitor (Invitrogen) and incubated on ice for 10 minutes on ice. Lysates were then centrifuged at maximum speed for 10 minutes, supernatant was aliquotted and flash-frozen on liquid nitrogen, and stored at -80°C for downstream applications.

Protein was quantified using the Pierce BCA Protein Assay as per manufacturer's instructions. Samples were prepared using BioRad 2X SDS/Laemmli Sample Buffer in at least a 1:1 volume ratio with samples, to which was added a 10% volume of 1M DTT.

Western Blot Protocol

For all Western Blot experiments, the following procedures were followed.

First, samples were separated by size using protein gel electrophoresis. Samples were prepared on ice, then boiled at 95°C for 5 minutes, and replaced immediately on ice before undergoing protein gel electrophoresis.

Afterwards, proteins were transferred to an Immun-Blot PVDF membrane (BioRad) using the BioRad Mini Trans-Blot Apparatus. Transfer was set to 100V and limited to 350 milliamps for 55 minutes.

For tagging of proteins on the membrane, the membrane was placed immediately in Block Buffer (5% dry milk in 1X Tris-Buffered Saline [TBS] plus 0.1% Tween) for 1 hour in a pipet box lid on a slow shaker. Afterwards, primary antibody solutions were prepared in fresh Block Buffer at their necessary dilutions. The protein membrane was transferred to the inside of a plastic page protector, which was then sealed on 3 sides by a Super-Sealer heat sealer (Traco). Sufficient antibody solution was pipetted over the membrane and then the fourth side of the page protector was sealed, ensuring no bubbles over the membrane. The membrane was taped to a fast shaker and placed at 4°C overnight or at room temperature for 2 hours. The membrane was transferred to a pipet box lid, and quick-washed twice in Wash Solution (1X TBS plus 0.1% Tween). Then the membrane was covered in Wash Solution and placed on a shaker for 10 minutes; this procedure was repeated twice. The membrane was then transferred to a new page protector using the same procedure described previously, and a secondary antibody solution prepared in Block Buffer was added to the membrane. The membrane was then placed on a fast shaker

at room temperature for 1 hour. Washes using the same procedure described previously were performed.

For imaging, Thermo Scientific SuperSignal West Dura Chemiluminescent Substrate components were mixed in a 1:1 ratio and incubated on each membrane for 5 minutes. Substrate was drained and membranes were imaged using film and a Konica Minolta Medical Film Processor (Model SRX-101A).

Chapter 2.8: Co-Immunoprecipitation of FMRP with P-Body Components

For co-immunoprecipitation experiments in S2 cells, 1 µg of each tagged P-body component was transfected into the stable-expression pAFHW-*DFmr1* S2 cells—except for control cells, which did not receive a transfection mixture—as described previously (Chapter 2.6, "Stable Expression of FLAG-HA-FMRP in S2 Cells") using a 6-well plate. Protein extracts were prepared and quantified as described previously (Chapter 2.7, "S2 Cells Protein Sample Preparation"). For the immunoprecipitation procedure, the Pierce HA-Tag Magnetic IP/Co-IP Kit was used as per manufacturer's instructions. Briefly, 25 µl magnetic beads were transferred to a 1.5 mL microcentrifuge tube, to which was added 175 µl NET Buffer. Beads were mixed briefly by vortexting, placed on a magnet, and supernatant was removed. This wash process was repeated with 1 mL NET Buffer. Next, 110 µg samples for each protein were prepared in a 220 µl volume using NET Buffer on ice. 20µl of each sample was saved at the 10% "input" on ice, while the remaining 200 µl were added to the magnetic beads. Tubes were placed on a rotator for 30 minutes, then washed 3 times with 300 µl NET Buffer, and once with nanopure water. Protein was eluted from the beads by adding 100 µl 1X Non-Reducing Sample Buffer to the beads,

plus 5 µl of 1M DTT, then heating the samples at 95°C for 5 minutes. Each tube was placed against a magnet for 2 minutes and the supernatant was transferred to a new 1.5 mL tube, which was immediately placed on ice. For input control, 5 µl of 5X Non-Reducing Sample Buffer was added to each tube, plus 1.1 µl 1M DTT. These were heated at 95°C for 5 minutes, then placed immediately on ice. All samples then underwent the same procedures described previously (Chapter 2.7, "Western Blot Protocol").

Chapter 2.9: Co-Localization Studies of FMRP and P-Body Components in Primary Neuron Cultures From *Drosophila* Larvae

Primary Neuron Culture

For co-localization experiments, male flies expressing either YFP-tagged FMRP or GFP-tagged HPat were crossed to virgin females expressing the C380 Cha-Gal80 driver for expression of the YFP-tagged FMRP in glutamatergic but not in cholinergic neurons (Kuehn and Duch, 2013). Fluorophore-positive larvae were selected, and from these, ventral ganglia were dissected in Complete Scheider's Media plus 1X Normocin (InvivoGen). At least ten ventral ganglia from each genotype were pooled for a single experiment and incubated in a 1X Liberase DH Research Grade enzyme (Roche) solution prepared in Rinaldini's Saline for 1 hour. Cells were then transferred to Complete Schneider's Media plus 1X Normocin, washed 3 times in this solution by centrifugation and removal of the supernatant, then triturated using a fire-polished glass pipet 55-60 times, and triturated using a p200 pipet tip 90-95 times. These solutions were then pipetted onto a coated coverslip in a 35 mm poly-d-lysine coated glass-bottom petri dish (MatTek) in a 200 µl volume. Cells were allowed to adhere for 1-2 hours before the

solution was gently pipetted off and 2 mL fresh media was added. Each dish was allowed to grow at room temperature for 3-5 days before fixation and staining.

Primary neuron cultures were fixed for 5 minutes in 4% paraformaldehyde, then quick-washed twice with 1X PBS, and 3 times for 10 minutes each with 1X PBS, followed by one time for 10 minutes with 1X PBS plus 0.1% Triton X-100. Cells were then incubated with primary antibody solutions in block buffer overnight in a humid chamber at 4°C. Primary antibody was washed off using 2 quick-washes followed by six 10-minute washes with 1X PBS plus 0.1% Triton X-100. Cells were then incubated with secondary antibody for 1 hour in a humid chamber at room temperature, then quick-washed twice with 1X PBS plus 0.1% Triton X-100. Cells were then washed once for 10 minutes with 1X PBS and immediately imaged on the Olympus FV1000 Scanning Confocal microscope.

Imaging and Image Analysis

Confocal images were thresholded (increased laser power) to exhibit maximum fluorescence in granules for each fluorophore individually in neurites (oversaturated in cell bodies), then overlapped in Adobe PhotoShop. Multiple neurons were imaged in each primary culture dish. Co-localization was examined by visualizing a single channel in black and white, and using a hand tool to circle discernible punctae. After circling all punctae from a single neuron, the HRP image was overlaid to ensure circled punctae resided within the neuronal structures. Next, both channels were turned back on, and the number of punctae exhibiting overlap was counted and divided by the total number of punctae circled. "Punctae" consisted of 6 pixels or more of a color grouped together

unbroken. “Overlap” was defined as 33% yellow pixels in any punctae, or 33% of red pixels in generally green punctae or 33% of green pixels in generally red punctae. From each set of neurons from the same dish, a weighted average % co-localization was then calculated.

Chapter Three: Results

Chapter 3.1: Differential Expression of miRNAs in the *Drosophila* CNS of Third-Instar Larvae Versus Adults

The goal of this research is to investigate the roles of RNP components, including miRNAs, FMRP, and P-bodies, in synaptic structure. As stated previously, microRNAs play a key role in synaptic development (Follert et al., 2014). Given this fact, it is presumed that the most abundant microRNAs in a given tissue play the most critical role in homeostasis for that tissue, and the targets of that tissue are therefore most important in normal tissue function. Given that brain development underlies learning and long-term memory, it is essential to understand which miRNAs contribute to this development. Thus, we performed differential analysis on *Drosophila* larval CNS and adult brain to learn what the most abundant miRNAs are at different developmental stages to better understand how these miRNAs may contribute to learning and memory processes.

For the purposes of analyzing miRNA abundance in brain tissue, dissections were performed to isolate brains from *Drosophila* larvae and adults. 100 CNS's were dissected out of $w1118^{(Iso31)}$ *Drosophila* larvae and 100 brains from adult flies; RNA was extracted using Trizol, purified, and submitted for Next-Generation Sequencing (NGS) analysis. Approximately 44 million reads from the larval extract and 50 million reads from the adult extract were trimmed of the adapter sequences and filtered for quality, reducing the numbers of reads to approximately 1 million reads for the larval extract and 1.2 million

for the adult extract. These reads were then processed using the miRPIPE miRNA quantification developed by Kuenne et al. (in press). Reads were converted to reads per million, essentially converting each miRNA value to a percentage of the total miRNAs, and quantification analyses were performed. Since we are interested in larval enrichment, the number of normalized reads in the adult tissue were subtracted from the number of normalized reads in the larval tissue and the results were graphed; for readability, only the top and bottom 10 miRNAs are shown (See Figure 4); the full dataset can be viewed in the Appendix (Figure A1). From this analysis, it is apparent that by far, the most abundant and larvally-enriched miRNA is miR-315, followed closely by miR-184, then miR-276A; these top three enriched miRNAs together comprise nearly 55% of the total reads for larval miRNA expression. The next most enriched miRNAs in the larval CNS, in order are: miR-92B, which comprises an additional 3.3% of the total reads in the larval CNS, miR-10 (3%), miR-305 (2%), miR-9C (1.2%) and miR-995 (1.7%).

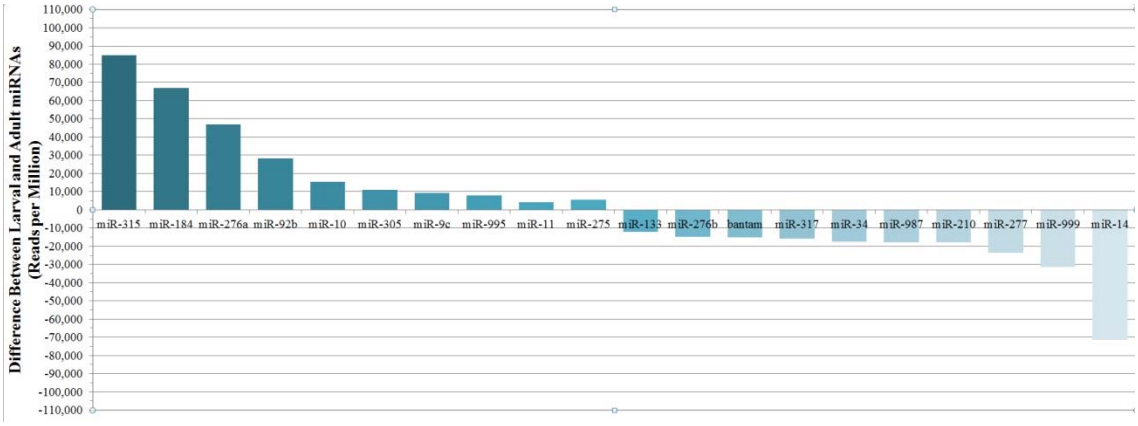

Figure 4: Differential Expression of miRNAs in Larval Versus Adult CNS

The expression of each miRNA was quantified and processed in *Drosophila* larval CNS and adult brain using Next Generation Sequencing and miRPIPE. Each quantification was normalized to reads per million in each tissue. The normalized reads in the adult

brain was then subtracted from the normalized reads in the larval CNS. The top and bottom ten larval-enriched miRNAs are shown.

When plotted against a linear regression assuming a 1:1 larva:adult ratio of miRNA expression, all of these show significant deviation from that ratio (See Figure 4). Interestingly, although miRs -315, -184, and -276A are by far the most numerically enriched miRNAs in the CNS, the greatest fold-change for the top 15 most enriched miRNAs in larval tissue was seen with miRs -92B and -92A, which showed over a 175-fold increase each in abundance from adult tissue to larval tissue. The next greatest fold-enrichments occurred in miRs -275, -9C, -315, and -9A, with fold-changes of 29-, 16-, 7-, and 4-, respectively (see Table 4).

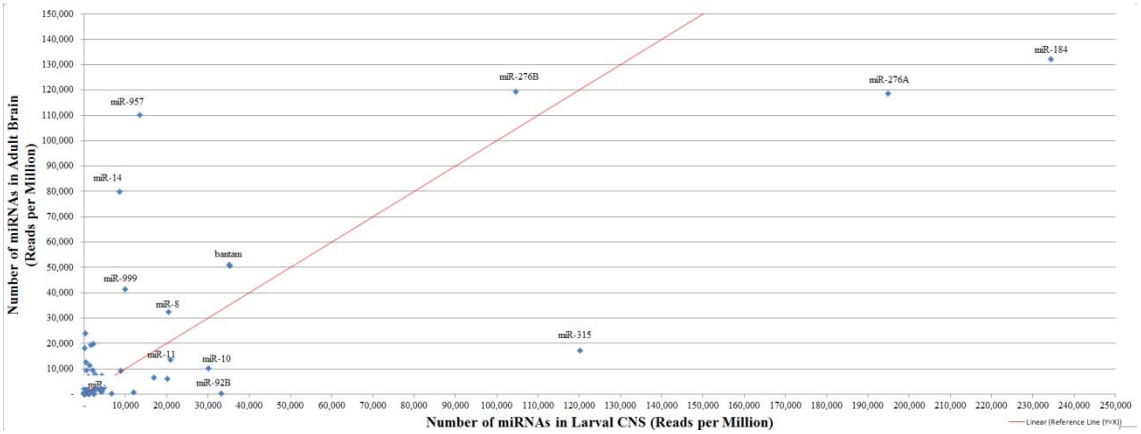

Figure 5: Differential Expression of miRNAs in Larval Versus Adult CNS Compared to a Linear Regression

The miRNA quantifications were plotted onto a scatterplot with larval expression as the x-axis and adult expression as the y-axis, then compared to a linear regression where x is equal to y, assuming a 1:1 ratio of larval to adult expression for each miRNA. Those points deviating most from the linear regression, or most abundant, are labeled.

Table 4: Fold-Enrichment of the Top 15 Most Enriched miRNAs in the Larval CNS

miRNA	Abundance (Reads per Million)	Fold-Enrichment
miR-92b	33,138	197.51
miR-92a	2,349	175.39
miR-275	6,478	28.94
miR-9c	11,192	15.57
miR-315	103,160	7.03
miR-9a	3,263	4.19
miR-306	2,896	3.64
miR-305	14,073	3.29
miR-10	19,839	2.94
miR-995	10,531	2.64
miR-993	2,646	2.43
miR-263a	2,172	2.19
miR-184	102,191	1.77
miR-31a	2,024	1.67
miR-276a	76,265	1.64

Next, miRNA families were grouped together for the purposes of target analysis. For example, the miR-9 family includes miRs -9A, -9B, and -9C, all of which share a seed region binding sequence, which is why they comprise a miRNA family, but are different at their 3' ends, which is why they are considered different miRNAs. These were grouped together because miRNA families share a seed region binding sequence, which substantially increases the likelihood of these miRNAs binding to the same target mRNAs. Each of the top 10 most larvally-enriched miRNAs/miRNA families was analyzed for potential targets using TargetScanFly6.2 (http://www.targetscan.org /fly_12/), which compares the seed region binding sequence of each miRNA/miRNA family for complementarity to a mRNA target and analyzes most likely targets by conservation of binding sites between different species of *Drosophila*. miR-315, the most absolutely abundant and numerically enriched miRNA in the larval CNS, was predicted

to regulate up to 417 target mRNAs. Number of potential targets varied significantly for each miRNA (Table 5).

Table 5: Number of Predicted Targets for each of the Top 10 most Larvally-Enriched miRNAs

miRNA	Number of Potential Targets
miR-315	417
miR-184	42
miR-276a	82
miR-92b	348
miR-10	11
miR-305	272
miR-9c	194
miR-995	54
miR-11	377
miR-275	46

To analyze the potential roles for each of these most abundant miRNAs, cluster function annotation analysis was performed on each set of miRNA/miRNA family potential targets using the Database for Annotation, Visualization and Integrated Discovery (DAVID) program version 6.2 (http://david.abcc.ncifcrf.gov/home.jsp). Interestingly, the potential targets for miR-315 showed a cluster with a large enrichment score of 8.75 that included clusters for neuron development, neuron differentiation, axonogenesis, etc., all with p-values less than $1x10^{-6}$ (see Table 6). The miR-9 family also showed strong enrichment of this same cluster, with an enrichment score of 5.08 (Table 7), all with p-values less than 8.1×10^{-2}. These were the only two miRNAs/miRNA families to show their most enriched functional annotation clusters associated directly with neuronal growth. In fact, of the ten most larvally-enriched miRNAs, only those and miR-275, miR-11 and the miR-92 family showed a functional annotation cluster enriched for neuron development with an enrichment score over 1.5 (Tables A1-A9).

While the miR-92 family and miR-275 did show functional annotation clusters including potential targets involved in neuron differentiation, dendrite morphogenesis, etc. (See Supplementary Tables A1 and A2), the most enriched cluster for the miR-92 family included potential targets involved in transcription regulation, and miR-275 was most predicted to target immunoglobulins. It is important to note that while the most highly-enriched functional annotation clusters of miR-11 targets were not related to neuron development, but rather to membrane development and transcription regulation, there was a functional annotation cluster of miR-11 targets with an enrichment score of 3.47 that was similar to the most highly-enriched functional annotation clusters for the miR-9 family and miR-315, including targets for neuron differentiation and development (Table A9).

Table 6: Functional Annotation Cluster for Predicted miR-315 Targets Enrichment Score 8.72	
Cluster Name	**P-Value**
Neuron development	1.30E-10
Neuron differentiation	1.80E-10
Cell morphogenesis involved in differentiation	3.20E-10
Neuron projection morphogenesis	3.40E-10
Neuron projection development	3.80E-10
Cell morphogenesis involved in neuron differentiation	4.10E-10
Cell projection organization	5.10E-10
Cell projection morphogenesis	1.30E-09
Axonogenesis	1.30E-09
Cell motion	1.60E-09
Cell part morphogenesis	2.80E-09
Cell morphogenesis	2.10E-08
Axon guidance	2.30E-07
Cellular component morphogenesis	1.00E-06

Table 7: Functional Annotation Cluster for Predicted miR-9 Family Targets Enrichment Score 5.08	
Cluster Name	**P-Value**
Cellular component morphogenesis	6.80E-09
Cell morphogenesis	3.10E-08
Cell morphogenesis involved in neuron differentiation	4.30E-07
Cell morphogenesis involved in differentiation	8.70E-07
Neuron projection morphogenesis	2.00E-06
Neuron projection development	2.10E-06
Cell projection organization	2.60E-06
Cell part morphogenesis	3.00E-06
Neuron differentiation	3.20E-06
Neuron development	5.60E-06
Cell projection morphogenesis	8.40E-06
Axonogenesis	1.90E-05
Axon guidance	6.10E-04
Dendrite morphogenesis	1.20E-03
Dendrite development	1.20E-03
Neuroblast proliferation	8.10E-02

Next, each of the miRNAs with target functional annotation clusters specific to neuronal growth was analyzed (miRs -315, -275, -11, and the miR-92 and miR-9 families). Lists of the predicted targets for each of these miRNAs were cross-compared using Microsoft Excel. Surprisingly, there was little overlap between the potential targets for these miRNAs. Only ten targets were predicted to be regulated by 3 or more of these miRNAs, and these targets did not form any functional annotation clusters with an enrichment score over 1.5. There were 21 potential targets that overlapped between the miR-9 family and miR-315, which showed a functional annotation cluster with an enrichment score of 2.62 that included targets involved in actin cytoskeleton reorganization (Table 8) and another functional annotation cluster with an enrichment

score of 2.28 including targets involved in neuron differentiation, neuron projection morphogenesis, etc. (Table 8). Similarly, six overlapping targets of miRs -315 and -275 showed a functional annotation cluster with an enrichment score of 1.97 that included potential targets involved in neuron development, neuron projection morphogenesis, etc. (Table 9). Lists of these potential targets can be found in the supplementary material (Tables A10-A14).

In contrast, overlapping potential targets for miRs -315 and the miR-92 family are strongly enriched in the transcription regulation category (Table A10); this is also the most enriched annotation cluster for overlapping potential targets of the miR-9 family and the miR-92 family (Table A11), and miR-11 and the miR-92 family (not shown). Potential targets for miR-11 did not overlap with any of the other examined miRNAs/miRNA families to form a functional annotation cluster pertaining to neuronal growth. Similarly, other lists of overlapping targets did not show enrichment for functional annotation clusters pertaining to neuronal development, differentiation, etc.

Table 8: Functional Annotation Cluster for Predicted miRs -9 and -315 Targets Enrichment Score: 2.65	
Cluster Name	**P-Value**
Cortical actin cytoskeleton organization	2.30E-02
Cortical cytoskeleton organization	2.30E-02
Cell projection organization	8.80E-02
Actin cytoskeleton organization	1.50E-01
Actin filament-based process	1.40E-01
Cytoskeleton organization	4.50E-01
Enrichment Score: 2.28	
Cell projection organization	8.80E-02
Neuron differentiation	9.00E-02
Sensory organ development	6.90E-02
Compound eye morphogenesis	1.20E-01
Eye morphogenesis	1.30E-01
Neuron projection morphogenesis	1.30E-01
Neuron projection development	1.20E-01
Cell morphogenesis involved in neuron differentiation	1.10E-01
Cell morphogenesis involved in differentiation	1.10E-01
Cell motion	1.00E-01
Compound eye development	9.60E-02
Cell projection morphogenesis	9.90E-02
Cell part morphogenesis	1.00E-01
Eye development	9.70E-02
Neuron development	9.80E-02
Regulation of cell morphogenesis	1.10E-01
Cell morphogenesis	1.50E-01
Cellular component morphogenesis	2.10E-01
Axonogenesis	2.10E-01
Cell projection organization	8.80E-02

Table 9: Functional Annotation Cluster for Predicted miRs -275 and -315 Targets Enrichment Score: 1.97	
Cluster Name	**P-Value**
Neuron projection morphogenesis	7.40E-03
Neuron projection development	7.40E-03
Cell morphogenesis involved in neuron differentiation	7.50E-03
Cell morphogenesis involved in differentiation	8.30E-03
Cell projection morphogenesis	9.20E-03
Cell part morphogenesis	9.80E-03
Neuron development	1.10E-02
Cell projection organization	1.20E-02
Neuron differentiation	1.50E-02
Cell morphogenesis	1.70E-02
Cellular component morphogenesis	2.30E-02
Neuron projection morphogenesis	7.40E-03

Ultimately, the analysis suggests that the most miRNAs most potentially involved in synaptic development in *Drosophila* larvae are miRs -315, -275, and the miR-9 family. The strong expression, enrichment, and functional cluster annotations emphasizing neuronal growth and development suggests these miRNAs play a key role in synaptic growth.

Chapter 3.2: Analyzing a *Futsch* Reporter as a Potential *In vitro* Target of Larvally-Enriched miRNAs

When analyzing the potential targets for the most enriched miRNAs in the larval CNS by *in silico* analysis, a previous graduate student Leslie Rozeboom, noted that four of the most abundant miRNAs are predicted to target the mRNA for *Futsch*, the *Drosophila* homolog for mammalian MAP1B (Table A12). Thus, we investigated this potential interaction by the *in vitro* analysis of a dual-luciferase assay. The initial

experiment was performed by Leslie Rozeboom, who also generated all of the constructs for this procedure. I later repeated the experiment to verify the results.

The *Futsch* 3'UTR was inserted into the 3'UTR region of Firefly Luciferase (FLuc) to act as a reporter for *Futsch* expression. When miRNAs base-pair match to their predicted targets, the RISC represses translation of the target, leading to down-regulation compared to a control not regulated by the miRNA—Renilla Luciferase (RLuc; Figure 6A). Thus, the decreased FLuc/RLuc ratio is indicative of target repression. When S2 cells were transfected with miRNA overexpression vectors for miR-9A, miR-9B, miR-9C, miR-315, or an empty vector control, along with the *Futsch* 3'UTR reporter, and RLuc control, a statistically significant decrease in the FLuc/RLuc ratio was seen, in all cases demarcating at least a 2-fold decrease in *Futsch* reporter expression (Figures 5C-F).

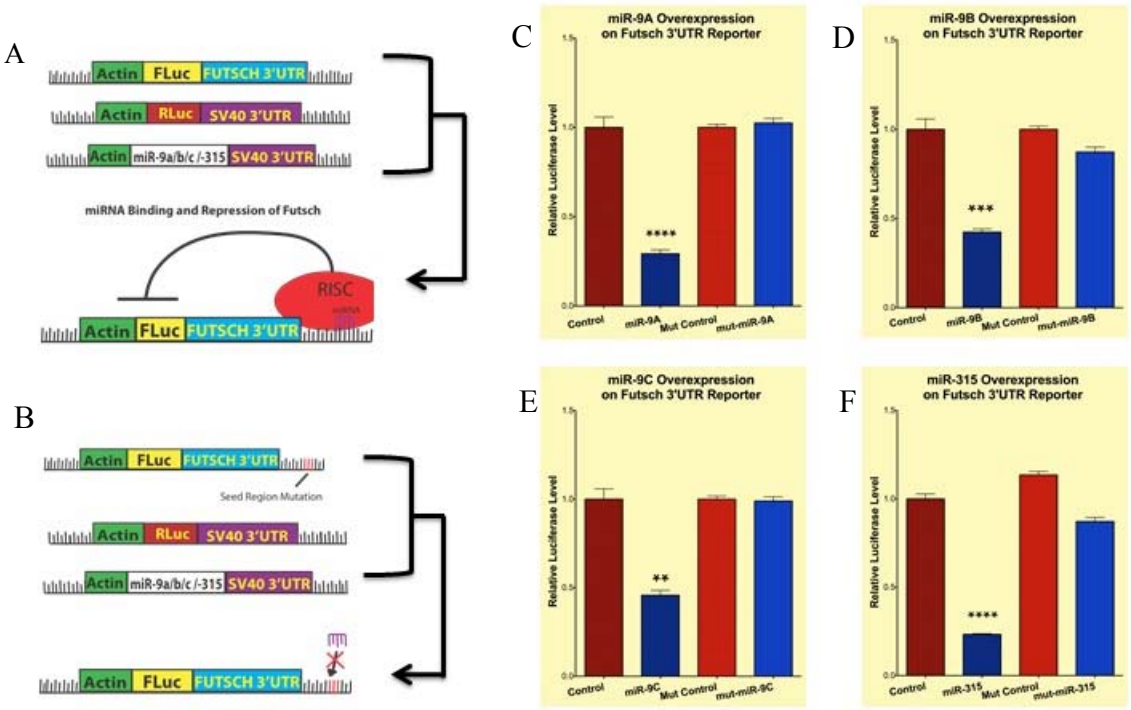

Figure 6: The miR-9 Family and miR-315 Specifically Regulate Translation of a Futsch 3'UTR Reporter

(A) Cartoon of 3 constructs inserted into the S2 cells including the *Futsch* 3'UTR reporter, and the model for repression by the miRNA base-pair matching to the target mRNA containing the *Futsch* 3'UTR sequence and using the RISC to repress translation. (B) Cartoon of 3 constructs inserted into S2 cells including the mutagenized *Futsch* 3'UTR reporter, and the model for de-repression by preventing base-pair matching and subsequent binding of the miRNA to the target mRNA containing the *Futsch* 3'UTR. S2 cells were transfected with a Renilla Luciferase control, one of two reporters: an FLuc-*Futsch* 3'UTR construct (first two columns), or a mutagenized FLuc-*Futsch* 3'UTR construct (last two columns), which was mutagenized at the binding site for either the miR-9 family or miR-315, and finally, the cells were also transfected with either an empty vector (control), or an overexpression construct for: (C) miR-9A, (D) miR-9B, (E) miR-9C, or (F) miR-315. Cells were lysed and Firefly Luciferase and Renilla Luciferase luminescence were quantified. Raw Firefly Luciferase values were normalized to raw Renilla Luciferase ratios, the mean value for the empty vector control was calculated, then the ratios were normalized to this mean value to demonstrate % change. Error bars indicate mean ± SEM. Statistics: One-way ANOVA with a Dunn's post-test. **$p < 0.01$, *** $p < 0.001$ and **** $p < 0.0001$.

To test the specificity of the interaction between each individual miRNA and the *Futsch* reporter, we employed site-directed mutagenesis to alter the binding site for the miRNA on the *Futsch* 3'UTR (Figure 6B). miRNA binding is dependent upon 100% complementarity in the "seed region" binding sequence between the mRNA target and the miRNA to induce translational repression. Thus, altering even a single nucleotide in the seed region binding site on the target should prevent binding of the miRNA and lead to de-repression of the target if the interaction is sequence-specific. In this case, Leslie Rozeboom mutagenized three nucleotides in the seed region sequences. Only two mutagenized constructs were required, as miRs -9A, -9B, and -9C share a seed region. Upon expression of the *Futsch* reporter mutagenized at the miR-9 binding site along with the RLuc control, and either an empty vector control, or overexpression construct for miR-9A, miR-9B, or miR-9C, complete de-repression occurred (Figures 5C-E). Similarly, expression of the *Futsch* reporter mutagenized at the binding site for miR-315 along with the RLuc control, and either an empty vector control, or overexpression construct for miR-315 led to complete de-repression (Figure 6F).

Since overexpression of miRNAs -9A, -9B, -9C and -315 led to repression of a *Futsch* reporter *in vitro*, we next sought to examine if decreased expression of these miRNAs would lead to increased expression of a *Futsch* reporter. For this purpose, miRNA "sponge" constructs were designed as outlined in Ebert et al. (2007). These constructs express ten repeats of an ideal binding site for the miRNAs, such that the miRNAs bind to this construct instead of their endogenous targets, thereby creating the phenotypic effect of decreased miRNA expression (Figure 7A). The construct is designed

with mismatches between the sponge and miRNA so that the miRNAs will act as repressors of the target, but will not induce degradation of the sponge construct. Because the miR-9 family shares a seed region binding site, we theorized that all of the miR-9 family should bind to a sponge designed for miR-9A. We chose to focus on miR-9A because miR-9A precisely base-pair matches to human miR-9, making it a more relevant target for human health implications (Li et al., 2006). To test the effectiveness of these constructs, I altered the miR-9 sponge to express 15 repeats of the binding site, and the miR-315 sponge to express 20 repeats of the binding site, then cloned these constructs into a vector expressing the sponge construct downstream of Firefly Luciferase in the place of the Firefly Luciferase 3'UTR under the control of an actin promoter for expression in S2 cells. Then, each of these constructs was co-expressed with a Renilla Luciferase control, and an empty vector control or overexpression vector for miR-9A, miR-9B, miR-9C or miR-315, and FLuc/RLuc ratios were measured. Overexpression of miR-9A and miR-9C with the FLuc-miR-9sponge vector demonstrated a significant decrease in the FLuc/RLuc ratio compared to an empty vector control (Figure 7B), and overexpression of miR-315 with the FLuc-miR-315sponge showed a significant decrease in the FLuc/RLuc ratio compared to an empty vector control (Figure 7C). Interestingly, overexpression of miR-9B with the FLuc-miR-9sponge did not lead to a significant decrease in the FLuc/RLuc ratio, and even increased the FLuc/RLuc ratio above control levels.

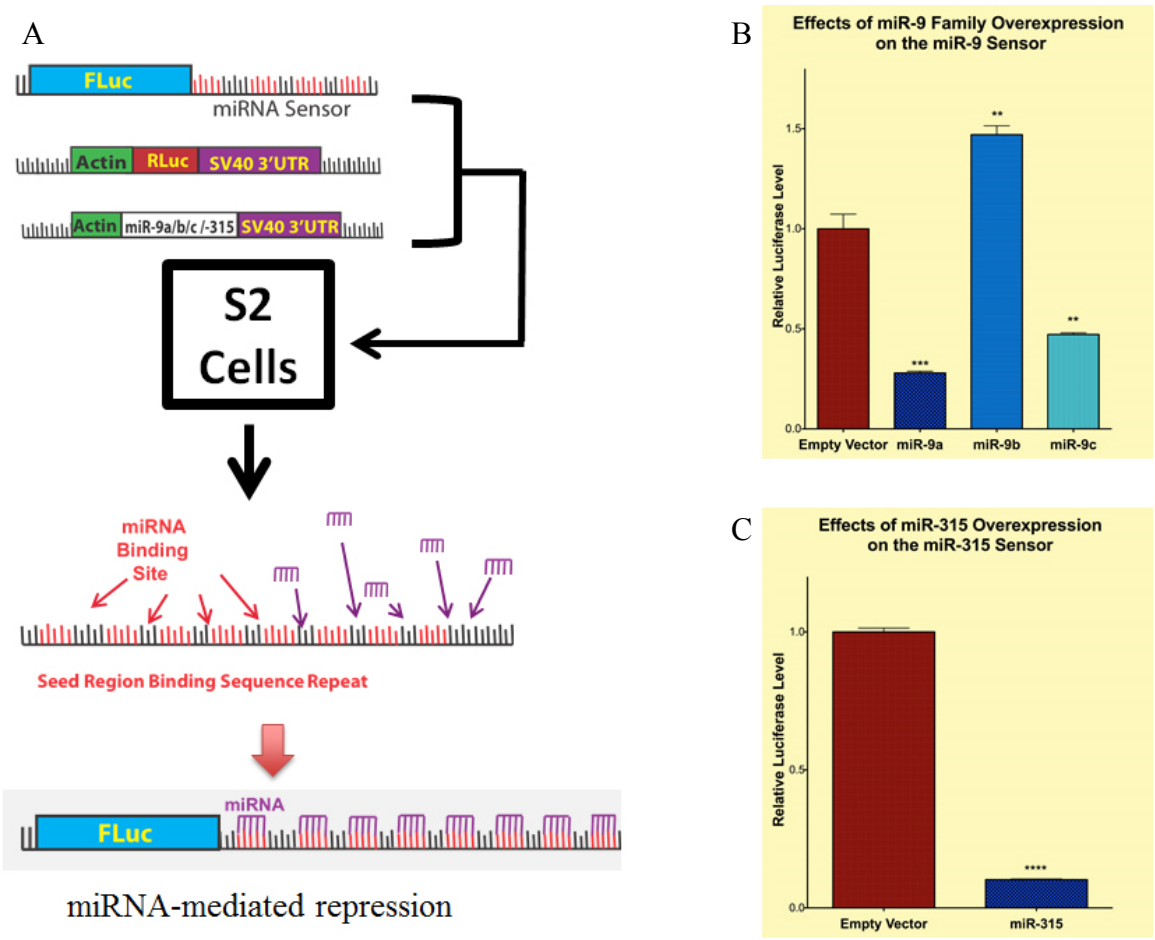

Figure 7: The miRs -9A, -9C, and -315 Bind to Their Respective miR-9 or miR-315 Sponge Sequences in an in vitro reporter but miR-9B Does Not

(A) Cartoon depicting the transfection method and mechanism for a miRNA sponge sequence reporter experiment (B) A 15X repeat of an ideal target sequence for miR-9A or (C) a 20X repeat of an ideal target sequence for miR-315, was inserted into the 3'UTR of a Firefly Luciferase reporter, then transfected into S2 cells with a Renilla Luciferase plasmid, and either an empty vector (control) or an overexpression vector for (B) miR-9A, miR-9B, miR-9C, or (C) miR-315. Cells were lysed and Firefly Luciferase and Renilla Luciferase luminescence were quantified. Raw Firefly Luciferase values were normalized to raw Renilla Luciferase ratios, the mean value for the empty vector control was calculated, then the ratios were normalized to this mean value to demonstrate % change. Error bars indicate mean ± SEM. Statistics: One-way ANOVA with a Dunn's post-test. **$p < 0.01$, *** $p < 0.001$ and **** $p < 0.0001$.

Once the sponge sequences had been validated as targets for each of the miRNAs, expression plasmids containing these sponge constructs were transfected individually into S2 cells along with the *Futsch* 3'UTR reporter. An increase in FLuc/RLuc ratios corresponding to increased *Futsch* 3'UTR reporter expression resulting from decreased abundance of miRNAs was expected. Multiple trials with this experiment produced varied results, none of which showed consistent increases in the FLuc/RLuc ratios in response to transfection with the miR-9 or miR-315 sponges compared to empty vector controls (Figures 7).

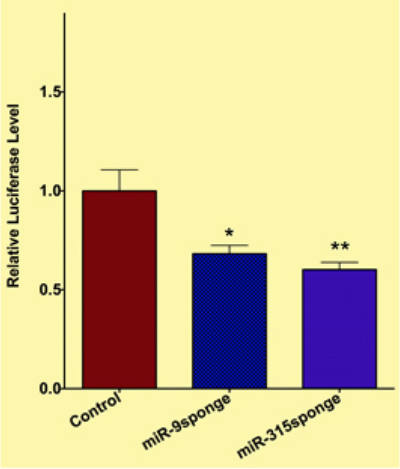

Figure 8: Transfection of S2 Cells with a miR-9 or miR-315 Sponge Does Not Lead to Increased Expression of a Futsch 3'UTR Reporter

S2 cells were transfected with a Renilla Luciferase control, an FLuc-*Futsch* 3'UTR reporter, and with either an empty vector (control), or an overexpression construct for the miR-9sponge (15x repeat), or for the miR-315sponge (20x repeat). Cells were lysed and Firefly Luciferase and Renilla Luciferase luminescence were quantified. Raw Firefly Luciferase values were normalized to raw Renilla Luciferase ratios, the mean value for the empty vector control was calculated, then the ratios were normalized to this mean value to demonstrate % change. Error bars indicate mean ± SEM. Statistics: One-way ANOVA with a Dunn's post-test. *$p < 0.05$, **$p < 0.01$ and **** $p < 0.0001$.

Chapter 3.3: Analyzing the Effects of Larvally-Enriched miRNAs on *Drosophila* NMJ Structure *In vivo*

After demonstrating the effects of the miR-9 family and miR-315 on a *Futsch* reporter *in vitro*, the next step was to test the effects of these miRNAs on Futsch *in vivo*. To do this, C155-Gal4 driver flies (pan-neuronal Gal4 expression) were crossed to transgenic flies designed by Leslie Rozeboom, which expressed the UAS construct upstream of mCherry followed by the same miRNA sequences used in the S2 cells experiments. Because we did not know which fly lines would produce the best overexpression of each miRNA, the effects of miRNA overexpression for two transgenic fly lines for each construct were tested. Overall, the number of 1B ("big") boutons at muscles 6/7 did not significantly decrease in response to pan-neuronal overexpression of miRs -9A, -9B, -9C and -315 (Figure 9A) in either of the transgenic fly lines tested. Similarly, neuronal overexpression of miRs -9A, -9B, -9C, and -315 had no effect on 1S bouton quantities and therefore, total bouton counts were not affected (Figures 8B-C).

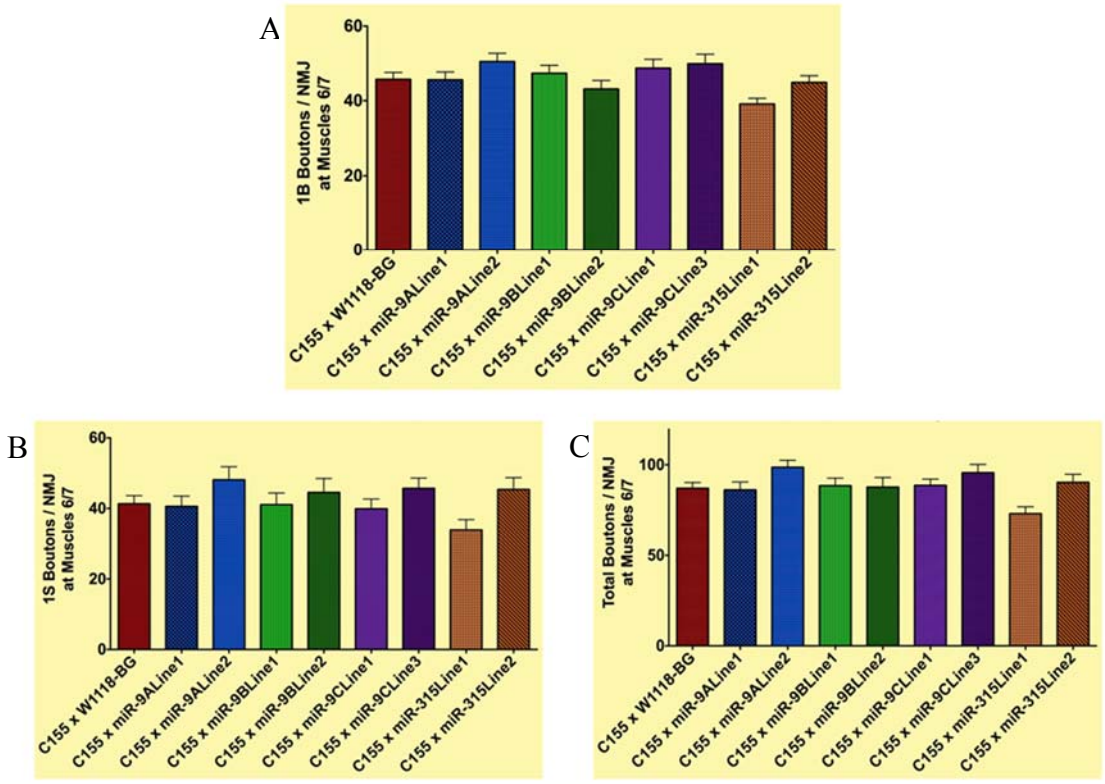

Figure 9: Pan-Neuronal Overexpression of miRs -9A, -9B, -9C, or -315 Does Not Decrease Bouton Numbers at Muscles 6/7 of the NMJ in Drosophila

Virgin flies containing the elav-C155-Gal4 driver were crossed to male flies containing the transgene UAS: mCherry-miRNA construct for each of miRNAs -9A, -9B, -9C, and -315. Third-instar larval offspring were screened for mCherry fluorescence, then dissected, fixed, and stained with Mouse anti-Discs Large antibody followed by Goat anti-Mouse AlexaFluorophore-488 and Goat anti-HRP-Dylight649 (far red). Muscles 6/7 from segment A3 were imaged on a confocal microscope, then the number of (A)1B, (B) 1S, and (C) total boutons were quantified. Error bars indicate mean ± SEM. Statistics: One-way ANOVA with a Dunn's post-test. **$p < 0.01$, *** $p < 0.001$ and **** $p < 0.0001$.

Futsch expression can affect not only bouton number at the *Drosophila* NMJ, but also bouton size (Roos et al., 2000). Therefore, morphology analysis was performed on the boutons of NMJs from the C155-Gal4 crossed to the miRNA overexpression lines. The more promising of the two transgenic fly lines tested for each miRNA was chosen

for this analysis. In other words, the transgenic lines that showed the greatest shift in bouton number in response to pan-neuronal miRNA overexpression. Morphology analysis revealed a very slight but statistically significant decrease in the total area of the boutons resulting from overexpression of miR -9A, but no change in bouton roundness or Feret's Diameter. Additionally, there was no statistically significant increase in bouton area, roundness, or Feret's Diameter, in response to overexpression of miRs -9B, -9C, or -315 (Figure 10A-9C).

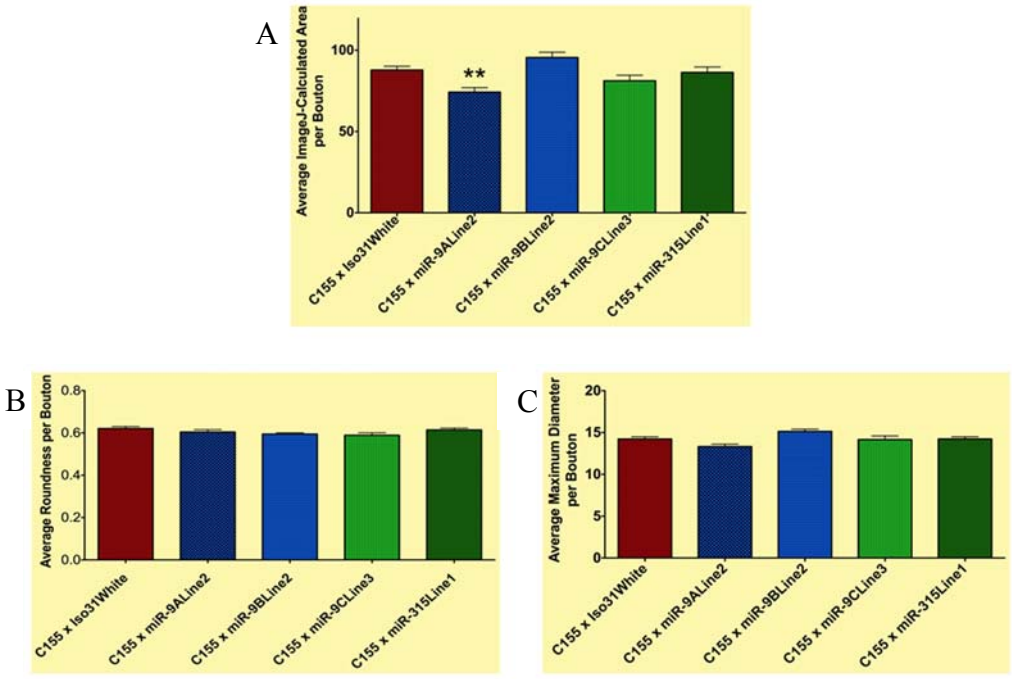

Figure 10: Effects of Pan-Neuronal Overexpression of miRs -9A, -9B, -9C and -315 on Bouton Morphology at the *Drosophila* NMJ Muscles 6/7

Images utilized in Figure 9 were further analyzed. The red channel showing HRP staining was split from the green channel showing Discs Large staining, and each individual bouton was then circled in ImageJ and analyses were performed on bouton size using the (A) Average area per bouton, and shape was analyzed using average (B) "Roundness" and (C) Feret's Diameter of each individual bouton. Error bars indicate mean ± SEM. Statistics: One-way ANOVA with a Dunn's post-test. **$p < 0.01$.

Our lab has previously experienced difficulties with using the C155-Gal4 driver in flies to examine phenotypes at the NMJ. Furthermore, it is possible that with pan-neuronal expression, the effects of overexpressed miRNAs would be masked by the effect of neuronal feedback loops, which compensate for changes in mRNA expression. miRNAs can be key components of these feedback loops (Ernsberger, 2012). Therefore, the experiment of overexpressing miRs -9A, -9B, -9C, and -315 was repeated, this time crossing the transgenic lines to the C380-Gal4 driver, which drives expression only in motor neurons. Overexpression of miRNAs using the C380 driver resulted in a statistically significant increase in the number of 1B boutons at muscles 6/7 for both miR-9A overexpression transgenic lines that were analyzed, and for the first miR-315 overexpression transgenic line that was analyzed (Figure 11A); this was mimicked only in the second miR-9A transgenic line in muscle 4 (Figure 11F). Overexpression of miR-315 from the third transgenic line examined showed a decreased number in 1S boutons (Figure 11B). However, this did not result in a statistically significant change in the total number of boutons per NMJ at muscles 6/7, nor were significant changes observed from overexpression of miRs -9A or -315 using any of the three transgenic lines examined at muscles 6/7 (Figure 11C), at muscle 4 (Figures 11C-D), or in the number of terminal tips per NMJ at muscle 4 (Figure 11F).

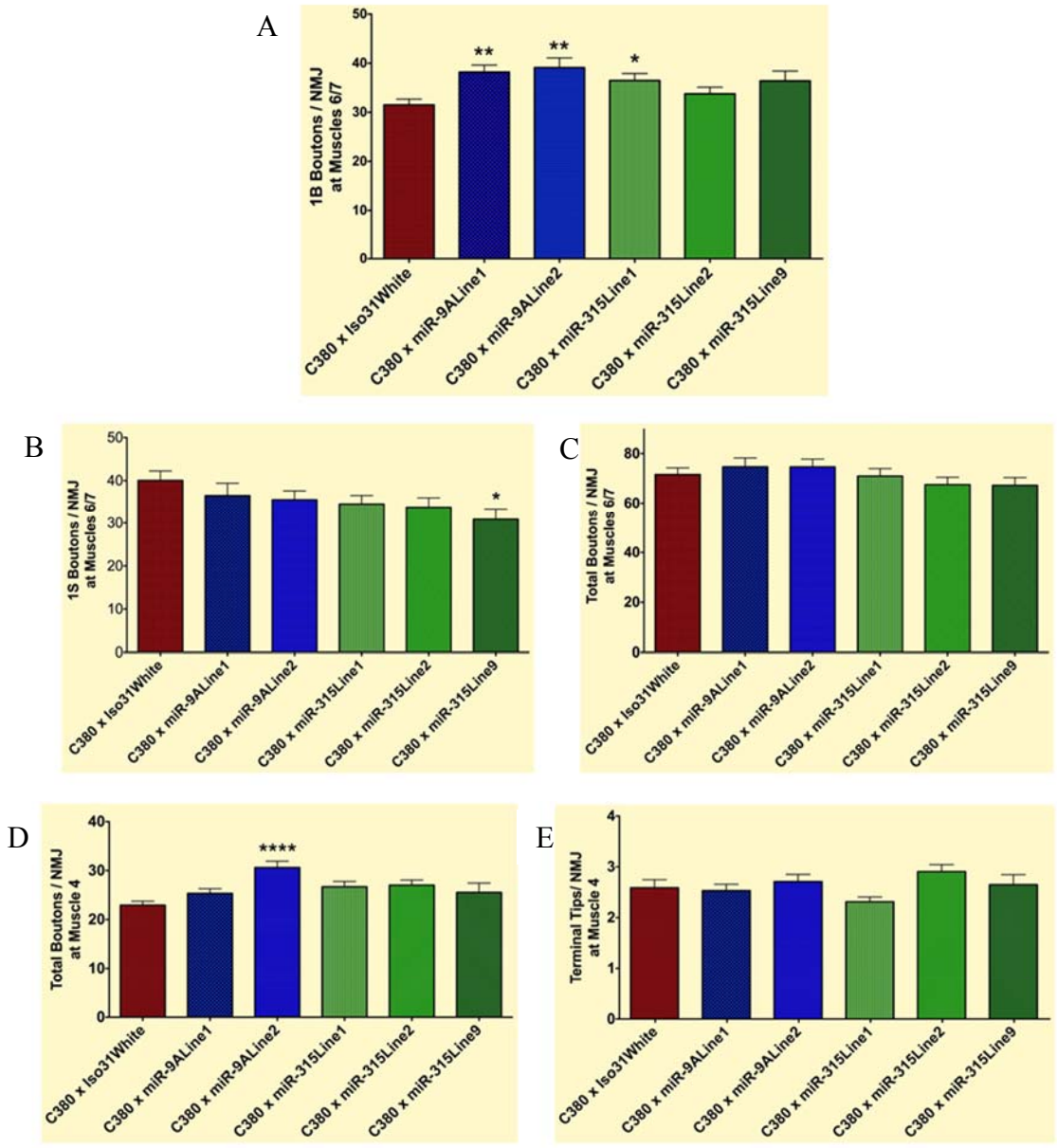

Figure 11: Overexpression of miRs -9A and -315 in Motor Neurons Actually Increases Bouton Numbers at Muscles 6/7 or Muscle 4 of the NMJ in *Drosophila* Rather Than Decreases These Numbers

Virgin flies containing the C380-Gal4 driver were crossed to male flies containing the transgene UAS: mCherry-miRNA construct for each of miRNAs -9A, -9B, -9C, and -315. Third-instar larval offspring were screened for mCherry fluorescence, then dissected, fixed, and stained with Mouse anti-Discs Large antibody followed by Goat anti-Mouse AlexaFluorophore-488 and Goat anti-HRP-Dylight649 (far red). Muscles 6/7

(A-C) and 4 (D and E) from segment A3 were imaged on a confocal microscope, then the number of (A)1B, (B)1S, and overall (C) boutons were quantified for muscles 6/7. (D) Number of total boutons and (E) terminal tips were quantified for muscle 4. Error bars indicate mean ± SEM. Statistics: One-way ANOVA with a Dunn's post-test. * $p < 0.05$, **$p < 0.01$ and **** $p < 0.0001$.

Overall, *in vivo* overexpression of miRs -9A and -315 induced statistically significant changes in the number of 1B boutons at the NMJ for muscles 6/7 only using the motor neuron driver C380; miR-9A overexpression also showed significant increases in bouton numbers at muscle 4 using this same driver. Overexpression of these miRNAs using a pan-neuronal driver did not appear to have significant effects on bouton size or shape, and minimal, conflicting effects on bouton numbers were seen in response to miR-315 overexpression in different transgenic lines using a motor neuron driver.

While overexpression of miRNAs of interest can potentially yield information about the role those miRNAs play at the NMJ, knocking down expression is a far more effective (and more physiological) method for examining miRNA function. Transgenic fly lines expressing miRNA sponges for the miR-9 family, and miR-315 were therefore generated, and crossed to a C380-Gal4 driver fly to induce miRNA knock-down for these miRNAs in motor neurons. Analysis of the NMJ at muscles 6/7 revealed no statistically significant change in the number of 1B boutons in response to the expression of a single sponge construct for any of 3 transgenic lines examined for either the miR-9 family or miR-315 (Figure 12A), though the second transgenic line for the miR-315 sponge yielded a statistically significant decrease in the number of 1S boutons compared to controls (Figure 12B) that resulted in a significant decrease in total boutons (Figure 12C). The third transgenic line expressing a single copy of the miR-9 family sponge also showed

significantly decreased 1S boutons (Figure 12B), but this did not affect total bouton numbers (Figure 12C). When two copies of the miR-9 family sponge were expressed, this led to a significant increase in the number of 1B boutons only (Figures 12A-C). None of the significant changes in bouton numbers were mimicked in muscle 4, nor did under-expression of any of these miRNAs lead to a significant change in the number of terminal tips per NMJ at muscle 4, though expression of the first miR-9 family sponge transgene did result in a significant increase in bouton numbers at muscle 4 (Figure 12E). Knockdown using a single construct for each of miRs -9 and -315 together did not induce any significant effects at muscles 6/7 or at muscle 4.

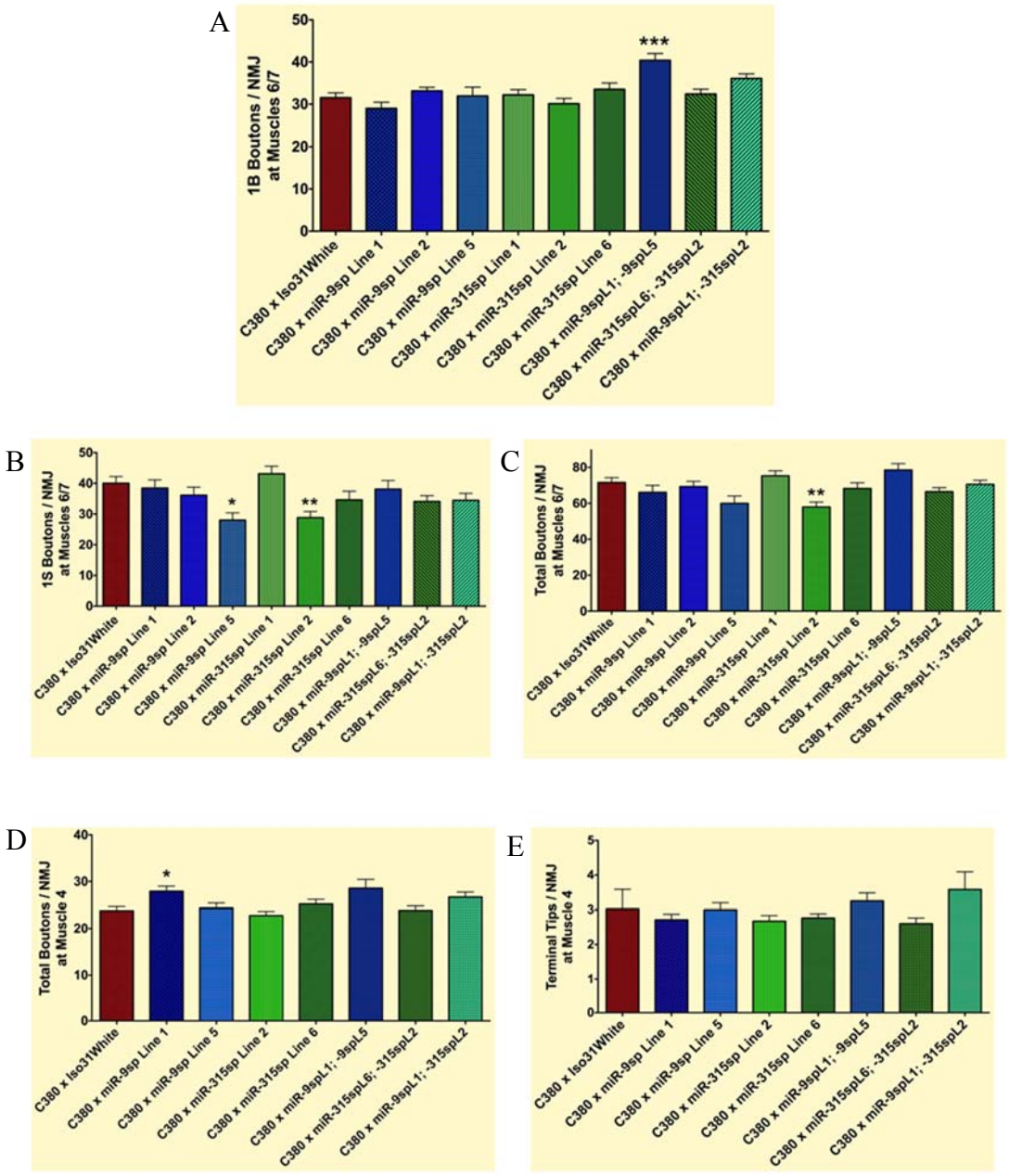

Figure 12: *In vivo* Knock-Down of miRs -9 and -315 Increases the Number of Boutons at Muscles 6/7 and Muscle 4 of the NMJ in *Drosophila*

Virgin flies containing the C380 motor neuron driver were crossed to male flies containing the transgene UAS: mCherry-miRNA sponge constructs for each of miRs -9 and -315. Third-instar larval offspring were screened for mCherry fluorescence, then dissected, fixed, and stained with Mouse anti-Discs Large antibody followed by Goat anti-Mouse AlexaFluorophore-488 and Goat anti-HRP-Dylight649 (far red). (A-C)

Muscles 6/7 and (D-E) muscle 4 from segment A3 were imaged on a confocal microscope, then the number of (A) 1B, (B)1S, and (C) total boutons were quantified from muscles 6/7. (D) Total boutons and (E) terminal tips were quantified from muscle 4. Error bars indicate mean ± SEM. Statistics: One-way ANOVA with a Dunn's post-test. * $p < 0.05$, ** $p < 0.01$ and *** $p < 0.001$.

Ultimately, decreased expression of miRs -9 and -315 had no more consistent effects at muscle segment A3 muscles 6/7, or muscle 4 for any of the transgenic lines examined than did overexpression. Statistically significant changes in 1B, 1S, and total boutons were observed, but none significant enough to affect overall bouton count or to remain consistent between the different muscles examined. However, miRNAs are known to interact with other repression mechanisms, and overexpression or under-expression of miRNAs by themselves may not be enough.

Chapter 3.4: Investigating the Repression of *Futsch* by FMRP *In Vitro*

FMRP is a known repressor of Futsch expression (Zhang et al., 2001), and interacts with the miRNA pathway (Jin et al., 2004). Because of this, and the fact that miRNAs repress translation of a *Futsch* reporter *in vitro* (Figure 6C-F), we hypothesized that FMRP might interact with miRs -9A, -9B, -9C, and -315 to repress *Futsch* translation. To analyze this potential interaction, the first goal was to figure out if FMRP binds directly to the *Futsch* mRNA, and if so, where that interaction occurs, using *in vitro* analysis. Thus, an FMRP overexpression construct was designed and verified in its ability to overexpress FMRP in S2 cells (Figures 12A-B) for co-expression with *Futsch* reporter constructs. Primers were designed for PCR amplification of 12 different *Futsch* reporter fragments (Figure 13D), and I trained an undergraduate in our lab, Nathan Boin, to clone the fragments into the vector and perform dual-luciferase assays in S2 cells. He performed

all of the assays seen in Figure 13B, with the exceptions of the UTRs. Leslie Rozeboom cloned the 3'UTR, and I performed the dual-luciferase assay for this fragment. I cloned the 5'UTR and performed the dual-luciferase assay. Ultimately, these results showed that there was no significant decrease in *Futsch* reporter expression in any fragment of the *Futsch* mRNA in response to FMRP overexpression compared to an empty vector control, and there was even significant overexpression of the reporters in many cases (Figure 13C).

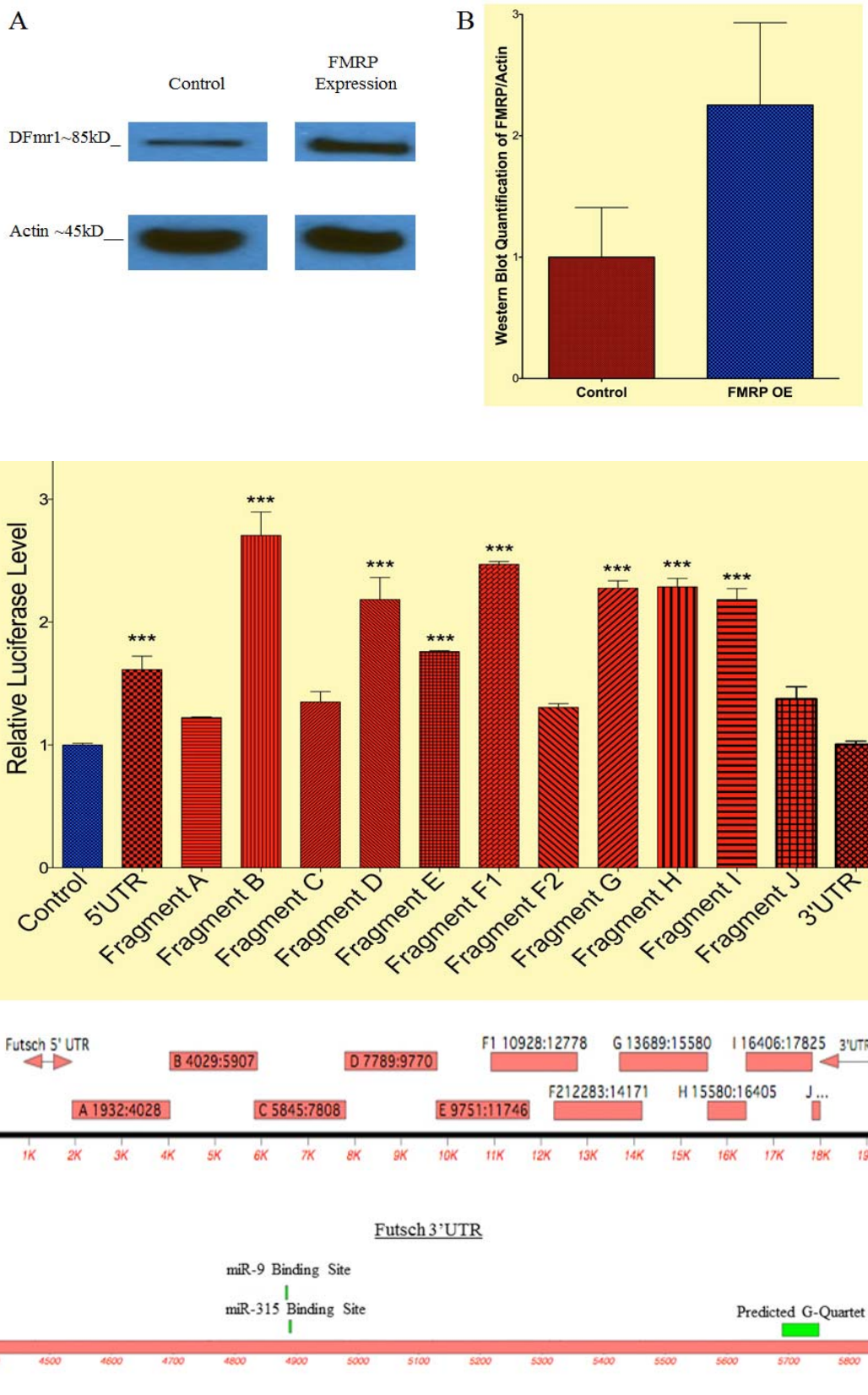
A
Control
FMRP Expression
DFmr1~85kD_
Actin ~45kD__
B
Western Blot Quantification of FMRP/Actin
Control
FMRP OE
C
Relative Luciferase Level
***
Control
5'UTR
Fragment A
Fragment B
Fragment C
Fragment D
Fragment E
Fragment F1
Fragment F2
Fragment G
Fragment H
Fragment I
Fragment J
3'UTR
D
Futsch 5' UTR
B 4029:5907
D 7789:9770
F1 10928:12778
G 13689:15580
I 16406:17825
3'UTR
A 1932:4028
C 5845:7808
E 9751:11746
F212283:14171
H 15580:16405
J ...
E
Futsch 3'UTR
miR-9 Binding Site
miR-315 Binding Site
Predicted G-Quartet

Figure 13: FMRP Significantly Increases, Rather Than Decreases Expression of *Futsch* Reporters *In vitro*

Boin (unpublished). (A) An FMRP overexpression vector was tested by transecting into S2 cells and performing a Western Blot against FMRP using a protein extract from lysed cells and comparing to extract from cells transfected with an empty expression vector (B) FMRP overexpression was further validated by quantitative Western Blot analysis (C) S2 cells were transfected with a Renilla Luciferase control, an FLuc-*Futsch* fragment reporter, and with either an empty vector (control), or an overexpression construct for FMRP. Cells were lysed and Firefly Luciferase and Renilla Luciferase luminescence were quantified. Raw Firefly Luciferase values were normalized to raw Renilla Luciferase ratios, the mean value for the empty vector control was calculated, then the ratios were normalized to this mean value to demonstrate % change. (D) For cloning purposes, the entirety of the *Futsch* mRNA was divided into fragments, which were then inserted into Firefly Luciferase reporter vectors for co-expression with FMRP and dual-luciferase analysis. This is a linear image of the *Futsch* mRNA shown 5' to 3' measuring the length in kilobases (red numbers at the bottom), above which are shown the extents of each fragment (red boxes) labeled with their own corresponding letters and the base-pair locations as measured from the 5' end (black numbers inside red boxes). (E) Graphic depicting the *Futsch* 3'UTR demarcated by the red arrow, with numerical base-pair markers shown below. Included are labeled points for the predicted miR-9 family binding site (TargetScanFly.org) and a predicted G-quartet (http://bioinformatics.ramapo.edu/GQRS). Error bars indicate mean ± SEM. Statistics: One-way ANOVA with a Dunn's post-test. *** $p < 0.001$.

Even if FMRP does not bind directly to the *Futsch* mRNA, it is still possible that FMRP interacts with miRNAs to induce translational repression of target mRNAs. Knowing that *Futsch* is a target of both FMRP (albeit indirectly), and four of the most enriched miRNAs in the *Drosophila* CNS in an *in vitro* assay, it is plausible that if FMRP interacts with any miRNAs to regulate its targets, miRs -9A, -9B, -9C and -315 are likely candidates. Immunoprecipitation of FMRP was therefore performed on fly head extract (Figure 14A), RNA was isolated, and qRT-PCR was performed using primer assays for each of miRs -9A, -9B, -9C, -315, and U1 for a negative control. Extract from an FMRP immunoprecipitation showed no enrichment of any of these five miRNAs over an IgG

immunoprecipitation or immunoprecipitation with unconjugated magnetic beads. A sample containing 10% of the input showed enrichment of all five miRNAs.

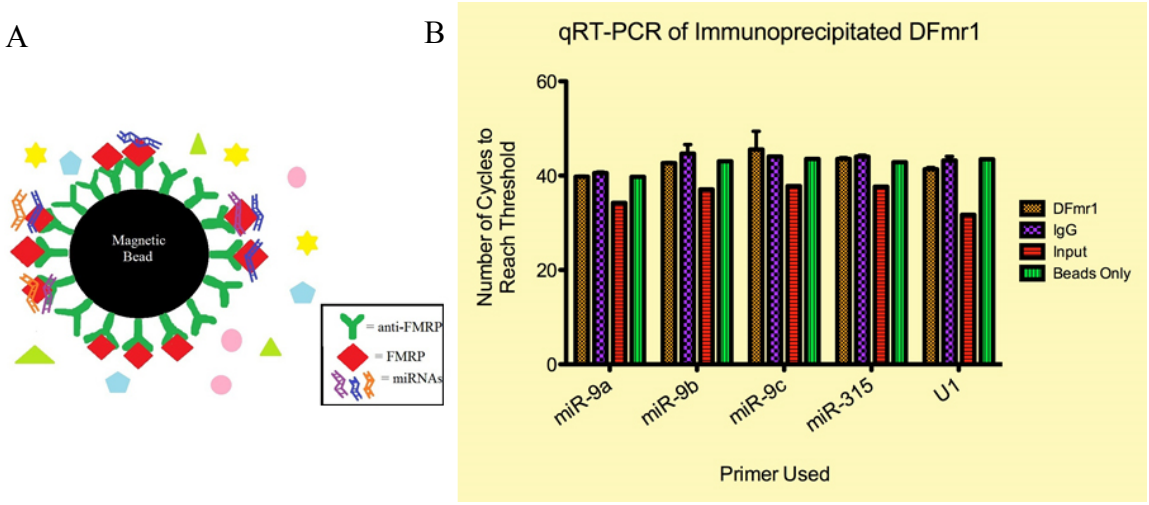

Figure 14: FMRP-Immunoprecipitated Extracts Are Not Enriched for miRs -9A, -9B, -9C or -315

(A) Cartoon depicting the use of an antibody-coated magnetic bead to co-immunoprecipitate FMRP with bound miRNAs. (B) FMRP was immunoprecipitated from protein extracted from homogenized *w1118* fly heads using Mouse anti-DFmr1 antibody (6A15) conjugated to magnetic beads. qRT-PCR analysis using SYBR Green was performed on the eluant using primers for miRs -9A, -9B, -9C, -315, and negative control U1. Results were compared to 10% protein extraction input, extract eluted from immunoprecipitations using Mouse IgG antibody conjugated to magnetic beads, and extract eluted from immunoprecipitations unconjugated magnetic beads.

Ultimately, the results show that FMRP does not significantly repress any portion of the *Futsch* mRNA using *in vitro* reporters for each fragment, nor does it interact physically with miRs -9A, -9B, -9C, or -315. However, miRNAs and FMRP are known to interact with other translational repression pathways, including, particularly, P-bodies (Pascual et al., 2012). Previous research has shown that FMRP not only co-localizes with P-body components Me31B, Trailerhitch, and HPat, but also interacts genetically with these P-body components (Barbee et al., 2006; Pradhan, unpublished). Knowing the

importance of understanding translational repression mechanisms for the purposes of synaptic structure modifications, the next step was to further examine the extent of the relationships between DFmr1 P-body components.

Chapter 3.5: Analysis of Co-Localization of FMRP with P-Body Components

Though FMRP is known to co-localize and interact physically with some P-body components, others have yet to be investigated. Thus, the first step was to analyze whether FMRP co-localizes with Twin, and verify that it co-localizes with HPat (Pradhan, unpublished) and Me31B (Barbee et al., 2006). Primary neuron cultures were prepared using flies expressing YFP-FMRP, and stained with antibodies against Twin, HPat and Me31B. Cultures were allowed to grow 3-5 days before fixing and immunostaining with antibodies against P-body components, as well as a neuronal marker, Horse Radish Peroxidase (HRP). Clear overlap was seen not only in the cell body, but also in substantial amounts of the punctae in neurites (Figure 15). Quantification of co-localization in the neurite punctae showed that Twin had the least co-localization with FMRP, with only 30.8% overlap with YFP fluorescence. Me31B showed substantially more overlap, averaging 51.9%. The greatest co-localization was seen between FMRP and HPat, which showed approximately 67.5% overlap between YFP-FMRP and endogenous HPat, and 62.3% overlap between GFP-HPat and endogenous FMRP (Table 10). Proximity of these particles suggests the possibility of a physical interaction between FMRP and these P-body components.

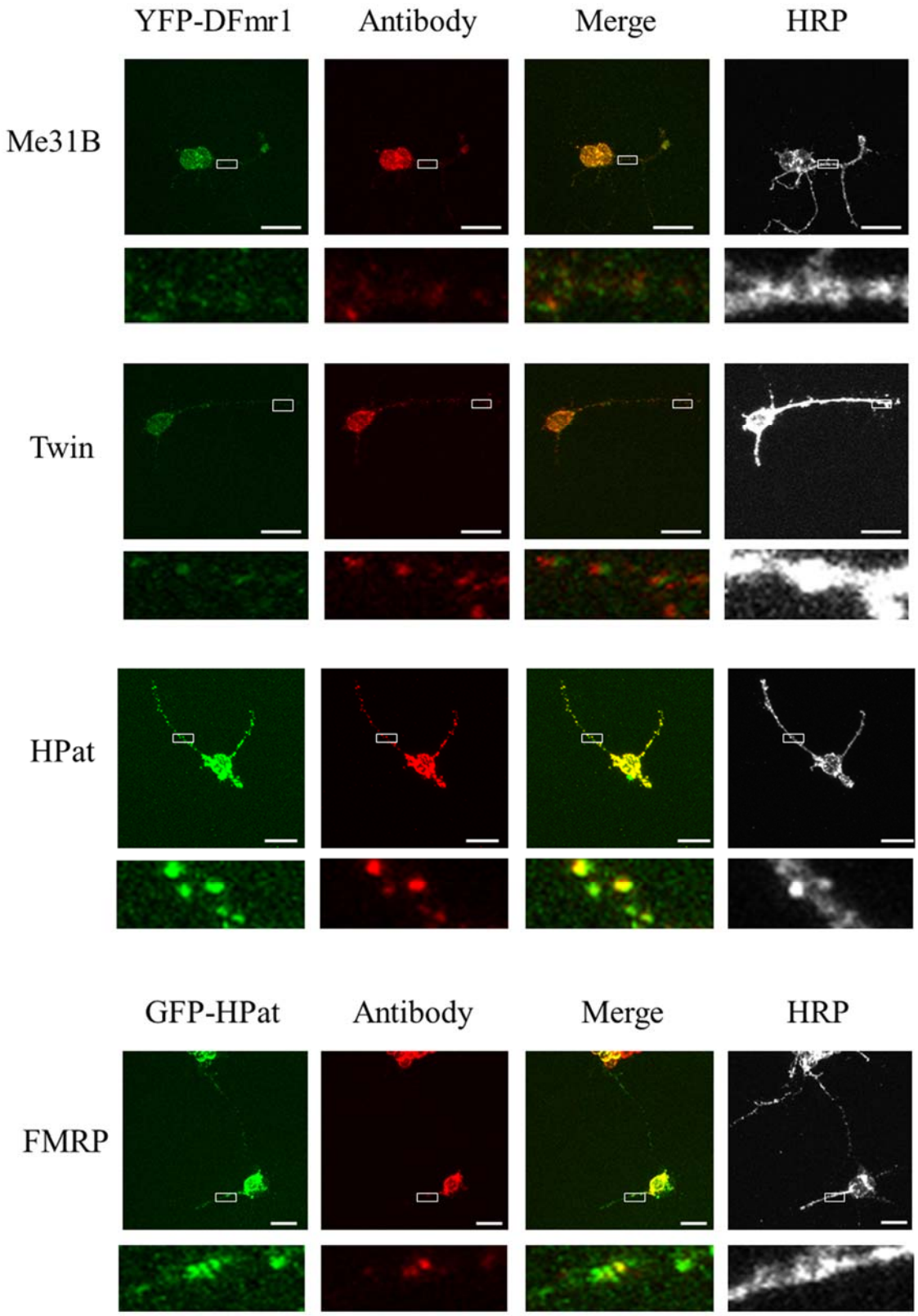
YFP-DFmr1
Antibody
Merge
HRP
Me31B
Twin
HPat
GFP-HPat
Antibody
Merge
HRP
FMRP

Figure 15: Images of Co-Localization of FMRP and P-Body Components in Primary Neuron Culture

Primary neuron cultures were prepared from the ventral ganglia of third-instar larvae expressing the indicated fluorphore-tagged proteins. Cultures were allowed to grow for 3-5 days prior to fixing for 5 minutes, and staining with primary antibody followed by secondary antibody conjugated to AlexaFluorophore-568 and Goat anti-HRP-Dylight649 (far red). Images were taken separately and overlaid using Adobe Photoshop. P-body components tested by antibody are labeled on the left. Below each neuron image is an expanded inset from the image depicted by the white box. Scale bars are equal to 5 µm.

Table 10: Percent Co-Localization of FMRP and P-Body Components

Genotype:			YFP-FMRP	GFP-HPat
Antibody used as a Reference:	# of punctae	# of neurons		
Mouse ∝ Me31B	210	4	51.9	—
Rabbit ∝Twin	127	4	30.8	—
Rabbit ∝ HPat	295	10	67.5	—
Mouse ∝ DFmr1	114	3	—	62.3

Images like those seen in Figure 15 were examined in Adobe Photoshop using separated channels to initially circle punctae, then observing co-localization in circled punctae using the channels overlay feature. A weighted average was calculated for each set of neurons. Co-localization of fluorescence from P-body particles overlapping with FMRP particles is expressed as a percent of total punctae.

To investigate whether FMRP physically interacts with P-body components, co-immunoprecipitation was used. An HA-tagged version of FMRP was designed and permanently expressed it in an S2 cell line, into which V5-His-tagged P-body components were then transfected: Twin, HPat, Me31B, and Dcp1, which I designed. I verified a tagged version of FMRP was being expressed in S2 cells by isolating protein extract from normal S2 cells, cells transfected with a normal FMRP overexpression plasmid, and cells transfected with the HA-tagged FMRP, and performed a Western Blot using antibody against FMRP. The control (untransfected) cells and cells transfected with normal FMRP

show a single band between 75 kDa and 100 kDa. The cells transfected with HA-tagged FMRP showed this same band, but also a higher band right at 100 kD (Figure A1). To verify if this band was higher due to the HA tag, a blot with the same extracts was stained with an antibody against HA. No bands were seen in the untransfected cells or cells transfected with normal FMRP, but a single band matching in size at 100 kDa to the higher band in the cells transfected with HA-tagged FMRP was seen (Figure A1).

To verify that tagged versions of Twin, Me31B, HPat, and Dcp1 were being expressed in S2 cells, each P-body component was transfected into the cells, protein was isolated, and Western Blot was performed for each using an antibody against V5. Without a tag, endogenous Me31B typically appears at 50-55 kD (Igreja and Izaurralde, 2011; Nakamura et al., 2001), Twin at around 63 kD (Temme et al., 2004), HPat at around 102 kD and 108 kD (Pradhan et al., 2012), and Dcp1 at around 43 kD (Braun et al., 2012). The addition of the V5-His tag should increase each protein's size by approximately 7 kD (Stothard, 2000). Bands appeared at the correct sizes on a Western Blot to suggest tagged versions of Me31B, Twin, and Dcp1 were being successfully expressed, though the tagged version of HPat did not show a band.

Protein extracts from each set of transfected cells were then added to commercially-available magnetic beads coated with antibody against HA (Pierce) for immunoprecipitation, then extracts were run on a protein gel and blotted for expression of V5, and each respective protein, with the exception of Dcp1, for which we could not obtain an antibody. 10% of the input from each immunoprecipitation reaction was also

run on a gel in parallael for verification of initial expression of each protein in the S2 cells.

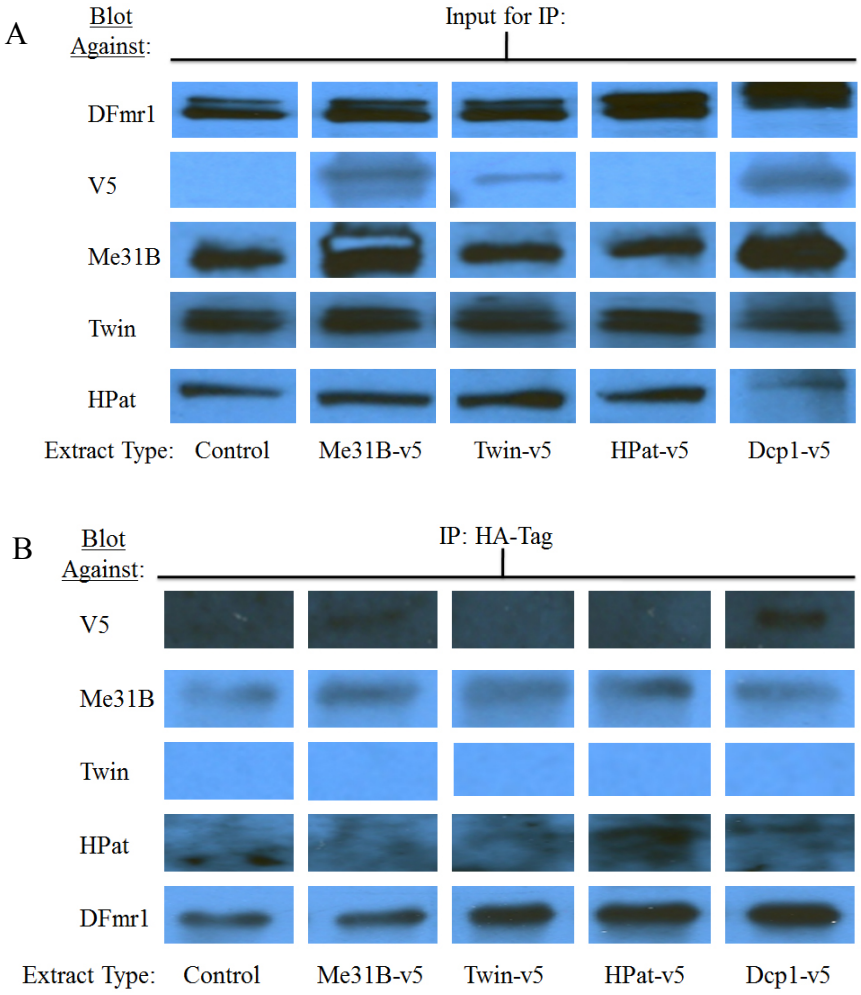

Figure 16: Co-Immunoprecipitation and Western Blot of HA-Tagged DFmr1 with V5-His-Tagged P-Body Components

Cells with stable expression of HA-tagged FMRP were transfected with V5-His-tagged versions of either Me31B, Twin, HPat, or Dcp1; negative controls were non-transfected cells (bottom row labels). Protein extract (Input) was run on a protein gel and blotted for (A) the V5 tag or endogenous proteins (left column labels), then (B) immunoprecipitations (IP) against HA were performed on each extract, and the eluants were run on a gel and blotted for the V5 tag or endogenous proteins (left column labels).

The input control Western Blot shows expression of tagged FMRP (indicated by the double bands) in all extracts. The V5 tag appears in all extracts except for the control cells, which were not transfected with a V5-tagged P-body component, and cells transfected with V5-tagged HPat. When probed using antibodies against endogenous proteins, all extracts show expression of Me31B, Twin, and HPat (antibody was not available for Dcp1). In the extract transfected with V5-tagged Me31B, two bands appear at different sizes in the range of 50-60 kD, one matching the endogenous bands found in other extracts, the other a bit higher. Antibody against Twin shows two bands very close to each other in all extracts in the range of 60-70 kD, with the possible shadow of a third, higher band in the extract transfected with V5-tagged Twin, and curiously, also in the extract transfected with V5-tagged Dcp1. Interestingly, in the extract transfected with V5-tagged Dcp1, HPat expression was not as strong, as the band appeared faint in comparison to the band seen from other cell extracts, and slightly higher on the gel.

Blots of HA-FMRP immunoprecipitated extracts from each set of transfected cells show a strong band indicating successful immunoprecipitation of the HA-tagged FMRP using anti-DFmr1 antibody. The V5 tag co-precipitated with HA-FMRP in Me31B-V5-transfected cells, Dcp1-V5-transfected cells, and, although it is very difficult to see in this image, a very faint band appeared suggesting minimal co-precipitation with Twin-V5 in transfected cells. The V5 tag did not appear to co-precipitate with HA-FMRP in cells that were not transfected with any tagged proteins, or with HPat-V5 in HPat-V5-transfected cells. Antibody against endogenous Me31B shows co-precipitation of Me31B with FMRP in all extracts, though interestingly, two bands are not seen in the extract from

Me31B-V5-transfected cells. Also, endogenous HPat appears to have co-precipitated with HA-FMRP in extracts transfected with HPat-V5, where a very strong band is seen, with Dcp1-V5-transfected extracts and Twin-V5-transfected extracts, where a fainter, but visible band is also seen, and finally, in control cells, though the band appears slightly lower than in the HPat-V5-transfected cells or the Dcp1-V5-transfected cells. Curiously, there was no band suggesting co-precipitation of HPat with FMRP in cells transfected with V5-Me31B. Twin did not appear to co-precipitate with FMRP in any of the extracts.

Ultimately, these results suggest that FMRP co-immunoprecipitates strongly with Me31B and Dcp1. It also co-immunoprecipitates with endogenous HPat, though strangely not in extracts overexpressing V5-tagged Me31B. FMRP also does not co-immunoprecipitate with V5-tagged HPat, or with endogenous Twin, though it may weakly co-immunoprecipitate with the tagged version of Twin.

Chapter 3.6: Analyzing the Effects of Genetic Interactions Between FMRP and P-Body Components at the *Drosophila* NMJ

As stated previously, FMRP has been shown to interact with P-body components not only physically, but also genetically. After examining the interactions between FMRP and P-body components by physical proximity and physical association in an immunoprecipitated complex, the next step was to see if these genetic interactions between FMRP and P-body components can, in fact, affect the structure of the *Drosophila* NMJ.

The first step in examining the genetic role of *DFmr1* and P-body components at the NMJ was to repeat previous unpublished experiments by Sarala Pradhan to validate her results suggesting a genetic interaction between FMRP and HPat to influence NMJ

structure. NMJ analysis at muscles 6/7 and muscle 4 showed that larvae that were heterozygous for two different deletions of FMRP (*DFmr1*$^{\Delta 50}$ and *DFmr1*$^{\Delta 113}$), or heterozygous for a single deletion of HPat (*HPat*$^{\Delta 3}$), showed no significant change in 1B bouton numbers compared to a *CantonS*/*w1118* $^{(Iso31)}$ control. This was also true for total bouton count, except in the case of the *DFmr1*$^{\Delta 113}$ heterozygote, which showed a significant increase in total bouton numbers (Figure 17C). In contrast, trans-heterozygotes *DFmr1*$^{\Delta 113}$/*HPat*$^{\Delta 3}$ and *DFmr1*$^{\Delta 50}$/*DFmr1*$^{\Delta 113}$ showed a significant increase in 1B bouton numbers at muscles 6/7 (Figure 17A) and also in total bouton numbers at muscles 6/7 and at muscle 4 over wildtype controls (Figure 17C-D). Homozygotes for *HPat*$^{\Delta 3}$ showed an increase in 1B boutons only (Figure 17A). Larvae that were trans-heterozygous *DFmr1*$^{\Delta 50}$/*HPat*$^{\Delta 3}$ showed a significant increase in 1B bouton numbers only at muscle 4 (Figures 17A and 17D), and the only significant shift in number of 1S boutons at muscles 6/7 or terminal tips at muscle 4 observed, were with a trans-heterozygous deletion of *DFmr1* (Figure 17B).

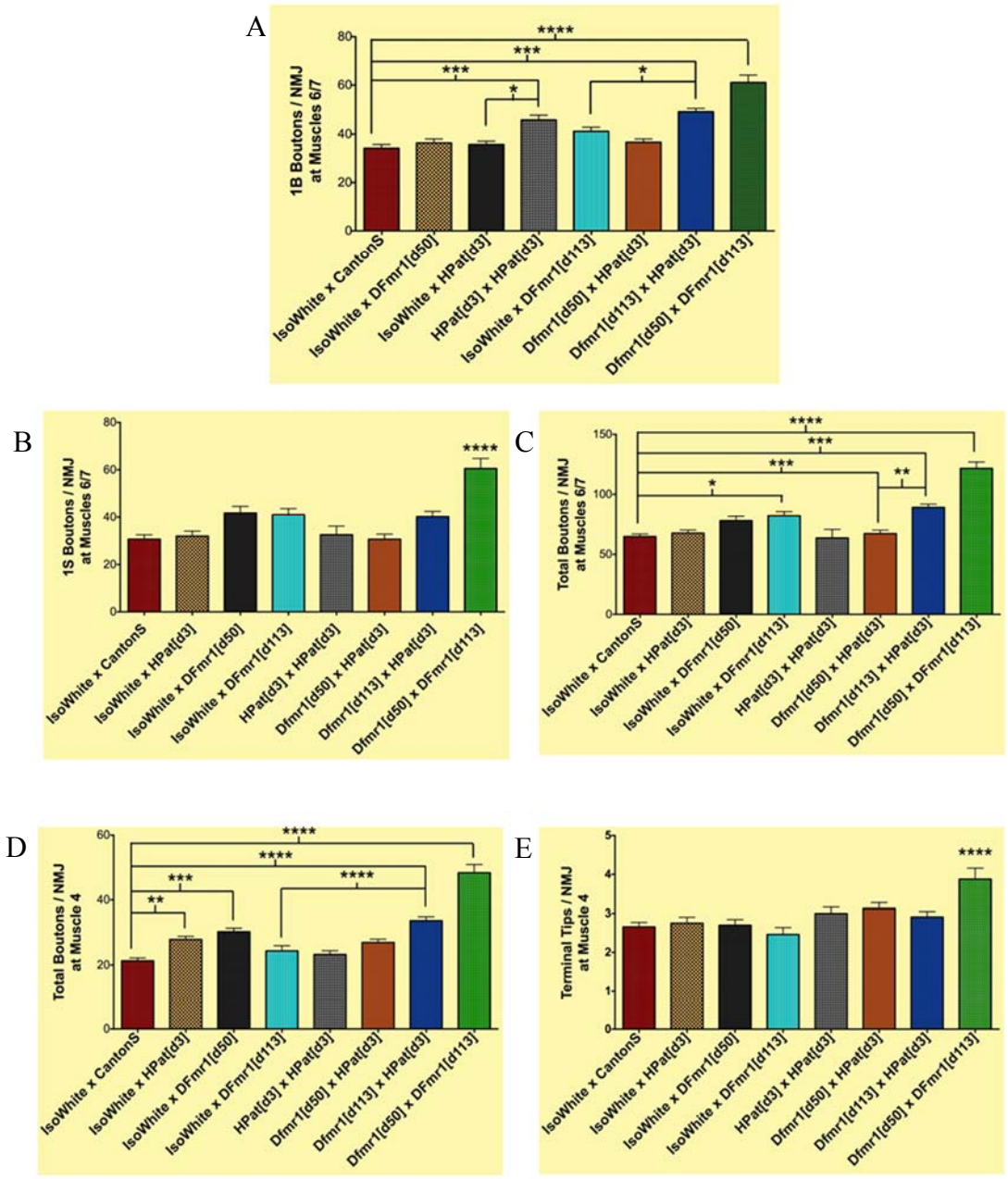

Figure 17: FMRP Interacts Genetically with P-Body Component *HPat* to Affect Synaptic Growth

Virgin *w1118*$^{(Iso31)}$ flies were crossed to the *Δ113* allele and the *Δ50* allele for *DFmr1*, and the *Δ3* allele for *HPat*. Virgin flies containing the *Δ113* allele or *Δ50* allele for *DFmr1* were crossed to male flies containing the *Δ3* allele for *HPat*, and each of the *DFmr1* alleles were also crossed to each other. Third-instar larval offspring were screened for absence of a larval marker, then dissected, fixed, and stained with Mouse anti-Discs Large

antibody followed by Goat anti-Mouse AlexaFluor-488 and Goat anti-HRP-Dylight649 (far red). (A-C) Muscles 6/7 and (D-E) muscle 4 from segment A3 were imaged on a confocal microscope, then the number of (A) 1B, (B)1S, and (C) total boutons were quantified from muscles 6/7. (D) Total boutons and (E) terminal tips were quantified for muscle 4. Error bars indicate mean ± SEM. Statistics: One-way ANOVA followed by Tukey's post-test. **p < 0.01, *** p < 0.001 and **** p < 0.0001.

Analysis of NMJ modifications in response to FMRP knock-down or HPat knock-down not only served to investigate the potential interaction between these two proteins, but also to indicate which FMRP deletion line was most effective for FMRP-induced increase in bouton numbers. The average number of boutons was greater for the *DFmr1*$^{\Delta 113}$ line than the *DFmr1*$^{\Delta 50}$ line for all muscles and boutons examined, suggesting it is the superior line for NMJ analysis for this purpose. Thus, to investigate the interaction between FMRP and other P-body components, I next performed crosses for deletions of each of these components and *DFmr1*$^{\Delta 113}$.

When compared to a *CantonS*/*w1118*$^{(Iso31)}$ control, only the *DFmr1*$^{\Delta 113}$/*HPat*$^{\Delta 3}$, *Dfmr1*$^{\Delta 113}$/*Twin*^{12209}, and *DFmr1*$^{\Delta 50}$/*Dfmr1*$^{\Delta 113}$ trans-heterozygotes showed a significant increase in the number of 1B boutons and total boutons over wildtype controls (Figures 17A and 17C). When compared to the *Dfmr1*$^{\Delta 113}$ heterozygote, only the *DFmr1*$^{\Delta 113}$/*HPat*$^{\Delta 3}$ and *DFmr1*$^{\Delta 113}$/*Dfmr1*$^{\Delta 50}$ trans-heterozygote showed a significant increase in 1B bouton numbers, and none of the genotypes showed significant increases in total bouton numbers over the *DFmr1*$^{\Delta 113}$ heterozygote. Heterozygotes and trans-heterozygotes for Me31B and Dcp1 showed no significant changes in 1B bouton or total bouton numbers compared to the *CantonS*/*w1118*$^{(Iso31)}$ control or the *DFmr1*$^{\Delta 113}$ heterozygote (Figures 17A and 17C). Interestingly, only the *Dcp1*^{442P} heterozygote and

DFmr1$^{\Delta 50}$/*Dfmr1*$^{\Delta 113}$ trans-heterozygote showed a significant increase in 1S bouton numbers over the *CantonS*/*w1118*$^{(Iso31)}$ controls (Figure 18B).

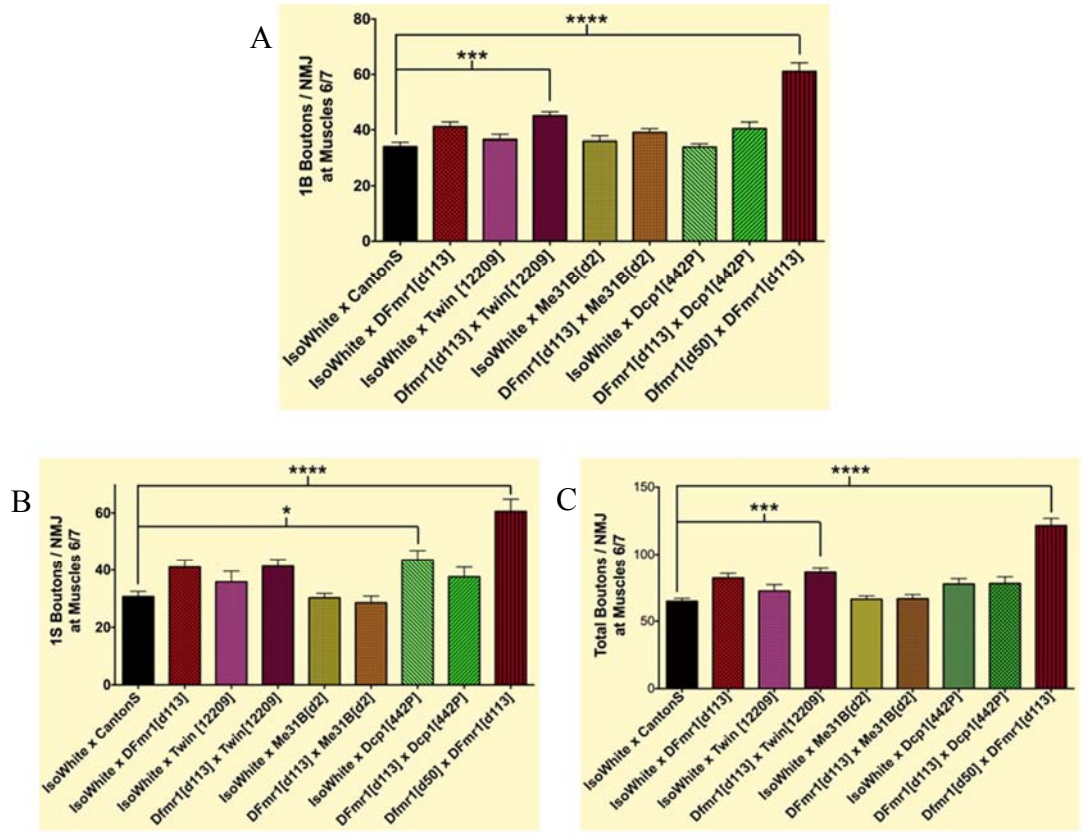

Figure 18: Genetic Effects of the Loss of P-Body Components and FMRP at the *Drosophila* NMJ

Virgin flies from the *w1118*$^{(Iso31)}$ line, as well as virgin flies from the DFmr1$^{\Delta 113}$ lines were crossed to males containing the *HPat*$^{\Delta 3}$ allele, the *Twin*^{12209} allele, and *Dcp1*^{442P} allele. Third-instar larval offspring were screened for absence of a larval marker, then dissected, fixed, and stained with Mouse anti-Discs Large antibody followed by Goat anti-Mouse AlexaFluor-488 and Goat anti-HRP-Dylight649 (far red). (A-C) Muscles 6/7 from segment A3 were imaged on a confocal microscope, then the number of (A) 1B, (B)1S, and (C) total boutons were quantified from muscles 6/7. Error bars indicate mean ± SEM. Statistics: One-way ANOVA followed by Tukey's post-test. **p < 0.01, *** p < 0.001 and **** p < 0.0001.

Given that the larvae homozygous for *HPat*$^{\Delta 3}$ showed a statistically significant increase in bouton numbers compared to controls, this suggests that P-body components may play a role in influencing NMJ structure independently of FMRP. Therefore, the next experiment was to test this possibility. New deletion lines for Twin, Me31B, and Dcp1 were crossed to a *w1118*$^{(Iso31)}$ control and to the deletion lines previously tested, and it was found that both Twin^{8115} and Dcp1^{442P} heterozygous expression produced a significant increase in 1B boutons at muscles 6/7, which was increased in Twin by the trans-heterozygous expression of *Twin*^{12209}, but not in Dcp1 with additional expression of the *Dcp1*^{b53} allele. Homozygous expression of *HPat*$^{\Delta 3}$ also produced a significant increase in 1B boutons over controls, but heterozygous expression did not (Figure 18A). The increase in bouton numbers resulting from *Twin*^{8115} was seen only in 1B boutons, not 1S (Figure 18B), though the increase in 1B boutons was significant enough from trans-heterozygous expression of both *Twin* knock-down alleles that it still caused a significant increase in total boutons over controls (Figure 18C). *HPat*$^{\Delta 3}$ expression did not produce a significant increase in 1S boutons or overall bouton numbers. Heterozygous expression of the *Dcp1*^{442P} allele did lead to an increase in 1S boutons (Figure 18B), which also led to a significant increase in total boutons over controls (Figure 18C). However, this did not culminate in a more significant increase in bouton numbers when *Dcp1*^{442P} was trans-heterozygously expressed with *Dcp1*^{b53}.

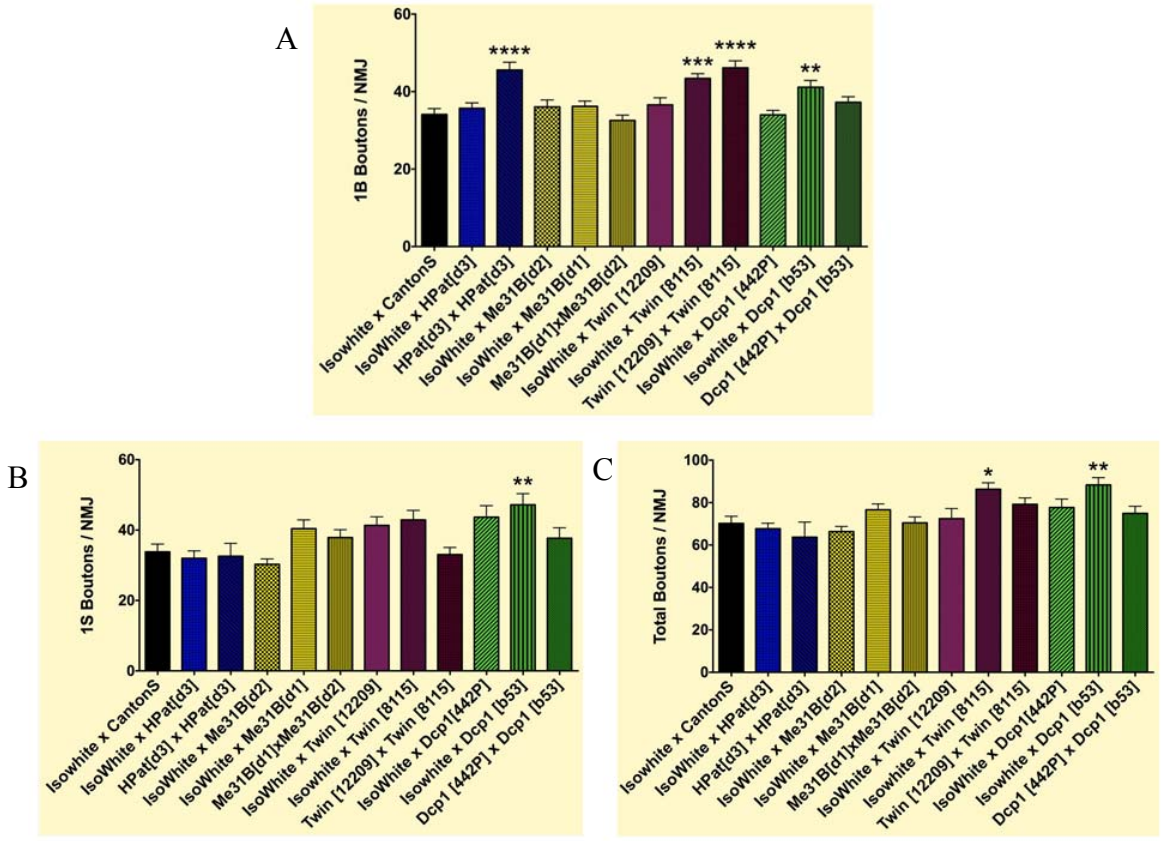

Figure 19: The Genetic Effects of P-Body Component Knock-Down on Bouton Numbers at the *Drosophila* Neuromuscular Junction

Virgin female *w1118*$^{(Iso31)}$ flies were crossed to males of each of *CantonS* wildtype flies, or flies containing each of the following alleles: *HPat*$^{\Delta 3}$, *Me31B*$^{\Delta 2}$, *Me31B*$^{\Delta 1}$, *Twin*^{12209}, *Twin*^{8115}, *Dcp1*^{442P} and *Dcp1*^{b53}, and flies for either allele for each P-body component were crossed to each other. Larvae were selected using a larval balancer marker for each gene, then dissected, fixed, and stained with Mouse anti-Discs Large antibody followed by Goat anti-Mouse AlexaFluor-488 and Goat anti-HRP-Dylight649 (far red). (A-C) Muscles 6/7 and (D-E) muscle 4 from segment A3 were imaged on a confocal microscope, then the number of (A) 1B, (B)1S, and (C) total boutons were quantified from muscles 6/7. Error bars indicate mean ± SEM. Statistics: One-way ANOVA followed by Tukey's post-test. **p < 0.01, *** p < 0.001 and **** p < 0.0001.

Chapter Four: Analysis and Discussion

Chapter 4.1: Analysis of Differential Expression of miRNAs

Processes of learning and long-term memory are largely dependent upon new protein synthesis and fine-tuned expression at the synapse in response to activity stimulation (Saab et al., 2014). As translational repressors, miRNAs underlie processes of protein expression from pathways ranging from neurogenesis (Follert et al., 2014) to cancer regulation (Li et al., 2014), and therefore hold the potential to regulate protein expression associated with learning and long-term memory. miRNAs have shown involvement in the fine-tuning expression of proteins underlying synaptic plasticity (Sosanya et al., 2013) and dendritic spine formation (Schratt et al., 2006). However, each miRNA is capable of repressing many targets (Lewis et al., 2005; Friedman et al., 2009; Li et al., 2014), and each potential target mRNA may be regulated by multiple miRNAs (Bartel, 2009), so there is still much to be discovered regarding which miRNAs regulate expression of which proteins involved in synaptic growth and modifications. Part of unveiling precisely which miRNAs may be involved neuronal development is first to establish which miRNAs are expressed in neurons in the first place, and second, how that expression changes in different stages of development. For the purposes development and growth in *Drosophila*, including the growth of neurons and overall development of the neuromuscular junction, the most important

transition may be the transition from the larva to the adult. Therefore, we utilized Next-Generation Sequencing (NGS) and analysis for comparison of absolute expression of miRNAs from the larval Central Nervous System (CNS) to the adult brain.

Initially, the number of reads generated from this dataset was approximately 94 million reads. Trimming of adapter sequences, filtering for quality and size decreased these numbers to little over 1 million reads per extract. Though this process substantially decreased the number of reads, it helped to ensure the reliability of our data by ensuring analysis of only the highest quality reads, and 1 million reads is still a large dataset for the purposes of miRNA analysis. The reads were then processed using the MPI-HLR miRNA pipeline (MIRPIPE; Kuene et al., in press). MIRPIPE clusters NGS reads together that differ only at the 3' end, which can be classified as isomers of miRNAs "isomiRs," which can result from Dicer and Drosha processing errors (Morin et al., 2008; Martí et al., 2010). Other databases and processing techniques do not necessarily take isomiRs into account, and therefore can underestimate the number of reads for a particular miRNA when those reads do not match database records one hundred percent (Lee et al., 2010). However, studies show that these isoforms are still valid, as they typically deviate by only 1-2 nucleotides at the 3' end, which is far less stringent in its requirements for precise base-pair matching to targets (Guduric-Fuchs et al., 2012); therefore, these isomiRs still target the same mRNAs and thus were counted in the total number of reads in each tissue.

One of the best-known molecular models for synaptic growth associated with learning and long-term memory in *Drosophila* is analysis of the neuromuscular junction

(NMJ) after trains of synaptic stimulation (Shen and Ganetzky, 2010). Because of this, our greatest interest was examining the expression of miRNAs in the larval CNS. Comparison of absolute expression of miRNAs in terms of reads-per-million between the larval CNS and adult brain showed the strongest enrichment for miRs-315, -184, -276A, -92B, and -10 (Figure 3) in the larval CNS compared to the adult brain. This list of miRNAs is interesting in and of itself because of the difference in overall expression. However, as this study's focus is on the roles of miRNAs to regulate neuronal growth, it seemed that the even more interesting miRNAs would be those that were not only most enriched in the larval CNS, but also those with the greatest number of potential targets pertaining to neuronal development.

To analyze the significance of these miRNAs relative to potential targets, we utilized the fact that miRNAs typically require 100% complementarity to their targets in a 7-8 base-pair seed region—base-pairs 2-8 or 2-9 of the miRNA (Lucas and Raikhel, 2013), and the online program TargetScanFly, which compares the seed region sequences of known miRNAs to potential target mRNAs. TargetScanFly compares miRNA seed regions to potential matches in mRNAs, and examines conservation of these sites between *Drosophila* species. The idea behind this process is that if a miRNA binding to a target mRNA is important for development, those sequences will be conserved throughout many species. Thus, an increase in the conservation of a miRNA-mRNA binding site increases the likelihood of a relevant interaction (Ruby et al., 2007).

To further analyze the potential role of these miRNAs, the compiled lists of mRNA targets for each miRNA were processed using the Database for Annotation,

Visualization and Integrated Discovery (DAVID). DAVID compiles lists of functional annotations for each given gene, then groups these functional annotations together into groups where the functions are similar or seemingly related. It also gives the value for the enrichment of the given genes by a modified Fisher Exact P-Value (Huang et al., 2009A; Huang et al., 2009B). Ultimately, this analysis revealed that the miR-9 family and miR-315 are strongly predicted to regulate mRNAs involved in neuronal development and differentiation; both the miR-9 family and miR-315 also are predicted to regulate overlapping targets, which in turn, are strongly enriched in the functions for cytoskeleton rearrangement, which is key for neuronal growth (Prokop et al., 2013), and neuronal development (Table 8). Overlapping targets for miR-315 and miR-275 showed enrichment for a similar functional annotation group (Table 9). Altogether, these results strongly support the notion that these miRNAs are of key interest to us for better understanding the processes underlying learning and long-term memory. However, it is important to note that while these functional annotation groups were formed between miRs -315 and the miR-9 family and miR-275, the other 2 most abundant miRNAs/ miRNA families, the miR-92 family and miR-11, formed more unpredictable groups.

Interestingly, the most-enriched functional annotation clusters for miR-11 with enrichment scores of 7.04 and 5.04 from the DAVID program predicted miR-11 to bind mostly to targets involved in cellular membranes or DNA transcription (Table A9 and data not shown). These include members of immunoglobulin families and transmembrane signaling proteins. Members of the immunoglobulin superfamily include cell adhesion molecules (Ig-CAMs), which are essential for synaptic plasticity (Lüthl et al., 1994;

Muller et al., 2000), LTP (Staubli et al., 1998), and Long-Term Depression (LTD; Bukalo et al., 2004), by regulating the activities of NMDA receptors and calcium ion channels (Dityatev et al., 2008). The role of cell adhesion molecules in synaptic growth is well-understood, as interactions between these molecules can trigger signaling cascades to induce new synaptic formation or structural modifications of existing synapses (Dalva et al., 2007; Wainwright and Galea, 2013). Similarly, transmembrane signaling proteins, such as Frizzled, a predicted target of miR-11, are highly involved in synaptic growth. These signaling pathways trigger neuron outgrowth, cell proliferation and differentiation, and thus affect synaptic growth (Shah et al., 2009; Zhong, 2008).

The miR-92 family, which was by far, the most fold-enriched of the abundance-enriched miRNAs in the larval CNS, was most predicted to regulate targets associated with transcription regulation and DNA binding (Table A1). As mentioned previously, this was also the second-most enriched functional annotation target cluster for miR-11. While immediate modifications to the synapse such as those involved in early Long-Term Potentiation (LTP) require immediate increase in protein synthesis from pools of translationally inhibited mRNAs, further modifications associated with long-term memory, such as late LTP, require an increase in protein transcription (Costa-Mattioli et al., 2009). Current models of long-term memory formation stipulate that, prior to synaptic stimulation, mRNAs necessary for neuronal growth and synaptic modification are transcribed in the neuronal cell body and held in a state of repression by RNA transport granules, which include translational repressor proteins, as well as miRNAs. These granules move into the dendrites and maintain the mRNAs in a state of repression until

they are needed—upon synaptic stimulation—at which point, the granules dissociate, allowing for rapid translation and synthesis of proteins essential for synaptic growth (Sánchez-Carbente and Desgroseillers, 2008). Thus, it is conceivable that while some miRNAs such as miRs -315, -275, and the miR-9 family are associated with such granules involved in temporary repression of mRNAs related to neuronal development, others, such as the miR-92 family, and potentially miR-11, are more involved with the transcriptional activation necessary for late LTP.

Overall, the significant enrichment of miRs -315, -275, -11, the miR-9 family, and the miR-92 family in the larval CNS compared the adult brain, and the fact that most of these miRNAs are predicted to regulate targets with known involvement in neuronal growth, differentiation, and synaptic plasticity strongly implicates these miRNAs in neuronal development. The only deviant from this pattern is the miR-92 family, which, incidentally, also showed the strongest fold-enrichment in the larval CNS compared to the adult brain. While the other enriched miRNAs seem to show heavy and direct involvement with regulating members of neuronal growth pathways, the miR-92 family is most strongly predicted to regulate targets involved in transcription. It is possible, given the evidence that transcription is also an essential component of learning and long-term memory, that the miR-92 family is contributing to synaptic modifications underlying these processes in this way.

Overall, the miRNAs of greatest interest for investigating processes of learning and long-term memory, based on their abundance and fold-enrichment, as well as their predicted ability to regulate targets associated with these processes, are miRs -315, -275,

-11, and the miR-9 family. By temporarily repressing translation of mRNAs key to synaptic growth, these small molecules potentially provide the mechanism for specific expression to induce growth at synapses in response to synaptic stimulation, serving as the basis for strengthened synaptic connections thought to underlie learning and long-term memory formation. It is important to recognize that while the seed region sequence is essential for miRNA binding to mRNA targets, it is by no means the only determining factor for this association. To identify mRNAs with a greater likelihood of being true targets, it is important to consider other factors using other target prediction algorithms (Tarang and Weston, 2014). This would be a good idea for future studies trying to find the relevant targets of these miRNAs, as targets that appear using multiple algorithms are more likely to be true targets. This evaluation would also help to narrow down the list of possible targets. However, the only true way to determine if a mRNA is a specific target of a miRNA, is to test this interaction directly. Thus, the next step in our process of understanding learning and long-term memory is to figure out what these miRNAs are targeting.

Chapter 4.2: Larvally-enriched miRNAs Target *Futsch in vitro* but Not Necessarily *in vivo*

Based on our results, the miR-9 family and miR-315 clearly show repression of a *Futsch* 3'UTR reporter *in vitro* (Figure 6) when overexpressed, and this interaction is sequence-specific to the miRNA binding sites. Each of miRs -9A, -9B, -9C, and -315 strongly repressed Firefly Luciferase to Renilla Luciferase ratios more than two-fold compared to an empty vector control, and this effect was obliterated by mutagenesis of the seed-region binding sequences for the miR-9 family and miR-315, as previously

shown by Leslie Rozeboom (unpublished). However, this interaction is not necessarily seen *in vivo* (Figure 9 and 10). Even with the observance of phenotypes from multiple lines expressing the sequences used to overexpress miRNAs in S2 cells, there was no apparent decrease in bouton number or bouton size that would be indicative of a decrease in Futsch expression (Figure 10; Roos et al., 2000). In fact, the only significant phenotypes observed in response to overexpression of the miR-9 family or miR-315 using a pan-neuronal or motor neuron driver was an increase in the number of boutons—the opposite of what would be expected if Futsch levels were decreased. Thus, it is possible that although these miRNAs target and repress a *Futsch* reporter *in vitro*, they may not target *Futsch in vivo*. However, there are other possible explanations for the absence of a *Futsch*-deficient phenotype.

One possible explanation for the absence of a phenotype indicative of decreased Futsch expression is that the miRNA overexpression constructs are not functional. It is important to note that while we have tested the efficacy of these miRNAs *in vitro* using a target reporter, we have not yet verified that these constructs overexpress the miRNAs *in vivo*. Our lab is working on a Venus reporter under the control of the tubulin promoter for insertion into fly lines. Once this reporter is generated, we could insert the target sequence for these miRNAs into the 3'UTR of the reporter, then cross the flies expressing the reporter to flies overexpressing the miRNA under a Patched Gal-4 driver to express these constructs in wing discs, and examine for decreased reporter expression to verify that the miRNA constructs function properly *in vivo* as well.

Another potential explanation for the absence of an effect for miRNA overexpression is the fact that these miRNAs are already so abundant in the larval CNS (Figure 3), that increasing expression might produce little tangible effect. An overabundance of miRNAs would saturate the potential targets, preventing additional miRNAs from binding to them. Additionally, every miRNA has numerous potential targets (Chi et al., 2009; Helwak et al., 2013; Iyengar et al., 2014), therefore, it is possible that the miRNAs being overexpressed in each of these fly lines is affecting multiple targets, some of which may normally repress synaptic growth. If a repressor of synaptic growth were a greater target for the miR-9 family and miR-315, overexpression of these miRNAs would lead to a decrease in synaptic growth. Therefore, while the overexpression of the miR-9 family and miR-315 did not produce the phenotype expected of Futsch repression, these results are by no means surprising.

Chapter 4.3: Knock-Down of the miR-9 Family and miR-315 *in vitro* Does Not Show De-Repression of a *Futsch* Reporter

Futsch reporter expression does not increase when miRNA sponges are transfected into S2 cells (Figure 8) nor do larvae express increased bouton numbers or decreased bouton size when these sponges are expressed in fly lines using the UAS-Gal4 system (Figure 12). Dual-luciferase assays including the *Futsch* 3'UTR reporter and miR-9 or miR-315 sponges produced ambiguous results, suggesting that down-regulation of these miRNAs does not lead to up-regulation of this reporter *in vitro*. We know that the sponges function, because insertion of each sponge into its own Firefly Luciferase reporter and transfection with miRNA overexpression plasmids led to strong repression of this reporter in S2 cells. However, miR-9B was unable to bind to the miR-9 sponge

sequence in order to repress the reporter (Figure 7). The reason for this may be due to a single nucleotide shift in the miR-9B sequence compared to the miR-9A and miR-9C sequences, which could affect the ability of the miRNA to bind to the target. This shift in nucleotides and the inability of miR-9B to bind to the miR-9 sponge could explain why there is no up-regulation of a *Futsch* 3'UTR reporter *in vitro*. Even if the sponges transfected into S2 cells are able to knock down miR-9A and miR-9C expression, endogenous miR-9B still exists and is capable of repressing the *Futsch* 3'UTR reporter on its own (Figure 6), therefore, transfection of the miR-9 sponge would not necessarily induce an increase in *Futsch* 3'UTR reporter expression. Contrastingly, miR-315 is not at all abundant in S2 cells (Chung et al., 2008), therefore, introduction of an overexpression vector into the cells would indeed lead to the repression of the *Futsch* 3'UTR reporter, but introduction of a miR-315 sponge might have no effect because there are so few endogenous miRNAs to repress the reporter in the first place, preventing any visible de-repression from occurring.

Chapter 4.4: Knock-Down of the miR-9 Family *in vivo* Shows Increased Synaptic Growth Characteristic of an Increase in *Futsch* Expression, But Knock-Down of miR-315 Does Not Produce the Same Effect

Our experiments suggest that miR-9B is somewhat abundant in the *Drosophila* larval CNS, though the expression is the least of any of the miR-9 family, and its abundance is little over 1,000 reads per million (0.1%). Ergo, expression of a miR-9 sponge that affects only miR-9A and miR-9C might be ineffective at de-repressing *Futsch*. However, a significant phenotype was observed at the NMJ when two copies of a miR-9 sponge were expressed in a single fly, suggesting that miR-9A and miR-9C may

in fact be important in repressing a target—or multiple targets—essential for synaptic growth. Whether or not that target is *Futsch* is a question to be examined with future studies. A simple way to examine this would be to use the same larvae examined in Figures 10 and 11, isolate protein and RNA from the CNS from these larvae, and perform a quantitative Western Blot and qRT-PCR on these two separate extracts to analyze for Futsch abundance compared to a control in response to expression of the miR-9 overexpression plasmid or the miR-9 sponge.

miR-9 in mammals matches the *Drosophila* miR-9A sequence completely (Aravin et al., 2003), and is highly enriched in the mammalian brain (Lagos-Quintana et al., 2002; Sempere et al., 2004). In mammalian embryonic stem cells, inhibition of miR-9 results in decreased neuronal differentiation (Krichevsky et al., 2006). In *Drosophila*, miR-9A affects sensory neuron and organ development, but does not absolutely switch expression of its targets off by its expression. Ergo, while the expression of miR-9A may be essential for neuronal development, it is not the sole determining factor of whether or not synaptic growth is repressed (Li et al., 2006). Numerous models have proposed that miRNAs, while obviously relevant for study, may act more as a buffering system for translational regulation rather than sole managers of mRNA fate. The effects seen in these studies potentially support this idea, though the significant changes in the number of boutons resulting from miR-9 knock-down suggest otherwise.

One potential caveat to the absence of a synaptic phenotype in response to miR-315 knock-down is that miR-315 is so much more abundant than any other miRNA in the larval CNS (Figure 3), that it may be impossible to knock down this miRNA sufficiently

to see a phenotype. Its abundance and the fact that it is predicted to regulate groups of targets responsible for synaptic growth (Figure 3 and Table 7) suggests that it is playing a very important role in synaptic development; therefore, it would be worth investigating the role of miR-315 further. One way to knock down miRNA expression *in vivo* more efficiently would be to generate a miR-315 deletion line. Currently, no commercially-available deletion fly lines exist for miR-315 according to FlyBase.org, though one was generated and published using the Clustered Interspersed Short Palindromic Repeat (CRISPR) technique (Kondo and Ueda, 2013). Using commercially-available plasmids and the plasmid used in that experiment, it may be possible to generate a stable miR-315 deletion fly line using the CRISPR technique. I have generated primer sequences for this purpose and borrowed the plasmid used in Kondo and Ueda (2013) for generating miR-315 deletion fly line, and in the near future, our lab can generate this line for analysis of miR-315's effects on NMJ structure. Further, if deletion of one copy of miR-315 is insufficient and a homozygous deletion is not viable, it would also be possible to cross a miR-315 deletion fly to any of the miR-315 sponge lines I have generated to knock down miR-315 expression further without completely eliminating it to see if such a decrease in expression would have an effect.

Chapter 4.5: FMRP Does Not Interact Directly with the *Futsch* mRNA or miRs -9A, -9B, -9C and -315

Although we have not yet verified repression of *Futsch in vivo* by the miR-9 family or miR-315, the *in vitro* results are compelling. Further, there is strong evidence suggesting that FMRP not only binds to the *Futsch* mRNA and represses Futsch expression (Zhang et al., 2001), but also interacts directly with miRNAs (Edbauer et al.,

2010) and components of the miRNA pathway (Jin et al., 2004). Thus, we were interested in finding out if FMRP and miRs -9A, -9B, -9C, and -315 interact to physically bind and repress *Futsch* translation.

The first step in this process was to figure out if and where FMRP may bind to *Futsch* to repress expression. For this, we used an *in vitro* approach. An FMRP overexpression was generated from a cDNA clone available from DGRC (see Materials and Methods) and verified its role as an overexpression plasmid by Western Blot (Figure 13). Generation of a *Futsch* reporter was more involved. The *Futsch* mRNA is extremely large, encompassing close to 20 kilobases in length (Flybase.org; St. Pierre et al., 2014), and forming a product over 500 kilodaltons (Hummel et al., 2000), which is too large for insertion into a single vector for examination by *in vitro* analysis. Hence, I broke up the *Futsch* mRNA into 12 manageable fragments (in addition to the 3'UTR reporter already generated by Leslie Rozeboom) for insertion into a Firefly Luciferase reporter for expression in S2 cells (Figure 13D).

Results demonstrated that not only did FMRP not significantly repress any of the *Futsch* reporter fragments, but also significantly increased the FLuc/RLuc ratio for many fragments. There is one important caveat to the analysis performed here, and that is the fact that each of these *Futsch* reporters was inserted into a vector originally designed to test 3'UTRs. Therefore, the reporters occur within the 3'UTR region of Firefly Luciferase, and do not contain a 3'UTR or polyadenylation sequence of their own. Absence of a polyA signal can affect mRNA translation and stability (Ford et al., 1997; Preiss and Hentze, 1998). Therefore, to be sure these unexpected results are not artifacts

of improper mRNA processing, these experiments could be repeated by adding an SV40 3'UTR with a polyadenylation signal like that included in the RLuc control vector. However, in the absence of a proper polyadenylation signal, previous research suggests that translation should be hindered, not enhanced (Zhao et al., 1999). Furthermore, there is recent evidence that the polyadenylation signal may not be essential for RNA translation (Searfoss and Wickner, 2012), indicating that the enhanced FLuc/RLuc ratio is most likely due to FMRP overexpression alone, rather than some combination with improper translation of the Firefly Luciferase reporter. This suggests a potential role for FMRP as a translational activator, rather than a translational repressor, which has been seen in previous research (Bechara et al., 2009; Soden and Chen, 2010; Gross et al., 2011), even pertaining to MAP1B expression (Chen et al., 2003). The possibility of FMRP acting as a translational activator would contradict the study by Zhang et al. (2001) off of which this study was based, but it could be investigated by examining Futsch abundance in FMRP-deficient flies using Western Blot of head extract, or quantification of a unique loop structure formed by Futsch at the NMJ (Roos et al., 2000).

Another possible explanation for the up-regulation, rather than down-regulation of *Futsch* reporters by FMRP is that FMRP has previously been shown to bind and repress expression of Renilla Luciferase (Chen et al., 2014). If FMRP selectively represses Renilla Luciferase, then overexpression of FMRP in S2 cells with a dual-luciferase assay could lead to a significant increase in the FLuc/RLuc ratio by decreasing RLuc expression. Additionally, if the artificially-introduced RLuc reporter is a better target for FMRP in this *in vitro* assay than the *Futsch* reporters we are testing, then we will not be

able to see the *Futsch* reporter repression. This possibly explains why none of the assays including a *Futsch* reporter show a decrease in the FLuc/RLuc ratio compared to controls in which FMRP was not overexpressed. Further, this proposition is supported by the fact that when increased amounts of FMRP were added to S2 cells with one of the *Futsch* reporters, we saw a dose-dependent increase in the FLuc/RLuc ratio (Figure A2). Future studies should examine whether or not RLuc expression is being affected by co-transfection with an FMRP overexpression plasmid by performing quantitative Western Blot analysis on transfected S2 cells. Antibodies against Firefly Luciferase and Renilla Luciferase are commercially available for this purpose (www.pierce-antibodies.com). If, in fact, RLuc expression is being manipulated by FMRP, it might be more prudent to co-trasfect the FLuc reporter and FMRP overexpression plasmid, and instead of performing a dual-luciferase assay, simply perform quantitative Western Blot analysis to see if the reporter is being down-regulated.

Although we were not able to show direct binding of FMRP to *Futsch* reporters in an *in vitro* assay, the evidence suggesting that FMRP translationally represses *Futsch* *in vivo* is compelling (Zhang et al., 2001). Plus there is the possibility that despite being and RNA-binding protein, FMRP's interaction with *Futsch* is more indirect. Regardless of whether FMRP is interacting directly with the *Futsch* mRNA or some other target, the fact remains that FMRP has a known role as a repressor of translation (Laggerbauer et al., 2001; Li et al., 2001; Muddashetty et al., 2007) and that this is a potential mechanism for FMRP's inhibition of synaptic growth (Todd et al., 2003; Vanderkilsh and Edelman,

2005). Understanding not only which targets FMRP represses, but also how it represses targets is therefore essential.

FMRP interacts with components of the miRNA pathway in *Drosophila* and mammals (Caudy et al., 2002; Xu et al., 2004; Ishizuka et al., 2002; Lugli et al., 2005; Kelley et al. 2012; Xu et al., 2012; Tian et al., 2013), and immunoprecipitates with mature miRNAs that, when mis-expressed, affect synaptic growth (Edbauer et al., 2010). It has therefore been proposed that miRNAs may mediate FMRP translational repression for the purposes of affecting synaptic structure, which could provide an indirect link between FMRP and translational repression of the target *Futsch*. The overall enrichment of the miR-9 family and miR-315 in larval CNS and their demonstrated ability to repress a target known to affect synaptic growth *in vitro* therefore makes them excellent candidates as potential interactors with FMRP.

To examine a potential interaction between FMRP and the miRNAs of interest in a physical complex, an immunoprecipitation against FMRP was performed in fly head extract, the RNA was isolated from the eluant, and qRT-PCR analysis of these miRNAs was performed and compared to negative control immunoprecipitations (IgG and beads-only), and compared to a U1 negative control (small RNA that is not predicted to interact with FMRP). Figure 14 shows clearly that there is no enrichment of miRs -9A, -9B, -9C or -315 in an FMRP immunoprecipitation extract compared to an IgG immunoprecipitation extract or immunoprecipitation extract from magnetic beads only. All of the small RNAs did appear at a lower cycle number—suggesting greater abundance—in the input control, which contained 10% of the extract that was used for

the immunoprecipitation, demonstrating that these small RNAs were present in the initial extract.

Ultimately, the role of the miR-9 family and miR-315 are yet to be elucidated. The analysis provided thus far on Futsch suggests that it may be a target of repression by these miRNAs and thus they may affect synaptic growth. However, more detailed analysis using better knock-down techniques is needed to discern if these miRNAs do in fact, repress targets responsible for synaptic growth, and if *Futsch* is specifically the target underlying this modification. Furthermore, although FMRP is known to interact with both *Futsch* and miRNAs, it does not appear to interact with the miR-9 family or miR-315 to co-regulate *Futsch* translation. It is still possible that FMRP interacts with other miRNAs to repress other targets, but further analysis should be performed to investigate these potential interactions.

Chapter 4.6: FMRP Co-Localizes and Interacts in a Physical Complex with Some P-Body Components

The final translational repression pathway we wanted to investigate as a potential effector of synaptic structure was P-bodies. FMRP has known interactions with P-body components (Barbee et al., 2006; Wang et al., 2008). It also acts as a repressor of synaptic growth (Zalfa et al., 2003; Lu et al., 2004; Nahm et al., 2010). Therefore, we sought to investigate whether FMRP requires P-body components for this function.

In yeast, the homolog for Twin (CCR4) initiates 3' trimming of mRNAs designated for 5' to 3' degradation, and associates with both Pat1/Mrt1p (HPat homolog) and Dcp1/Dcp2 (Meyer et al., 2004; Tharun and Parker, 2001). It has thus been proposed that mRNAs targeted for 5' to 3' degradation are selectively deadenylated by Twin, which

is followed by association with Pat1/Mrt1p (HPat homolog) and Dcp1/Dcp2 for the purposes of decapping and 5' to 3' degradation. The mammalian homolog of Twin (CCR4) interacts with the homolog for Me31B (Rck) *in vivo*, and these two proteins are mutually dependent upon each other for expression in P-bodies (Andrei et al., 2005). Such tight associations as those required by interacting P-body components suggests that, at the very least, these proteins should be found in close proximity to each other in cells.

FMRP has been shown interact with P-body components by co-localization, but this co-localization is never one hundred percent. P-bodies are known to be very heterogeneous RNPs, and FMRP is known to associate with other granule types beyond P-bodies (Wang et al., 2008; Barbee et al., 2006). It is therefore not surprising that even with such strong interactions as those shown with HPat and Me31B, there is not complete overlap of these P-body components and FMRP (Figure 15). In fact, the percent co-localization between FMRP and Me31B is similar to previous published studies, albeit slightly lower (Barbee et al., 2006), and percent co-localization of FMRP with HPat nearly matches previous findings from our lab (Pradhan, unpublished). Surprisingly, the co-localization of FMRP with Twin was much lower than with that of either Me31B or HPat, though it was still significant, as the two proteins co-localized in nearly 31% of all observed punctae in cultured neurons. This again demonstrates the overall heterogeneity not only of P-bodies, but also of FMRP's association with RNP complexes. The overlap suggests that FMRP is associating with these P-bodies for a purpose, which is most likely translational regulation. This theory, however, would be better supported by

demonstration of actual interactions between FMRP and P-body components in physical complexes.

FMRP has previously shown to co-immunoprecipitate with Me31B (Barbee et al., 2006) and HPat (Pradhan, unpublished) in *Drosophila*, indicating that the proposed physical interaction with P-bodies does in fact, occur. However, to validate these prior findings and further elucidate FMRP's interaction with P-bodies, we co-immunoprecipitated FMRP with the P-body components Me31B, Twin, HPat, and Dcp1. Expression of tagged constructs in S2 cells was validated by Western Blot showing both the HA tag for FMRP, and the V5 tag for Me31B, Twin, and Dcp1, and by endogenous antibodies for all proteins examined except Dcp1 (Figure 16A).

Immunoprecipitation of FMRP was verified by Western Blot using anti-DFmr1 antibody. Tagged and endogenous Me31B co-immunoprecipitated with FMRP, as did tagged Dcp1, and endogenous HPat. There was a very faint association of tagged Twin with FMRP, but this was not mimicked with endogenous Twin, suggesting that the minor interaction may have been more of a byproduct of the V5-His tag rather than a real association of FMRP and Twin in a physical complex (Figure 16B). However, this should be further investigated, possibly by expressing more of the tagged Twin construct in S2 cells to enhance the interaction. An untagged construct could also be used to overexpress endogenous Twin in an attempt to view if there is any interaction between FMRP and the endogenous protein.

The fact that HPat was not seen intact with the V5 tag in the original extract indicates that the tag may have had an effect on the protein itself and prevented proper

folding and/or expression of HPat from the transgenic construct. However, the fact that endogenous HPat still co-immunoprecipitated with the tagged FMRP indicates that the two proteins do in fact, interact in a physical complex, even in the absence of overexpression or a tag. Interestingly, this interaction between tagged FMRP and endogenous HPat did not occur in the control (untransfected) extract, or the extract from cells transfected with tagged Me31B. However, it is important to note that these two extracts were on the other side of the original blot from the other three extracts that did show and interaction between FMRP and endogenous HPat, and the band in those three extracts was not incredibly strong, which suggests the absence of a band in the control lane and Me31B extract lane may be due to simple experimental variation. To verify the HPat results, this experiment should be repeated. And further enhancement of the interaction between HPat and FMRP could occur, similar to enhancing any potential interaction with Twin, by generating a construct for overexpression of native HPat and transfecting it into S2 cells prior to immunoprecipitation.

In any case, the fact that FMRP co-localizes with Me31B, Twin, and HPat, and previous studies have shown also, Dcp1 (Eystathioy et al., 2003), shows that FMRP physically interacts with these proteins and they exist together in a complex. P-bodies are known sites of translational repression and mRNA degradation (Sheth and Parker, 2003; Anderson et al., 2009; Walters et al., 2014), therefore, in a model where translational repression is key to control of synaptic growth, P-bodies are an essential component. Given FMRP's known role as a repressor of synaptic growth, and the fact that and this interaction with P-body components occurs in neurons, this suggests that the mechanism

by which FMRP represses synaptic growth may be translational repression mediated by P-bodies.

Chapter 4.7: FMRP Interacts Genetically with P-Body Component HPat to Affect NMJ Structure

A previous graduate student in our lab, Sarala Pradhan, performed NMJ analyses suggesting that the P-body component HPat is essential for FMRP repression of synaptic growth. I verified her results, demonstrating that a simultaneous deletion of one copy of *DFmr1* and *HPat* significantly enhances the number of boutons at the NMJ at muscles 6/7 and at muscle 4 over both wildtype controls and flies with the deletion of only a single copy of either gene (Figure 17). This increase in bouton numbers is modest, but significant as well as consistent, suggesting that HPat does in fact, affect FMRP's ability to repress synaptic growth at the NMJ. However, it must be noted that this increase in bouton numbers was not nearly as significant as the increase generated by knocking down two copies of FMRP. This indicates that while HPat does potentially mediate the role of FMRP as an inhibitor of synaptic growth, there are clearly other factors at work that could play a more major role in affecting synaptic structure.

Chapter 4.8: FMRP Does Potentially Interact with Other P-body Component Twin, But Not Me31B or Dcp1 to Affect NMJ Structure

To investigate whether any of the other potential factors affecting FMRP function at the NMJ could be additional P-body components, I performed additional fly crosses with deletion lines of Me31B, Twin, and Dcp1. We learned from the experiment demonstrating an FMRP interaction with HPat that the $DFmr1^{\Delta 113}$ allele is stronger in its effects on NMJ structure than the $DFmr1^{\Delta 50}$ allele. In all cases where either $DFmr1^{\Delta 50}$ or

DFmr1$^{\Delta 113}$ were used, crosses including *DFmr1*$^{\Delta 113}$ always showed more boutons at the NMJ than those including *DFmr1*$^{\Delta 50}$ (Figure 17). I therefore used the *DFmr1*$^{\Delta 113}$ allele for all crosses where knock-down of FMRP was investigated. These crosses showed no statistically significant change in the number of boutons at muscles 6/7 when a single copy of a *DFmr1* deletion was expressed with a single copy of a deletion for *Me31B*, *Twin*, or *Dcp1*, compared to a fly with a single copy of *DFmr1* deleted, suggesting that none of these factors assist FMRP in synaptic structure modification. However, the *DFmr1*$^{\Delta 113}$; *Twin*^{12209} trans-heterozygotes did show a significant increase in the number of boutons compared to wildtype controls, suggesting that Twin could potentially mediate FMRP modification of NMJ structure, but if so, its effect is even more modest than that of HPat, and not much more significant than the effect of the *DFmr1*$^{\Delta 113}$ allele by itself.

Chapter 4.9: P-body Component Twin May Affect NMJ Structure By Itself, But Dcp1 and Me31B Do Not

When investigating the interaction between HPat and FMRP at the NMJ, we found that deletion of 2 copies of HPat was sufficient to induce a statistically significant increase in bouton number compared to wildtype controls independent of FMRP. This was also previously published (Pradhan et al., 2012). Thus, P-body components are capable of affecting synaptic structure on their own. I next investigated the possible roles of other P-body components: Me31B, Twin, and Dcp1, in affecting synaptic structure at the NMJ by performing additional fly crosses with heterozygous expression of deletions of each of these components that I had not already investigated, and trans-heterozygous deletions using two different deletion lines for each component.

Heterozygous deletion of Twin using the *Twin*^{8115} allele led to a significant increase in 1B boutons, but this was further enhanced by double-deletion of Twin. However, this increase in 1B boutons only led to a significant increase in total boutons with the *Twin*^{8115} allele expressed heterozygously, not when co-expressed with the *Twin*^{12209} allele. This is likely due to the fact that there was a noticeable but not statistically significant decrease in the number of 1S boutons resulting from the double-deletion of Twin. Interestingly, this effect was not seen at all with either allele when expressed heterozygously; it was a cumulative effect from combining both deletion lines. Ultimately, Twin may have an effect on synaptic growth that increases the number of 1B boutons at the expense of 1S boutons.

Double-deletion of *Me31B*, or *Dcp1* produced no statistically significant increase in the number of boutons at muscles 6/7 like that seen with a double-deletion of *HPat*. The *Dcp1*^{442P} allele did lead to a very significant increase in both 1B boutons and 1S boutons, and therefore, total boutons when expressed heterozygously, but not when co-expressed with another *Dcp1* deletion allele *Dcp1*^{b53}. *Dcp1*^{442P} is a null allele for Dcp1, while *Dcp1*^{b53} still expresses residual fragments of the protein. It may be possible that *Dcp1*^{b53} is somehow compensating for *Dcp1*^{442P}, but this is highly unlikely given previous published results indicating that *Dcp1*^{b53} also acts as a Dcp1 deletion line (Chen et al., 2006). Thus, the increase in bouton count resulting from *Dcp1*^{442P} is more likely due to some other effect beyond the absence of Dcp1. Given that *Dcp1*^{442P} results an imprecise excision, it is possible that other genes were excised with *Dcp1*, which in turn, could have unforeseen effects on synaptic growth. This suggests that although these components

Me31B and Dcp1 exist in the same P-body complexes, they do not necessarily perform the same functions to inhibit synaptic structural growth. Thus, among the P-body components examined, HPat and Twin appear to have a genetic effect on synaptic structure, while Me31B and Dcp1 do not.

Chapter 4.10: Concluding Remarks

Altogether, the research presented here elucidates the role of translational regulation mechanisms in affecting synaptic structure by examination of the interactions between different components of ribonucleoproteins. Analysis of differential expression of miRNAs in the *Drosophila* CNS at different developmental stages implicates miRs -315, miR-275, miR-11, and the miR-9 family as strong potential regulators of neuronal growth and development. The substantial enrichment of these miRNAs in the *Drosophila* larval CNS compared to the adult brain and enrichment of potential targets with functional annotations pertaining to neuronal growth strongly suggests these miRNAs should be examined to determine what their targets are, and the effects of those targeted interactions.

In these studies, we investigated the roles of miRs -315 and the miR-9 family as potential regulators of *Futsch*. We validated the specific targeting of a *Futsch* reporter by these miRNAs *in vitro*, and further investigation could potentially show this effect *in vivo*. The small changes in structure that occurred at the NMJ in response to miRNA overexpression, and larger structural modifications that occurred in response to miRNA under-expression suggest that knocking down miRNA expression is a superior method for examining their effects at the NMJ.

Although we could not demonstrate an interaction between neuronally-enriched miRNAs and FMRP to co-regulate *Futsch*, the fact remains that FMRP interacts with the miRNA pathway potentially to mediate repression of synaptic growth. Our results suggest that this repression is somewhat mediated by P-body components, particularly HPat and potentially Twin. We verified that FMRP does co-immunoprecipitate with Me31B and HPat, both of which were shown in previous unpublished studies. However, the physical association of FMRP with Dcp1 is a novel interaction, as is co-localization with Twin. Together, these results suggest a mechanism by which FMRP interacts with P-bodies for translational repression resulting in repression of synaptic growth. The interaction is weak in all cases, suggesting it may not be the most important mechanism in this process, or that stronger mediators of this process may exist. As stated previously, all of the P-body components investigated in this study are involved in the 5' to 3' mRNA degradation pathway, whereas the miRNA pathway can lead to either translational repression or degradation. FMRP associates in heterogeneous complexes; it is possible that part of the time it associates with P-bodies as part of a mRNA degradation pathway, and at other times, associates with miRNAs for translational repression.

Clearly, there is still a significant amount of investigation necessary to elucidate the processes of translational repression as they relate to neuronal growth. However, the research presented here demonstrates the importance of enriched miRNAs in the *Drosophila* CNS, their potential role in affecting neuronal growth independently and interacting with FMRP, the interactions between FMRP and multiple P-body components, and the role of individual P-body components in affecting neuronal growth.

Together, these translational mechanisms can result in significant structural changes at the neuromuscular junction, indicative of the potential for functional effects, as well.

List of References Cited

Anderson P., Kedersha N. (2009). RNA granules. Post-transcriptional and epigenetic modulators of gene expression. *Nature Reviews. Molecular Cell Biology*, 10, 430–436.

Andrei, M.A., Ingelfinger, D., Heintzmann, R., Achsel, T., Rivera-Pomar, R., and Lührmann, R. (2005). A role for eIF4E and eIF4E-transporter in targeting mRNPs to mammalian processing bodies. *RNA*, 11(5), 717-27.

Aravin, A.A., Lagos-Quintana, M., Yalcin, A., Zavolan, M., Marks, D., Snyder, B., Gaasterland, T., Meyer, J., and Tuschl, T. (2003). *Developmental Cell*, 5(2), 337-50.

Ashley, C.T. Jr., Wilkinson, K.D., Reines, D., and Warren, S.T. (1993). FMR1 protein: conserved RNP family domains and selective RNA binding. *Science*, 262(5133), 563-6.

Bailey, C.H. and Chen, M. (1983). Morphological Basis of Long-Term Habituation and Sensitization in *Aplysia*. *Science*, 220, 91-93.

Bakker, C.E., and Oostra, B.A. (2003). Understanding fragile X syndrome: insights from animal models. *Cytogenetic and Genome Research*, 100(1-4), 111-23.

Barbee, S.A., Estes, P.S., Cziko, A.M., Hillebrand, J., Luedeman, R.A., Coller, J.M. … and Ramaswami, M. (2006). Staufen- and FMRP-containing neuronal RNPs are structurally and functionally related to somatic P bodies. *Neuron*, 52(6), 997-1009.

Bardoni, B., Mandel, J.L., and Fisch, G.S. (2000). FMR1 gene and fragile X syndrome. *American Journal of Medical Genetics*, 97(2), 153-63.

Behm-Ansmant, I., Rehwinkel, J., Doerks, T., Stark, A., Bork, P., Izaurralde, E. (2006). mRNA degradation by miRNAs and GW182 requires both CCR4:NOT deadenylase and DCP1:DCP2 decapping complexes. *Genes and Development*, 20(14), 1885-98.

Bernstein, E., Caudy, A.A., Hammond, S.M., and Hannon, G.J. (2001). Role for a bidentate ribonuclease in the initiation step of RNA interference. *Nature*, 409(6818), 363-6.

Blankenberg, D., Von Kuster, G., Coraor, N., Ananda, G., Lazarus, R., Mangan, M. … and Taylor, J. (2010). Galaxy: a web-based genome analysis tool for experimentalists. *Current Protocols in Molecular Biology*, Chapter 19:Unit 19.10.1-21.

Bliss, T.V.P. and Lomo, T. (1973). Long-lasting potentiation of synaptic transmission in the dentate area of the anaesthetised rabbit following stimulation of the perforant path. *Journal of Physiology*, London. 232, 331-356.

Braun, J.E., Truffault, V., Boland, A., Huntzinger, E., Chang, C.T., Haas, G., Weichenrieder, O., Coles, M., and Izaurralde, E. (2012). Direct interaction between DCP1 and XRN1 couples mRNA decapping to 5' exonucleolytic degradation. *Nature Structural and Molecular Biology*, 19(12), 1324-31.

Bukalo, O., Fentrop, N., Lee, A.Y., Salmen, B., Law, J.W., Wotjak, C.T. et al. (2004) Conditional ablation of the neural cell adhesion molecule reduces precision of spatial learning, long-term potentiation, and depression in the CA1 subfield of mouse hippocampus. *Journal of Neuroscience*, 24, 1565–1577.

Caudy, A.A., Myers, M., Hannon, G.J., and Hammond, S.M. (2002). Fragile X-related protein and VIG associate with the RNA interference machinery. *Genes and Development*,16(19), 2491-6.

Chan, S.P., and Slack, F.J. (2006). microRNA-mediated silencing inside P-bodies. *RNA Biology*, 3(3), 97-100.

Chen, E., Sharma, M.R., Shi, X., Agrawal, R.K., and Joseph, S. (2006). Fragile X Mental Retardation Protein Regulates Translation by Binding Directly to the Ribosome. *Molecular Cell*, In Press.

Chi, S. W., Zang, J. B., Mele, A., and Darnell, R. B. (2009). Argonaute HITS-CLIP decodes microRNA-mRNA interaction maps. *Nature*, 460, 479–486.

Chu C.Y., and Rana, T.M. (2006). Translation repression in human cells by microRNA-induced gene silencing requires RCK/p54. *PLoS Biology*, 4(7), e210.

Chung, W.J., Okamura, K., Martin, R., and Lai E.C. (2008). Endogenous RNA interference provides a somatic defense against Drosophila transposons. Current Biology, 18(11), 795-802.

Coller J., and Parker, R. (2004). Eukaryotic mRNA decapping. Annual Review of Biochemistry, 73, 861-90.

Collins, C.A., and DiAntonio, A. (2007). Synaptic development: insights from Drosophila. *Current Opinion in Neurobiology*, 17(1), 35-42.

Costa-Mattioli, M., Sossin, W.S., Klann, E., and Sonenberg, N. (2009). Translational control of long-lasting synaptic plasticity and memory. *Neuron*, 61(1):10-26.

Dalva, M.B., McClelland, A.C., Kayser, M.S. 2007. Cell adhesion molecules: signalling functions at the synapse. *Nature Reviews. Neuroscience*, 8(3), 206-20.

Darnell, J.C., Fraser, C.E., Mostovetsky, O., Stefani, G., Jones, T.A., Eddy, S.R., and Darnell, R.B. (2005). Kissing complex RNAs mediate interaction between the Fragile-X mental retardation protein KH2 domain and brain polyribosomes. *Genes and Development*, 19(8), 903-18.

Darnell, J.C., Jensen, K.B., Jin, P., Brown, V., Warren, S.T., and Darnell, R.B. (2001). Fragile X mental retardation protein targets G quartet mRNAs important for neuronal function. *Cell*, 107(4), 489-99.

Daugeron, M.C., Mauxion, F., Seraphin, B. (2001). The yeast POP2 gene encodes a nuclease involved in mRNA deadenylation. *Nucleic Acids Research*, 29, 2448–2455.

Davis, R.L. (1993). Mushroom bodies and *Drosophila* learning. *Neuron*, 1, 1-14.

De Boulle, K., Verkerk, A.J., Reyniers, E., Vits, L., Hendrickx, J., Van Roy, B., … Willems, P.J. (1993). A mutation in the FMR-1 gene associated with fragile X mental retardation. *Nature Genetics*, 3(1), 31-5.

de Valoir, T., Tucker, M.A., Belikoff, E.J., Camp, L.A., Bolduc, C., Beckingham, K. (1991). A second maternally expressed Drosophila gene encodes a putative RNA helicase of the "DEAD box" family. *Proceedings of the National Academy of Sciences, U.S.A.*, 88(6), 2113-7.

Dityatev, A., Bukalo, O., Schachner, M. (2008). Modulation of synaptic transmission and plasticity by cell adhesion and repulsion molecules. *Neuron Glia Biology*, 4(3), 197-209.

Dokudovskaya, S., Williams, R., Devos, D., Sali, A., Chait, B.T., and Rout, M.P. (2006).Protease accessibility laddering: proteomic tool for probing protein struct ure. *Structure*, 14(4), 653-60.

Dölen, G., Osterweil, E., Rao, B.S., Smith, G.B., Auerbach, B.D., Chattarji, S., and Bear, M.F. (2007). Correction of fragile X syndrome in mice. *Neuron*, 56(6), 955-62.

Dostie, J., Mourelatos, Z., Yang, M., Sharma, A., and Dreyfuss, G. (2003). Numerous microRNPs in neuronal cells containing novel microRNAs. *RNA*, 9(2), 180-6.

Ebert, M.S., Neilson, J.R., Sharp, P.A. (2007). MicroRNA sponges: competitive inhibitors of small RNAs in mammalian cells. *Nature Methods*, 4(9), 721-6.

Edbauer, D., Neilson, J.R., Foster, K.A., Wang, C.F., Seeburg, D.P., … Sheng, M. (2010). Regulation of synaptic structure and function by FMRP-associated microRNAs miR-125b and miR-132. *Neuron*, 65(3), 373-84.

Ernsberger, U. (2012). Regulation of gene expression during early neuronal differentiation: evidence for patterns conserved across neuron populations and vertebrate classes. *Cell and Tissue Research*, 348(1):1-27.

Eulalio, A., Behm-Ansmant, I., Schweizer, D. and Izaurralde, E. (2007). P-body formation is a consequence, not the cause, of RNA-mediated gene silencing. Molecular and Cellular Biology, 27(11), 3970–3981.

Eystathioy T,, Jakymiw, A., Chan, E.K.L, Séraphin, B., Cougot, N., Fritzler, M.J. (2003). The GW182 protein co-localizes with mRNA degradation associated proteins hDcp1 and hLSm4 in cytoplasmic GW bodies. *RNA*, 9, 1171–1173.

Filipowicz, W., Jaskiewicz, L., Kolb, F.A., and Pillai, R.S. Post-transcriptional gene silencing by siRNAs and miRNAs. (2005). *Current Opinion in Structural Biology*,15(3), 331-41.

Follert, P., Cremer, H., and Béclin, C. (2014). microRNAs in brain development and function: a matter of flexibility and stability. *Frontiers in Molecular Neuroscience*, 7(7), 5.

Ford L.P., Bagga P.S., and Wilusz, J. (1997). The poly(A) tail inhibits the assembly of a 3′-to-5′ exonuclease in an in vitro RNA stability system. *Molecular and Cellular Biology*, 17, 398–406.

Friedman, R.C., Farh, K.K., Burge, C.B., and Bartel, D.P. (2009). Most mammalian mRNAs are conserved targets of microRNAs. *Genome Research*, 19, 92–105.

Friedman, R.C., Farh, K.K., Burge, C.B., and Bartel, D.P. (2009). Most mammalian mRNAs are conserved targets of microRNAs. *Genome Research*, 19, 92-105.

Fritzsche, R., Karra, D., Bennett, K.L., Ang, F.Y., Heraud-Farlow, J.E., Tolino, M., … Kiebler, M.A. (2013). Interactome of two diverse RNA granules links mRNA

localization to translational repression in neurons. *Cell Reports (Cambridge)*, 5(6),1749-62.

Garza-Manero, S., Pichardo-Casas, I., Arias, C., Vaca, L., Zepeda, A. (2013). Selective distribution and dynamic modulation of miRNAs in the synapse and its possible role in Alzheimer's Disease. *Brain Research*, ii: S0006-8993(13), 01536-9.

Giardine, B., Riemer, C., Hardison, R.C., Burhans, R., Elnitski, L., Shah, P., … and Nekrutenko, A. (2005). Galaxy: a platform for interactive large-scale genome analysis. *Genome Research*, 15(10), 1451-5.

Goecks, J., Nekrutenko, A., Taylor, J. and The Galaxy Team. (2010). Galaxy: a comprehensive approach for supporting accessible, reproducible, and transparent computational research in the life sciences. *Genome Biology*, (8), R86.

Gorter, J.A., Iyer, A., White, I., Colzi, A., van Vliet, E.A., Sisodiya, S., and Aronica, E. (2014). Hippocampal subregion-specific microRNA expression during epileptogenesis in experimental temporal lobe epilepsy. *Neurobiology of Disease*, 62, 508-20.

Griffiths-Jones S. (2004). The microRNA Registry. Nucleic Acids Research, 1,32(Database issue), D109-11.

Griffiths-Jones, S., Grocock, R.J., van Dongen, S., Bateman, A., Enright, A.J. (2006). miRBase: microRNA sequences, targets and gene nomenclature. Nucleic Acids Research, 1, 34(Database issue), D140-4.

Griffiths-Jones, S., Saini, H.K., van Dongen, S., and Enright AJ. (2008). miRBase: tools for microRNA genomics. Nucleic Acids Research, 36(Database issue), D154-8.

Gross, C., Yao, X., Pong, D.L., Jeromin, A. and Bassell, G.J. (2010). Fragile X Mental Retardation Protein Regulates Protein Expression and mRNA Translation of Potassium Channel Kv4.2. *The Journal of Neuroscience*, 31(15), 5693-5698.

Guduric-Fuchs, J., O'Connor, A., Cullen, A., Harwood, L., Medina, R.J., O'Neill, C.L., Stitt, A.W., Curtis, T.M., and Simpson, D.A. (2012). Deep sequencing reveals predominant expression of miR-21 amongst thesmall non-coding RNAs in retinal microvascular endothelial cells.*Journal of Cell Biochemistry*, 113(6):2098-111.

Hagerman, R., Hoem, G., Hagerman, P. (2010). Fragile X and autism: Intertwined at the molecular level leading to targeted treatments. *Molecular Autism*, 1(1), 1-12.

Hammond, S.M. (2005). Dicing and slicing: the core machinery of the RNA interference pathway. *FEBS Letters*, 579(26), 5822-9.

Hammond, S.M., Bernstein, E., Beach, D., and Hannon, G.J. (2000). An RnA-directed nuclease mediates post-transcriptional gene silencing in Drosophila cells. *Nature*, 404(6775), 293-6.

Han, J., Lee, Y., Yeom, K.H., Kim, Y.K., Jin, H., Kim, V.N. (2004). The Drosha-DGCR8 complex in primary microRNA processing. *Genes and Development*, 18(24), 3016-27.

Hatton, D.D., Sideris, J., Skinner, M., Mankowski, J., Bailey, D.B., Jr, Roberts, J., and Mirrett, P. (2006). Autistic behavior in children with fragile syndrome: prevalence, stability, and the impact of FMRP. *American Journal of Medical Genetics Part A*, 140A(17), 1804-13.

Heisenberg, M., Borst, A., Wagner, S., and Byers, D. (1985). *Drosophila* mushroom body mutants are deficient in olfactory learning. *Journal of Neurogenetics*, 1, 1-30.

Helwak, A., Kudla, G., Dudnakova, T., and Tollervey, D. (2013. Mapping the human miRNA interactome by CLASH reveals frequent noncanonical binding. *Cell*, 153, 654–665.

Hillebrand, J., Barbee, S.A., and Ramaswami, M. (2007). P-body components, microRNA regulation, and synaptic plasticity. *Scientific World Journal*, 7, 178-90.

Höck, J., Weinmann, L., Ender, C., Rüdel, S., Kremmer, E., Raabe, M., … Meister, G. (2007). Proteomic and functional analysis of Argonaute-containing mRNA-protein complexes in human cells. *EMBO Reports*, 8(11), 1052-60.

Huang D.W., Sherman, B.T., and Lempicki, R.A. (2009. Systematic and integrative analysis of large gene lists using DAVID Bioinformatics Resources. *Nature Protocols*, 4(1), 44-57.

Huang, D.W., Sherman, B.T., Lempicki, R.A. (2009a) Systematic and integrative analysis of large gene lists using DAVID Bioinformatics Resources. Nature Protocols, 4(1), 44-57.

Huang, D.W., Sherman, B.T., Lempicki, R.A. (2009b) Bioinformatics enrichment tools: paths toward the comprehensive functional analysis of large gene lists. Nucleic Acids Research, 37(1), 1-13.Hummel, T., Krukkert, K., Roos, J., Davis, G., and Klämbt, C. (2000). *Drosophila* Futsch/22C10 is a MAP1B-like protein required for dendritic and axonal development. *Neuron*, 26(2), 357-70.

Huntzinger,E., Braun, J.E., Heimstädt, S., Zekri, L., and Izaurralde, E. (2010). Two PABPC1-binding sites in GW182 proteins promote miRNA-mediated gene silencing. *EMBO Journal*, 29(24), 4146-60.

Igreja C, and Izaurralde E. (2011). CUP promotes deadenylation and inhibits decapping of mRNA targets. *Genes & Development*, 25(18), 1955-67.

Irwin, S.A., Galvez, R., Greenough, W.T . (2000). Dendritic spine structural anomalies in fragile-X mental retardation syndrome. *Cerebral Cortex*, 10(10), 1038-44.

Irwin, S.A., Idupulapati, M., Mehta, A.B., Crisostomo, R.A., Rogers, E.J., Larsen, B.P, … Greenough, W.T. (1999). Abnormal dendritic and dendritic spine characteristics in fragile-X patients and the mouse model of fragile-X syndrome. *Social Neuroscience*, Abstr25, 2548.

Ishizuka, A., Siomi, M.C., and Siomi, H. (2002). A Drosophila fragile X protein interacts with components of RNAi and ribosomal proteins. *Genes and Development*, 16(19), 2497-508.

Iyengar, B.R., Choudhary, A., Sarangdhar, M.A., Venkatesh, K.V., Gadgil, C.J., and Pillai, B. (2014). Non-coding RNA interact to regulate neuronal development and function. *Frontiers in Cellular Neuroscience*, 8, 47.

Jin, P., Zarnescu, D.C., Ceman, S., Nakamoto, M., Mowrey, J., Jongens, T.A., … Warren, S.T. (2004). Biochemical and genetic interaction between the fragile X mental retardation protein and the microRNA pathway. *Nature Neuroscience*, 7(2), 113-117.

Kanai, Y., Dohmae, N., Hirokawa, N. (2004). Kinesin transports RNA: isolation and characterization of an RNA-transporting granule. *Neuron*, 43(4), 513-25.

Keene JD. (2010). Minireview: global regulation and dynamics of ribonucleic Acid. *Endocrinology*, 151(4), 1391-7. doi: 10.1210/en.2009-1250.

Kelley, K., Chang, S.J., and Lin, S.L. (2012). Mechanism of repeat-associated microRNAs in fragile X syndrome. *Neural Plasticity*, 2012, 104796.

Kheradpour, P., Stark, A., Roy, S., and Manolis, K. (2007). Reliable prediction of regulator targets using 12 Drosophila genomes. *Genome Research*, 17, 1919-1931.

Kiledjian, M., Dreyfuss, G. (1992). Primary structure and binding activity of the hnRNP U protein: binding RNA through RGG box. *EMBO Journal*, 11(7), 2655-64.

Kim, W., Im, M.J., Park, C.H., Lee, C.J., Choi, S., Yoon, B.J. (2013). Remodeling of the dendritic structure of the striatal medium spiny neurons accompanies behavioral recovery in a mouse model of Parkinson's disease. *Neuroscience Letters*, 557(B), 95-100.

Kondo, S., and Ueda R. (2013). Highly improved gene targeting by germline-specific Cas9 expression in Drosophila. *Genetics*, 195(3), 715-21.

Kozomara A, and Griffiths-Jones S. (2011). miRBase: integrating microRNA annotation and deep-sequencing data. *Nucleic Acids Research*, 39(Database issue), D152-7.

Kozomara, A., and Griffiths-Jones, S. (2014). miRBase: annotating high confidence microRNAs using deep sequencing data. *Nucleic Acids Research*, 42(Database issue):D68-73.

Krichevsky, A.M., Sonntag, K.C. Isacson, O., and Kosik, K.S. (2006). Specific microRNAs modulate embryonic stem cell-derived neurogenesis. *Stem Cells*, 24, 857–864.

Kuehn, C., Duch, C. 2013. Putative excitatory and putative inhibitory inputs are localised in different dendritic domains in a Drosophila flight motoneuron. *European Journal of Neuroscience*, 37(6), 860-75.

Kuenne, C., Preussner, J., Herzog, M. and Looso, M. (in press). MIRPIPE - quantification of microRNAs in niche model organisms. *BMC Bioinformatics*.

Laggerbauer, B., Ostareck, D., Keidel, E.M., Ostareck, L.A., and Fischer, Y. (2001). Evidence that FMRP is a negative regulator of translation. *Human Molecular Genetics*,10, 329–338.

Lagos-Quintana, M., Rauhut, R., Yalcin, A., Meyer, J., Lendeckel, W., and Tusch, T. (2002). Identification of tissue-specific microRNAs from mouse. *Current Biology*, 12(9), 735-9.

Lee, L.W., Zhang, S., Etheridge, A., Ma, L., Martin, D., Galas, D., Wang, K. (2010). Complexity of the microRNA repertoire revealed by next-generation sequencing. *RNA*, 16(11), 2170-80.

Lewis, B.P., Burge, C.B. and Bartel, D. (2005). Conserved Seed Pairing, Often Flanked by Adenosines, Indicates that Thousands of Human Genes are MicroRNA Targets. ***Cell***, 120, 15-20.

Li, X.L., Jones, M.F., Subramanian, M., and Lal, A. (2014). Mutant p53 exerts oncogenic effects through microRNAs and their target gene networks. *FEBS Letters*, S0014-5793(14)00273-7.

Li, Y., Wang, F., Lee, J.A., and Gao, F.B. (2006). MicroRNA-9a ensures the precise specification of sensory organ precursors in Drosophila. *Genes and Development*, 20(20), 2793-805.

Li, Z., Zhang, Y., Ku, L., Wilkinson, K.D., Warren, S.T., and Feng, Y. (2001). The fragile X mental retardation protein inhibits translation via interacting with mRNA. *Nucleic Acids Research*, 29, 2276–2283.

Lightbody, A.A., Reiss, A.L. (2009). Gene, brain, and behavior relationships in fragile X syndrome: evidence from neuroimaging studies. *Developmental Disabilities Research Reviews*, 15(4), 343-52.

Lin, M.D., Fan, S.J., Hsu, W.S., and Chou, T.B. (2006). *Drosophila* decapping protein 1, dDcp1, is a component of the oskar mRNP complex and directs its posterior localization in the oocyte. *Developmental Cell,* 10(5), 601-13.

Loesch, D.Z., Huggins, R.M., Hagerman, R.J. (2004). Phenotypic variation and FMRP levels in fragile X. *Mental retardation and developmental disabilities research reviews*, 10(1), 31-41.

Lorsch, J.R. (2002). RNA chaperones exist and DEAD box proteins get a life. *Cell*, 109(7), 797-800.

Lu, R., Wang, H., Liang, Z., Ku, L., O'Donnell, W.T., Li, … Feng, Y. (2004). The fragile X protein controls microtubule-associated protein 1B translation and microtubule stability in brain neuron development. *Proceedings of the National Academy of Sciences U.S.A.*, 101, 15201–15206.

Lucas, F.R., Goold, R.G., Gordon-Weeks, P.R., Salinas, P.C. (1998). Inhibition of GSK-3beta leading to the loss of phosphorylated MAP-1B is an early event in axonal remodeling induced by WNT-7a or lithium. *Journal of Cell Science*, 111(10), 1351-61.

Lucas, K., Raikhel, A.S. (2013). Insect microRNAs: biogenesis, expression profiling and biological functions. *Insect Biochemistry and Molecular Biology*, 43(1), 24-38.

Lucas, K., and Raikhel, A.S. (2013). Insect microRNAs: biogenesis, expression profiling and biological functions. *Insect Biochemistry and Molecular Biology*, 43(1), 24-38.

Lugli, G., Larson, J., Martone, M. E., Jones, Y., and Smalheiser, N. R. (2005). Dicer and eIF2c are enriched at postsynaptic densities in adult mouse brain and are modified by neuronal activity in a calpain-dependent manner. *Journal of Neurochemistry*, 94, 896–905.

Lüthl, A., Laurent, J.P., Figurov, A., Muller, D., Schachner, M. (1994). Hippocampal long-term potentiation and neural cell adhesion molecules L1 and NCAM. *Nature*, 372(6508), 777-9.

Mack, T.G., Koester, M.P., and Pollerberg, G.E. (2000). The microtubule-associated protein MAP1B is involved in local stabilization of turning growth cones. *Molecular and Cellular Neurosciences*, 15(1), 51-65.

Madsen, C., Grønskov, K., Brøndum-Nielsen, K., and Jensen, T.G. (2009). Normal RNAi response in human fragile x fibroblasts. *BMC Research Notes*, 2, 177.

Marnef, A., and Standart, N. (2010). Pat1 proteins: a life in translation, translation repression and mRNA decay. *Biochemical Society Transactions*, 38(6), 1602-7.

Martí, E., Pantano, L., Bañez-Coronel, M., Llorens, F., Miñones-Moyano, E., Porta, S., Sumoy, L., Ferrer, I., Estivill, X. (2010). A myriad of miRNA variants in control and Huntington's disease brainregions detected by massively parallel sequencing. *Nucleic Acids Research*, 38(20), 7219-35.

Matsuzaki, M., Honkura, N., Ellis-Davies, G.C., Kasai, H. (2004). Structural basis of long-term potentiation in single dendritic spines. *Nature*, 429(6993), 761–78.

Maurin, T., Zongaro, S., and Bardoni, B. (2014). Fragile X Syndrome: From molecular pathology to therapy. *Neuroscience and Biobehavioral Reviews*, ii, S0149-7634(14)00009-8 [Epub ahead of print].

McBride, S.M., Choi, C.H., Wang, Y., Liebelt, D., Braunstein, E., Ferreiro, D., Sehgal, A., Siwicki, K.K., Dockendorff, T.C., Nguyen, H.T., McDonald, T.V., and Jongens, T.A. 2005. Pharmacological rescue of synaptic plasticity, courtship behavior, and mushroom body defects in a Drosophila model of fragile X syndrome. *Neuron*, 45(5), 753-64.

McLennan, Y., Polussa, J., Tassone, F., Hagerman, R. (2011). Fragile x syndrome. *Current Genomics*, 12(3), 216-24.

Meyer, S., Temme, C., and Wahle, E. (2004). Review Messenger RNA turnover in eukaryotes: pathways and enzymes. *Critical Reviews in Biochemistry and Molecular Biology*, 39(4), 197-216.

Mikl, M., Vendra, G., Doyle, M., and Kiebler, M.A. (2010). RNA localization in neurite morphogenesis and synaptic regulation: current evidence and novel approaches. *Journal of Comparative Physiology, A, Neuroethology, Sensory, Neural and Behavioral Physiology*, 196(5), 321-34.

Monzo, K., Papoulas, O., Cantin, G.T., Wang, Y., Yates, J.R. 3rd, Sisson, J.C. (2006). Fragile X mental retardation protein controls trailer hitch expression and cleavage

furrow formation in Drosophila embryos. *Proceedings of the National Academy of Sciences, U.S.A*., 103(48), 18160-5.

Morin, R.D., O'Connor, M.D., Griffith, M., Kuchenbauer, F., Delaney, A., Prabhu, A.L., Zhao, Y., McDonald, H., Zeng, T., Hirst, M., Eaves, C.J., Marra, M.A. (2008). Application of massively parallel sequencing to microRNA profiling anddiscovery in human embryonic stem cells. *Genome Research*, 18(4), 610-21.

Morris, R.G.M., Davis, S. and Butcher, S.P. (1990). Hippocampal Synaptic Plasticity and NMDA Receptors: A Role in Information Storage? *Philosophical Transactions of the Royal Society of London, Series B, Biological Sciences*, 329(1253), 187-204.

Moser, J.J., Eystathioy, T., Chan, E.K., and Fritzler, M.J. (2007). Markers of mRNA stabilization and degradation, and RNAi within astrocytoma GW bodies. *Journal of Neuroscience Research*, 85(16), 3619-31.

Moss, E.G. (2002). MicroRNAs: hidden in the genome. *Current Biology*,12(4), R138-40.

Muddashetty, R. S., Kelic, S., Gross, C., Xu, M., and Bassell, G. J. (2007). Dysregulated metabotropic glutamate receptor-dependent translation of AMPA receptor and postsynaptic density-95mRNAs at synapses in a mouse model of fragile X syndrome. *Journal of Neuroscience*, 27, 5338–5348.

Muller, D., Djebbara-Hannas, Z., Jourdain, P., Vutskits, L., Durbec, P., Rougon, G., and Kiss, J.Z. (2000). Brain-derived neurotrophic factor restores long-term potentiation in polysialic acid-neural cell adhesion molecule-deficient hippocampus. *Proceedings of the National Academy of Sciences of the U.S.A.*, 97, 4315–4320.

Nahm, M., Lee, M.J., Parkinson, W., Lee, M., Kim, H., Kim, Y.J,, . . . and Lee, S. (2013).Spartin regulates synaptic growth and neuronal survival by inhibiting BMP-mediated microtubule stabilization. *Neuron*, 77(4), 680-95.

Nakamura A, Amikura R, Hanyu K, Kobayashi S. (2001). Me31B silences translation of oocyte-localizing RNAs through the formation of cytoplasmic RNP complex during Drosophila oogenesis. *Development*, 128(17), 3233-42.

Nesler, K.R., Sand, R.I., Symmes, B.A., Pradhan, S.J., Boin, N.G., Laun, A.E., Barbee, S.A. (2013). The miRNA pathway controls rapid changes in activity-dependent synaptic structure at the *Drosophila melanogaster* neuromuscular junction. *PLoS One*, 8(7), e68385.

Nottrott, S., Simard, M.J., and Richter, J.D. (2006). Human let-7a miRNA blocks protein production on actively translating polyribosomes. *Nature Structural and Molecular Biology*, 13(12), 1108-14.

Oeffinger, M., Wei, K.E., Rogers, R., DeGrasse, J.A., Chait, B.T., Aitchison, J.D., and Rout, MP. (2007). Comprehensive analysis of diverse ribonucleoprotein complexes. *Nature Methods*, 4(11), 951-6.

Oh, J.Y., Kwon, A., Jo, A., Kim, H., Goo, Y.S., Lee, J.A., Kim, H.K. (2013). Activity-dependent synaptic localization of processing bodies and their role in dendritic structural plasticity. *Journal of Cell Science*, 126(Pt 9), 2114-23.

Olde Loohuis, N.F., Kos, A., Martens, G.J., Van Bokhoven, H., Nadif, K.N., Aschrafi, A. (2012). MicroRNA networks direct neuronal development and plasticity. *Cellular and Molecular Life Sciences*, 69(1), 89-102.

Pascual, M.L., Luchelli, L., Habif, M., Boccaccio, G.L. (2012). Synaptic activity regulated mRNA-silencing foci for the fine tuning of local protein synthesis at the synapse. Communicative and Integrative Biology, 5(4), 388-92.

Penagarikano, O., Mulle, J.G., and Warren, S.T. (2007). The pathophysiology of fragile x syndrome. *Annual Review of Genomics and Human Genetics*, 8, 109-29.

Pieretti, M., Zhang, F.P., Fu, Y.H., Warren, S.T., Oostra, B.A., Caskey, C.T., Nelson, D.L. (1991). Absence of expression of the FMR-1 gene in fragile X syndrome. *Cell*, 66(4), 817-22.

Pradhan S.J., Nesler, K.R., Rosen, S.F., Kato, Y., Nakamura, A., Ramaswami, M., and Barbee, S.A. (2012). The conserved P body component HPat/Pat1 negatively regulates synaptic terminal growth at the larval Drosophila neuromuscular junction. *Journal of Cell Science,* 125(Pt 24), 6105-16.

Preiss T., and Hentze M.W. (1998). Dual function of the messenger RNA cap structure in poly(A)-tail-promoted translation in yeast. *Nature*, 392, 516–520.

Prokop, A., Beaven, R., Qu, Y., and Sánchez-Soriano, N. (2013). Using fly genetics to dissect the cytoskeletal machinery of neurons during axonal growth and maintenance. *Journal of Cell Science*, 126(Pt 11), 2331-41.

Rage, F., Boulisfane, N., Rihan, K., Neel, H., Gostan, T., Bertrand, E., Bordonné, R., and Soret, J. (2013). Genome-wide identification of mRNAs associated with the protein SMN whose depletion decreases their axonal localization. *RNA*, 19(12), 1755-66.

Reddy, K.S. (2005). Cytogenetic abnormalities and fragile-X syndrome in Autism Spectrum Disorder. BMC Medical Genetics, 6, 3.

Rehwinkel, J., Behm-Ansmant, I., Gatfield, D., and Izaurralde, E. (2005). A crucial role for GW182 and the DCP1:DCP2 decapping complex in miRNA-mediated gene silencing. *RNA*, 11(11), 1640-7.

Roos, J., Hummel, T., Ng, N., Klämbt, C., and Davis, G.W. (2000). *Drosophila* Futsch regulates synaptic microtubule organization and is necessary for synaptic growth. *Neuron*, 26(2), 371-82.

Rozeboom, Leslie. (2011). Thesis: microRNAs 9a, 9b, 9c and 315 regulate expression of the neuronal microtubule-associated protein Futsch/MAP1B. Denver: Denver Bookbinding Company.

Ruby, J.G., Jan, C.H., and Bartel, D.P. (2007). Intronic microRNA precursors that bypass Drosha processing. ***Nature***, 448, 83-86.

Ruby, J.G., Stark, A., Johnston, W.K., Kellis, M., Bartel, D.P., and Lai. (2007). E.C. Evolution, biogenesis, expression, and target predictions of a substantially expanded set of *Drosophila* microRNAs. *Genome Research*, 17, 1850-1864.

Saab, B.J., and Mansuy, I.M. (2014). Neuroepigenetics of memory formation and impairment: The role of microRNAs. *Neuropharmacology*, 80C, 61-69.

Sánchez-Carbente, M.R., and Desgroseillers, L. 2008. Understanding the importance of mRNA transport in memory. *Progress in Brain Research*, 169, 41-58.

Schratt, G. M., Tuebing, F., Nigh, E. A., Kane, C. G., Sabatini, M. E., Kiebler, M., et al. (2006). A brain-specific microRNA regulates dendritic spine development. *Nature*, 439, 283–289.

Schwartz, J.H., Castellucci, V.F., and Kandel, E.R. (1971). Functioning of Identified Neurons and Synapses in Abdominal Ganglion of *Aplysia* in Absence of Protein Synthesis. *Journal of Neurophysiology*, 34, 939-53.

Searfoss, A.M., and Wickner, R.B. (2000). 3' poly(A) is dispensable for translation. *Proceedings of the National Academy of Science*, U.S.A., 97(16), 9133-7.

Sempere, L.F., Freemantle, S., Pitha-Rowe, I., Moss, E., Dmitrovsky, E., and Ambros, V. (2004). Expression profiling of mammalian microRNAs uncovers a subset of brain-expressed microRNAs with possible roles in murine and human neuronal differentiation. *Genome Biology*, 5(3), R13.

Shah, S.M., Kang, Y.J., Christensen, B.L., Feng, A.S., Kollmar, R. (2009). Expression of Wnt receptors in adult spiral ganglion neurons: frizzled 9 localization at growth cones of regenerating neurites. *Neuroscience*, 164(2), 478-87.

Shen, W., and Ganetzky, B. 2010. Nibbling away at synaptic development. *Autophagy*, 6(1), 168-9.

Sheth, U., and Parker, R. (2003). Decapping and decay of messenger RNA occur in cytoplasmic processing bodies. *Science*, 300(5620), 805-8.

Siegel, G., Saba, R., and Schratt G. microRNAs in neurons: manifold regulatory roles at the synapse.(2011). *Current Opinion in Genetics and Development*, 21(4), 491-7.

Siomi, H., Choi, M., Siomi, M.C., Nussbaum, R.L., and Dreyfuss, G. (1994). Essential role for KH domains in RNA binding: impaired RNA binding by a mutation in the KH domain of FMR1 that causes fragile X syndrome. *Cell*, 77(1), 33-9.

Siomi, H., Matunis, M.J., Michael, W.M., and Dreyfuss, G. (1993a). The pre-mRNA binding K protein contains a novel evolutionarily conserved motif. *Nucleic Acids Research*, 21(5), 1193-8.

Siomi, H., Siomi, M.C., Nussbaum, R.L., and Dreyfuss, G. (1993b). The protein product of the fragile X gene, FMR1, has characteristics of an RNA-binding protein. *Cell*, 74(2), 291-8.

Sleeman, J. (2013). Small nuclear RNAs and mRNAs: linking RNA processing and transport to spinal muscular atrophy. *Biochemical Society Transactions*, 41(4):871-5.

Soden, M.E. and Chen, L. (2010). Fragile X Protein FMRP is Required for Homeostatic Plasticity and Regulation of Synaptic Strength by Retinoic Acid. *The Journal of Neuroscience*, 30(50), 16910-16921.

Sosanya, N.M., Huang, P. P., Cacheaux, L.P., Chen, C. J., Nguyen, K., Perrone-Bizzozero, N.I., et al. (2013). Degradation of high affinity HuD targets releases Kv1.1 mRNA from miR-129 repression by mTORC1. *Journal of Cell Biology*, 202, 53–69.

St. Pierre SE, Ponting L, Stefancsik R, McQuilton P, and the FlyBase Consortium (2014). FlyBase 102 - advanced approaches to interrogating FlyBase. *Nucleic Acids Research*, 42(D1), D780-D788.

Staley, J.P., and Woolford, J.L. Jr. (2009). Assembly of ribosomes and spliceosomes: complex ribonucleoprotein machines. *Current Opinion in Cell Biology*, 21(1), 109-18.

Staubli, U., Chun, D. and Lynch, G. (1998) Time-dependent reversal of long-term potentiation by an integrin antagonist. *Journal of Neuroscience*, 18: 3460–3469.

Steele, J.W., Brautigam, H., Short, J.A., Sowa, A., Shi, M., Yadav, A., … Dickstein, D.L. (2014). Early fear memory defects are associated with altered synaptic plasticity and molecular architecture in the TgCRND8 Alzheimer's disease mouse model. *Journal of Comparative Neurology*, doi: 10.1002/cne.23536. [Epub ahead of print].

Stewart, B.A., Atwood, H.L., Renger, J.J., Wang, J., & Wu, C.-F. (1994). Improved stability of Drosophila larval neuromuscular preparations in hemolymph-like physiological solutions. Journal of Comparative Physiology. *A Sensory, Neural, and Behavioral Physiology*, 175, 179–191.

Sun, A.X., Crabtree, G.R., and Yoo, A.S. (2013). MicroRNAs: regulators of neuronal fate. *Current Opinion in Cell Biology*, 25(2), 215-21.

Tarang, S., and Weston, M.D. (2014). Macros in microRNA target identification: A comparative analysis of in silico, in vitro, and in vivo approaches tomicroRNA target identification. *RNA Biology*, 11(4).

Temme, C., Zaessinger, S., Simonelig, M., and Wahle, E. (2004). A complex containing the CCR4 and CAF1 proteins is involved in mRNA deadenylation in *Drosophila*. *EMBO Journal*, 23, 2862–2871.

Temme, C., Zhang, L., Kremmer, E., Ihling, C., Chartier, A., Sinz, A., Simonelig, M., Wahle, E. (2010). Subunits of the *Drosophila* CCR4-NOT complex and their roles in mRNA deadenylation. *RNA*, 16(7), 1356-70.

Tharun S, Parker, R. (2001). Targeting an mRNA for decapping: displacement of translation factors and association of the Lsm1p-7p complex on deadenylated yeast mRNAs. *Molecular Cell*, 8(5), 1075-83.

Tian, H., Cao, Y.X., Zhang, X.S., Liao, W.P., Yi, Y.H., Lian, J., … and Sun, F. (2013). The targeting and functions of miRNA-383 are mediated by FMRP during spermatogenesis. *Cell Death and Disease*, 4, e617.

Todd, P.K., Mack, K.J. & Malter, J.S. (2003). The fragile X mental retardation protein is required for type-I metabotropic glutamate receptor-dependent translation of PSD-95. *Proceedings of the National Academy of Science, USA*, 100, 14374–14378.

Tucker, M., Valencia-Sanchez, M.A., Staples, R.R., Chen, J., Denis, C.L., and Parker, R. (2001).The transcription factor associated Ccr4 and Caf1 proteins are components of the major cytoplasmic mRNA deadenylase in *Saccharomyces cerevisiae*. *Cell*, 104, 377–386.

Vanderklish, P.W., and Edelman, G.M. (2005). Differential translation and fragile X syndrome. *Genes, Brain and Behavior*, 4(6), 360-84.

Verkerk, A.J., Pieretti, M., Sutcliffe, J.S., Fu, Y.H., Kuhl, D.P., Pizzuti, A., … Warren, S.T. (1991). Identification of a gene (FMR-1) containing a CGG repeat coincident with a breakpoint cluster region exhibiting length variation in fragile X syndrome. *Cell*, 65(5), 905-14.

Wainwright, S.R. and Galea, L.A.M. 2013. The Neural Plasticity Theory of Depression: Assessing the Roles of Adult Neurogenesis and PSA-NCAM within the Hippocampus. *Neural Plasticity*, 2013, 805497.

Walters, R.W., Shumilin, I.A., Yoon, J.H., Minor, W., and Parker, R. (2014). Edc3 Function in Yeast and Mammals Is Modulated by Interaction with NAD-Related Compounds. *G3 (Bethesda)*, 4(4), 613-22.

Wang, I.F., Wu, L.S., Chang, H.Y., and Shen, C.K. (2008). TDP-43, the signature protein of FTLD-U, is a neuronal activity-responsive factor. *Journal of Neurochemistry*, 105(3), 797-806.

Wang, X. (2014). Composition of seed sequence is a major determinant of microRNA targeting patterns. *Bioinformatics*, Feb 12. [Epub ahead of print]

Weil, T.T., Parton, R.M., Herpers, B., Soetaert, J., Veenendaal, T., Xanthakis, D. … Davis, I. (2012). Drosophila patterning is established by differential association of mRNAs with P bodies. *Nature Cell Biology*, 14(12), 1305-13.

Weiler, I.J. and Greenough, W.T. (1993). Metabotropic glutamate receptors trigger postsynaptic protein synthesis. *Proceedings of the National Academy of Sciences, U.S.A.*, 90(15), 7168-71.

Xu, K., Bogert, B. A., Li, W., Su, K., Lee, A., and Gao, F. B. (2004). The fragile X-related gene affects the crawling behavior of Drosophila larvae by regulating the mRNA level of the DEG/ENaC protein pickpocket1. *Current Biology*, 14, 1025–1034.

Xu, S., Poidevin, M., Han, E., Bi, J., and Jin, P. (2012). Circadian rhythm-dependent alterations of gene expression in Drosophila brain lacking fragile X mental retardation protein. *PLoS One*, 7(5), e37937.

Yamashita, A., Chang, T.C., Yamashita, Y., Zhu, W., Zhong, Z., Chen, C.Y.A., Shyu, A.B. (2005). Concerted action of poly(A) nucleases and decapping enzyme in mammalian mRNA turnover. *Nature Structural and Molecular Biology*, 12, 1054–1063.

Yi, R., Qin, Y., Macara, I.G., and Cullen, B.R. (2003). Exportin-5 mediates the nuclear export of pre-microRNAs and short hairpin RNAs. *Genes and Development*, 17(24), 3011-6.

Zalfa, F., Giorgi, M., Primerano, B., Moro, A., Di Penta, A., Reis, S., … and Bagni, C. 2003. The fragile X syndrome protein FMRP associates with BC1 RNA and regulates the translation of specific mRNAs at synapses. *Cell*, 112(3), 317-27.

Zhang, Y.Q., Bailey, A.M., Matthies, H.J., Renden, R.B., Smith, M.A., Speese, S.D., Rubin, G.M., Broadie, K. (2001). Drosophila fragile X-related gene regulates the MAP1B homolog Futsch to control synaptic structure and function. *Cell*, 107(5), 591-603.

Zhao, J., Hyman, L., and Moore, C. 1999. Formation of mRNA 3' ends in eukaryotes: mechanism, regulation, and interrelationships with other steps in mRNA synthesis. *Microbiology and Molecular Biology Reviews*, 63(2), 405-45.

Zhong, W. (2008). Going nuclear is again a winning (Wnt) strategy. *Developmental Cell*, 15(5), 635-6.

Appendix: Additional Tables and Figures

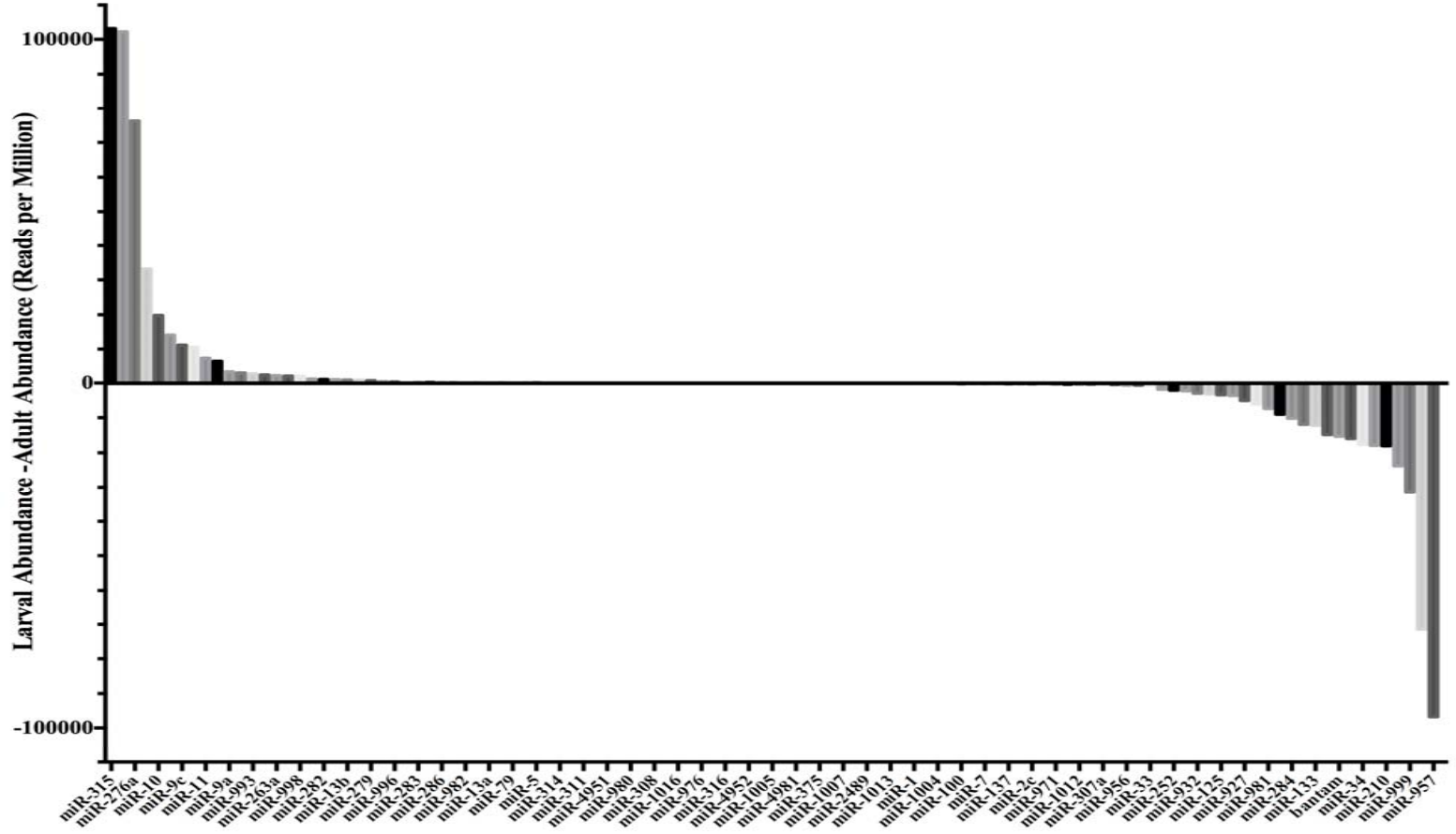

Figure A 1: Larval Enrichment of all miRNAs found in Larval CNS and Adult Brain

Table A 1: Functional Annotation Cluster for Predicted the miR-92 Family Targets	
Enrichment Score: 6.95	
Cluster Name	**P-Value**
Sequence-specific DNA binding	7.40E-13
Transcription factor activity	1.20E-11
DNA-binding	1.60E-10
Regulation of transcription, DNA-dependent	2.10E-08
Transcription regulator activity	2.10E-08
Regulation of RNA metabolic process	3.50E-08
Regulation of transcription	4.70E-08
DNA binding	4.90E-08
DNA binding	1.20E-07
RNA polymerase II transcription factor activity	1.60E-07
Homeobox	2.20E-07
Transcription	2.70E-07
Transcription regulation	2.80E-07
Homeobox	6.80E-07
Homeodomain-related	1.10E-06
Transcription	1.30E-06
Homeobox, conserved site	2.30E-06
Nucleus	1.60E-05
HOX	3.50E-05
DNA-binding region:Homeobox	4.80E-03
Enrichment Score: 3.51	
Cell morphogenesis	1.20E-07
Cellular component morphogenesis	3.80E-07
Cell projection organization	4.40E-06
Neuron differentiation	3.00E-05
Dendrite morphogenesis	4.20E-04
Dendrite development	4.20E-04
Neuron development	1.30E-03
Cell projection morphogenesis	1.40E-03
Cell part morphogenesis	2.00E-03
Cell morphogenesis involved in differentiation	2.10E-03
Neuron projection morphogenesis	3.00E-03
Neuron projection development	3.10E-03
Cell morphogenesis involved in neuron differentiation	3.20E-03
Axonogenesis	3.20E-01

Table A 2: Functional Annotation Cluster for Predicted miR-275 Targets	
Enrichment Score: 2.38	
Cluster Name	**P-Value**
Immunoglobulin	1.50E-04
Immunoglobulin-like fold	5.90E-04
Immunoglobulin-like	9.20E-04
Immunoglobulin subtype 2	3.70E-03
Immunoglobulin subtype	4.00E-03
IGc2	7.40E-03
IG	8.10E-03
Immunoglobulin V-set	1.00E-02
Immunoglobulin I-set	1.50E-02
Fibronectin, type III	1.90E-02
FN3	3.10E-02
Enrichment Score: 1.74	
Cell morphogenesis	2.10E-03
Cellular component morphogenesis	4.60E-03
Neuron projection morphogenesis	1.10E-02
Neuron projection development	1.20E-02
Cell morphogenesis involved in neuron differentiation	1.20E-02
Cell morphogenesis involved in differentiation	1.40E-02
Cell projection morphogenesis	1.70E-02
Cell part morphogenesis	1.90E-02
Neuron development	2.20E-02
Cell projection organization	2.60E-02
Neuron differentiation	3.70E-02
Dendrite morphogenesis	5.20E-02
Dendrite development	5.20E-02
Axonogenesis	1.30E-01

Table A 3: Functional Annotation Cluster for Predicted Targets of miR-282 **Enrichment Score: 1.48**	
Cluster Name	**P-Value**
Imaginal disc-derived wing vein specification	2.30E-03
Epidermal growth factor receptor signaling pathway	2.90E-03
Imaginal disc morphogenesis	3.30E-03
Post-embryonic organ morphogenesis	3.30E-03
Post-embryonic organ development	3.90E-03
Compositionally biased region:Gln-rich	4.40E-03
Instar larval or pupal morphogenesis	6.70E-03
Post-embryonic morphogenesis	7.20E-03
Metamorphosis	7.80E-03
Cell surface receptor linked signal transduction	1.10E-02
Imaginal disc development	1.20E-02
Imaginal disc-derived wing morphogenesis	1.20E-02
Wing disc morphogenesis	1.30E-02
Instar larval or pupal development	1.30E-02
Post-embryonic appendage morphogenesis	1.40E-02
Post-embryonic development	1.50E-02
Imaginal disc-derived appendage morphogenesis	1.60E-02
Appendage morphogenesis	1.60E-02
Imaginal disc-derived appendage development	1.60E-02
Appendage development	1.70E-02
Wing disc development	2.40E-02
Transmembrane receptor protein tyrosine kinase signaling pathway	2.50E-02
Enzyme linked receptor protein signaling pathway	4.20E-02
Developmental protein	8.40E-02
Pattern specification process	9.10E-02
Cell fate commitment	9.60E-02
Alternative splicing	1.10E-01
Splice variant	1.50E-01
Regionalization	2.80E-01
Nucleus	5.10E-01

Table A 4: Functional Annotation Cluster for Predicted Targets of miR-184 **Enrichment Score: 3.06**	
Cluster Name	**P-Value**
Septate junction assembly	7.70E-06
Apical junction assembly	3.30E-05
Cell-cell junction assembly	4.10E-05
Cell junction assembly	4.50E-05
Cell-cell junction organization	7.30E-05
Cell junction organization	7.90E-05
Endothelial cell development	4.20E-04
Epithelial cell development	4.20E-04
Endothelial cell differentiation	4.20E-04
Septate junction	9.80E-04
Regulation of tube size, open tracheal system	1.00E-03
Regulation of tube size	1.30E-03
Epithelial cell differentiation	1.50E-03
Occluding junction	1.50E-03
Regulation of tube architecture, open tracheal system	3.60E-03
Apical junction complex	3.80E-03
Apicolateral plasma membrane	4.50E-03
Respiratory system development	5.40E-03
Open tracheal system development	5.40E-03
Cell-cell junction	6.90E-03
Plasma membrane part	1.00E-02
Epithelium development	1.70E-02
Cell junction	3.60E-02

Table A 5: Functional Annotation Cluster for Predicted Targets of the miR-276 Family **Enrichment Score: 2.4**	
Cluster Name	**P-Value**
Positive regulation of adenylate cyclase activity	1.80E-03
Positive regulation of cyclase activity	1.80E-03
Positive regulation of lyase activity	2.10E-03
Regulation of adenylate cyclase activity	2.60E-03
Regulation of cAMP metabolic process	2.60E-03
Regulation of nucleotide biosynthetic process	2.60E-03
Regulation of cyclic nucleotide biosynthetic process	2.60E-03
Regulation of cyclic nucleotide metabolic process	2.60E-03
Regulation of cyclase activity	2.60E-03
Regulation of cAMP biosynthetic process	2.60E-03
Regulation of lyase activity	3.00E-03
Regulation of nucleotide metabolic process	3.50E-03
cAMP-mediated signaling	4.60E-03
Cyclic-nucleotide-mediated signaling	5.20E-03
Positive regulation of catalytic activity	7.90E-03
Positive regulation of molecular function	1.10E-02
Second-messenger-mediated signaling	1.80E-02
Intracellular signaling cascade	4.10E-02

Table A 6: Functional Annotation Cluster for Predicted Targets of miR-10 **Enrichment Score: 1.28**	
Cluster Name	**P-Value**
Sequence-specific DNA binding	1.20E-02
Transcription factor activity	3.20E-02
Regulation of transcription, DNA-dependent	5.10E-02
Regulation of RNA metabolic process	6.10E-02
Regulation of transcription	8.20E-02
Transcription regulator activity	8.80E-02
DNA binding	1.20E-01

Table A 7: Functional Annotation Cluster for Predicted Targets of miR-305	
Enrichment Score: 6.19	
Cluster Name	**P-Value**
Transcription regulator activity	2.00E-10
Transcription factor activity	7.60E-09
Transcription	2.80E-08
Regulation of transcription	3.30E-08
Transcription regulation	6.10E-07
Transcription	8.00E-07
Regulation of transcription, DNA-dependent	3.80E-06
Regulation of RNA metabolic process	3.90E-06
RNA polymerase II transcription factor activity	4.20E-06
Nucleus	6.00E-06
DNA binding	7.60E-06
Regulation of transcription from RNA polymerase II promoter	3.00E-05
DNA binding	6.40E-05
Enrichment Score: 3.26	
Neuroblast differentiation	1.60E-05
Neuroblast fate commitment	1.80E-04
Cell fate commitment	2.30E-04
Cell fate determination	1.10E-03
Neuroblast fate determination	1.40E-03
Ventral cord development	2.40E-02

Table A 8: Functional Annotation Cluster for Predicted Targets of miR-995	
Enrichment Score: 1.67	
Cluster Name	**P-Value**
Imaginal disc development	1.80E-03
Neuron differentiation	3.20E-02
Tube morphogenesis	5.30E-02
Tube development	7.00E-02

Table A 9: Functional Annotation Cluster for Predicted Targets of miR-11	
Enrichment Score: 7.04	
Cluster Name	**P-Value**
Integral to membrane	9.60E-11
Intrinsic to membrane	2.00E-10
Transmembrane	9.70E-06
Membrane	3.80E-04
Enrichment Score: 3.47	
cell morphogenesis	2.70E-05
cell part morphogenesis	5.80E-05
neuron differentiation	5.90E-05
cellular component morphogenesis	6.00E-05
neuron projection morphogenesis	7.30E-05
neuron projection development	7.60E-05
cell morphogenesis involved in neuron differentiation	8.00E-05
cell morphogenesis involved in differentiation	1.60E-04
cell projection morphogenesis	3.10E-04
cell projection organization	6.20E-04
neuron development	8.50E-04
cell motion	1.30E-03
dendrite morphogenesis	2.70E-05
dendrite development	5.80E-05
axonogenesis	5.90E-05
axon guidance	6.00E-05

Tables A1-A9: Predicted miRNA targets from TargetScanFly were analyzed with the DAVID bioinformatics program functional annotation cluster analysis tool. The top functional annotation cluster is shown for each miRNA, and any functional annotation cluster pertaining to neuronal growth with an enrichment score over 1.5 is shown at the bottom of each table.

Table A 10: Functional Annotation Cluster for Overlapping Predicted Targets of miR-315 and the miR-92 Family **Enrichment Score: 2.29**	
Cluster Name	**P-Value**
DNA-binding	3.40E-04
Zinc-finger	4.80E-04
Transcription regulation	1.40E-03
Transcription	1.50E-03
Steroid hormone receptor	1.80E-03
Nuclear hormone receptor, ligand-binding	2.10E-03
Nuclear hormone receptor, ligand-binding, core	2.10E-03
Steroid hormone receptor activity	3.10E-03
Zinc finger, nuclear hormone receptor-type	3.50E-03
zinc finger region:NR C4-type	4.00E-03
DNA-binding region:Nuclear receptor	4.50E-03
ligand-dependent nuclear receptor activity	4.50E-03
Zinc finger, NHR/GATA-type	4.80E-03
HOLI	6.50E-03
Transcription	6.60E-03
ZnF_C4	1.10E-02
Receptor	2.50E-02
Transcription factor activity	2.70E-02
Regulation of RNA metabolic process	3.80E-02
Regulation of transcription, DNA-dependent	7.70E-02
Sequence-specific DNA binding	8.00E-02

Table A 11: Functional Annotation Cluster for Overlapping Predicted Targets of the miR-9 Family and the miR-92 Family **Enrichment Score: 1.48**	
Cluster Name	**P-Value**
Zinc finger	1.50E-03
Cell fate determination	2.50E-03
Zinc ion binding	7.10E-03
Cell fate commitment	8.00E-03
Zinc finger, C2H2-type/integrase, DNA-binding	8.40E-03
Compound eye development	1.40E-02
Eye development	1.60E-02
Transition metal ion binding	1.90E-02
RNA polymerase II transcription factor activity	2.00E-02
Neuron differentiation	2.40E-02
Sensory organ development	2.40E-02
Zinc	2.70E-02
Transcription	3.00E-02
Zinc finger, C2H2-type	3.70E-02
Zinc finger, C2H2-like	3.80E-02
Metal ion binding	4.40E-02
Cation binding	4.80E-02
Ion binding	4.90E-02
Zinc-finger	5.00E-02
Metal-binding	6.00E-02
Transcription regulation	7.20E-02
Transcription	7.40E-02
DNA-binding	8.20E-02
Regulation of transcription	8.20E-02
ZnF_C2H2	9.60E-02
Transcription regulator activity	1.20E-01
DNA binding	1.60E-01
Phosphoprotein	2.40E-01
Nucleus	2.70E-01
Zinc finger	1.50E-03

Table A 12: List of Overlapping Targets for miR-315 and the miR-9 Family

FlyBase Gene ID	Gene
FBgn0001122	G protein alpha 47A
FBgn0003870	**Tramtrack**
FBgn0004579	spalt major
FBgn0005638	slow border cells
FBgn0015609	**Cadherin-N**
FBgn0020307	defective proventriculus
FBgn0020412	Chromosomal serine/threonine-protein kinase JIL-1
FBgn0030820	Dmel_CG5004
FBgn0031762	Dmel_CG9098
FBgn0034720	Liprin-gamma
FBgn0035011	Dmel_CG13589
FBgn0038320	**specifically Rac1-associated protein 1**
FBgn0040765	Dmel_CG33473
FBgn0041781	**SCAR**
FBgn0052062	Ataxin-binding protein 1
FBgn0052333	Dmel_CG32333
FBgn0063649	Dmel_CG6006
FBgn0083962	Dmel_CG34126
FBgn0085400	Dmel_CG34371
FBgn0085416	**Futsch**
FBgn0037585	
FBgn0001122	G protein oalpha 47A
FBgn0003870	Tramtrack
FBgn0004579	spalt major
FBgn0005638	slow border cells
FBgn0015609	Cadherin-N
FBgn0020307	Defective proventriculus
FBgn0020412	Chromosomal serine/threonine-protein kinase JIL-1
FBgn0030820	Dmel_CG5004
FBgn0031762	Dmel_CG9098

Table A 13: List of Overlapping Targets for miR-315 and miR-275	
FlyBase Gene ID	Gene
FBgn0086758	**Uzipped**
FBgn0044028	**Roundabout**
FBgn0005631	Notum
FBgn0033368	CG13743
FBgn0004055	**Chinmo**
FBgn0033551	CG7222

Table A 14: List of Overlapping Targets for miR-315 and the miR-276 Family	
FlyBase Gene ID	Gene
FBgn0052206	CG32206
FBgn0036725	CG18265
FBgn0051140	CG31140
FBgn0052062	Ataxin-binding protein 2
FBgn0000633	Faint sausage
FBgn0003715	Jim lovell
FBgn0036464	Synaptotagmin-beta
FBgn0033368	CG13743
FBgn0052830	Abrupt
FBgn0037976	Tachykinin
FBgn0015269	Neurofibromin 1
FBgn0050177	CG30177

Tables A10-A14: Predicted targets for each miRNA were determined using TargetScanFly, then combined in an Excel spreadsheet to look for overlap of potential targets. Overlapping target lists were compiled and processed using the DAVID bioinformatics program and the tool for functional annotation cluster analysis. The most enriched functional annotation cluster is shown for each set of overlapping miRNA potential targets. Targets with known roles in neuron development are shown in bold.

Table A 15: Potential miR-315 Targets Involved in Neuron Development	
FlyBase Gene ID	**Gene**
FBgn0015589	APC-like
FBgn0020510	Abelson Interacting Protein
FBgn0015609	Cadherin-N
FBgn0086758	Chronologically inappropriate morphogenesis
FBgn0024277	Dmel_CG18214
FBgn0036274	Dmel_CG4328
FBgn0041781	Dmel_CG4636
FBgn0022764	Dmel_CG8815
FBgn0000546	Ecdysone receptor
FBgn0028734	Fragile X mental retardation syndrome-related protein 1
FBgn0001085	Frizzled
FBgn0004435	G protein alpha49B
FBgn0001325	Kruppel
FBgn0000464	Leukocyte-antigen-related-like
FBgn0015773	Netrin-A
FBgn0015774	Netrin-B
FBgn0020912	Pituitary homeobox 1 homolog
FBgn0040294	Plenty of SH3s
FBgn0003380	Shaker
FBgn0085450	Sno oncogene
FBgn0013433	beaten path Ia
FBgn0023097	bonus
FBgn0023095	capricious
FBgn0016794	daughter of sevenless
FBgn0024245	doughnut on 2
FBgn0000578	enabled
FBgn0011592	frazzled
FBgn0016797	frizzled 2
FBgn0020294	knockout
FBgn0035106	rhinoceros
FBgn0005631	**roundabout**
FBgn0016061	sidestep
FBgn0038320	**specifically Rac1-associated protein 1**
FBgn0003870	**tramtrack**
FBgn0004055	**unzipped**

Table A15: Predicted targets of miR-315 from TargetScan were compiled and analyzed with the functional annotation cluster analysis tool from the DAVID bioinformatics program. This table shows the list of potential miR-315 targets involved in neuron development.

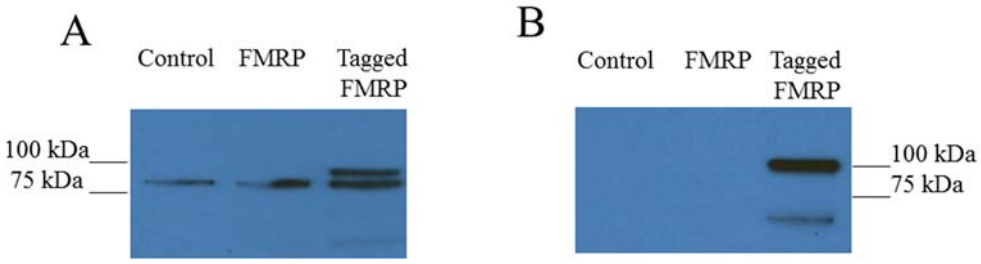

Figure A 2: An HA-tagged Version of FMRP Can Be Expressed in S2 Cells

Protein was isolated from untransfected S2 cells (control), S2 cells transfected with an endogenous FMRP overexpression vector (FMRP), and S2 cells transfected with a 3xHA-3x-FLAG-tagged version of FMRP (Tagged FMRP). A Western Blot was performed against each extract using (A) Mouse-anti-DFmr1 (6A15) antibody or (B) Rat anti-HA.

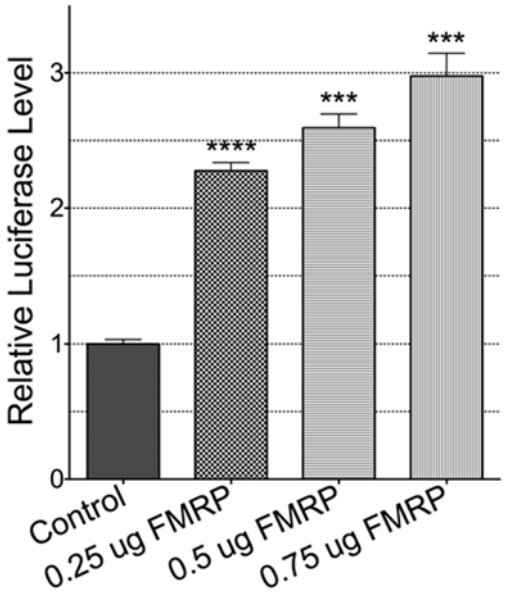

Figure A 3: Dose-Dependent Increased Expression of a Futsch Fragment G Reporter in Response to FMRP Overexpression

A dual-luciferase assay was performed using a Firefly-Luciferase reporter for *Futsch* Fragment G (Figure 13) in S2 cells and increasing amounts of FMRP (indicated below the x-axis) with a Renilla Luciferase transfection control. FLuc/RLuc ratios increased significantly with increasing amounts of FMRP transfected into S2 cells compared to cells transfected with an empty vector in place of FMRP.

List of Publications:

Nesler, K.R., Sand, R.I., Symmes, B. Pradhan, S.J., Boin, N.G., Laun, A.E., and Barbee, S.A. (2013). The miRNA Pathway Controls Rapid Changes in Activity-Dependent Synaptic Structure at the Neuromuscular Junction. *PLoS ONE* 8(7):e6835. DOI: 10.1371/journal.pone.0068385.

Mitchell, D.G., Rosen, G.M., Tseitlin, M., Symmes, B., Eaton, S.S. and Eaton, G.R. (2013). Use of Rapid-Scan EPR to Improve Detection Sensitivity for Spin-Trapped Radicals. *Biophysical Journal* 105(2): 338-342.

List of Manuscripts in Progress:

1. Breanna A. Symmes, Katherine R. Nesler, Scott A. Barbee. Profiling of the *Drosophila melanogaster* neuronal microRNA transcriptome by small RNA deep sequencing. In preparation for submission to Scientific Data

2. Breanna A. Symmes, Sarala J. Pradhan, Leslie M. Rozeboom, and Scott A. Barbee Drosophila HPat interacts with the fragile X mental retardation protein to regulate synaptic structure in preparation for submission to *PLoS ONE*.

3. Breanna A. Symmes, Nathan G. Boin, Scott A. Barbee. The role of larval-enriched miRNAs -9 and -315 in repression of *Futsch* at the *Drosophila* neuromuscular junction. In preparation for submission to *PLoS ONE*.

List of Plasmids Generated:

pENTR: miR-1
pENTR: miR-8
pENTR: miR-14
pENTR: miR-92B
pENTR: miR-277
pENTR: miR-289
pENTR: miR-958
pENTR: miR-9 sp(15x)
pENTR: miR-315sp(20x)
pBSTM: miR-9sp(10x)
pBSTM: miR-314sp(10x)
pBSTM: miR-315sp(10x)
pAc5.1: miR-1
pAc5.1: miR-8
pAc5.1: miR-14
pAc5.1: miR-92B
pAc5.1: miR-289
pAc5.1: miR-9sp(15x)
pAc5.1: miR-315sp(20x)
pAc5.1: FLuc-miR-9sp(15x)
pAc5.1: FLuc-miR-315sp(20x)
pAc5.1: FLuc-Futsch 5'/3'UTR
pAc5.1: DFmr1
pAc5.1: pAFHW-DFmr1
pAc5.1: Twin-V5-HisA
pAc5.1: Me31B-V5-HisA
pAc5.1: Dcp1-V5-HisA
pUASM: mCherry-miR-1
pUASM: mCherry-miR-8
pUASM: mCherry-miR-289
pUASM: mCherry-miR-958
pUASM: mCherry-miR-9sp(15x)
pUASM: mCherry-miR-315sp(20x)
pUASM: 3xFLAG-3xHA-DFmr1

Fly Lines/Groups of Fly Lines Generated:

UAS: mCherry-miR-9sp(15x) (Line 1) / CyO ; TbSb/DI
Kr/CyO; UAS: mCherry-miR-9sp(15x) (Line 2) / TbSb
Kr/CyO; UAS: mCherry-miR-9sp(15x) (Line 5) / DI
UAS: FH-FMRP
Kr/CyO; UAS: mCherry-miR-315sp(20x) (Line 1) / TbSb
Kr/CyO; UAS: mCherry-miR-315sp(20x) (Line 2) / TbSb
UAS: mCherry-miR-315sp(20x) (Line 6)/ CyO ; TbSb/DI
UAS: mCherry-miR-958 (Line 1) on II
Kr / CyO; UAS: mCherry-miR-958 (Line 3) / TbSb
Kr / CyO; UAS: mCherry-miR-958 (Line 5) TbSb
UAS: mCherry-miR-8
UAS: mCherry-miR-289
UAS: mCherry-miR-315
UAS: mCherry-miR-1